TITLE

Identification of Biomarkers in Bacteria by Pyrolysis-Tandem Mass Spectrometry

TYPE OF REPORT (TECHNICAL, FINAL, ETC.)

Final

AUTHOR(S)

Kent J. Voorhees

DATE

September 25, 1995

U.S. ARMY RESEARCH OFFICE

CONTRACT/GRANT NUMBER

DAAL03-92-G-003

INSTITUTION

Colorado School of Mines
Golden CO 80401

APPROVED FOR PUBLIC RELEASE;
DISTRIBUTION UNLIMITED.

REPORT DOCUMENTATION PAGE

Form Approved
OMB No. 0704-0188

1. AGENCY USE ONLY (Leave blank)	2. REPORT DATE	3. REPORT TYPE AND DATES COVERED
	Sep 25 1995	

4. TITLE AND SUBTITLE
Identification of Biomarkers in Bacteria by Pyrolysis-Tandem Mass Spectrometry

5. FUNDING NUMBERS
DAAL03-92-G-0033

6. AUTHOR(S)
Kent J Voorhees

7. PERFORMING ORGANIZATION NAME(S) AND ADDRESS(ES)
Colorado School of Mines
Golden CO 80401

8. PERFORMING ORGANIZATION REPORT NUMBER

9. SPONSORING / MONITORING AGENCY NAME(S) AND ADDRESS(ES)
U.S. Army Research Office
P.O. Box 12211
Research Triangle Park, NC 27709-2211

10. SPONSORING / MONITORING AGENCY REPORT NUMBER
ARO 29300.2-LS

11. SUPPLEMENTARY NOTES
The views, opinions and/or findings contained in this report are those of the author(s) and should not be construed as an official Department of the Army position, policy, or decision, unless so designated by other documentation.

12a. DISTRIBUTION / AVAILABILITY STATEMENT
Approved for public release; distribution unlimited.

12b. DISTRIBUTION CODE

13. ABSTRACT *(Maximum 200 words)*

The use of the biomarkers for the classification and identification of bacteria is discussed. Results on the pyrolysis-mass spectrometry of proteins, peptides, and fatty acids are described. In situ chemical reactions of fatty acids and fatty acid precursors using tetramethyl ammonium hydroxide produced fatty acid methyl ester FAME) distributions similar to those obtained from classical derivatization procedures. The FAME mass spectrometry data allowed for differentiation of Gram-positive and negative bacteria. Moreover, pathogenic bacteria were identified based on their FAME profiles generated using in situ derivatization in the Army's Chemical and Biological Mass Spectrometer. Three peer-reviewed papers and eleven oral presentations have resulted from the research.

14. SUBJECT TERMS
Pyrolysis-mass spectrometry bacteria, biomarkers, in situ derivatization.

15. NUMBER OF PAGES
150

16. PRICE CODE

17. SECURITY CLASSIFICATION OF REPORT	18. SECURITY CLASSIFICATION OF THIS PAGE	19. SECURITY CLASSIFICATION OF ABSTRACT	20. LIMITATION OF ABSTRACT
UNCLASSIFIED	UNCLASSIFIED	UNCLASSIFIED	UL

EXECUTIVE SUMMARY

The U.S. Army contracted in 1985 with Teledyne CME and Bruker Franzen to build a field portable chemical and biological detector system (CBMS). Pyrolysis with an ion trap mass spectrometry as the detector, was chosen as the technique to be used for the biological agents. Early tests conducted by Teledyne showed that the use of biomarkers for identification of biological agents provided a satisfactory approach for the system. The present report provides new research results on using fatty acids, nucleic acids, and proteins as biomarkers for the CBMS identification protocol. In addition, information on the identity of specific mass spectral ions used in the Teledyne and Army Dugway tests is discussed.

1. Fatty Acids

Two types of fatty acids, metabolic and bound, are present in a bacterium. It has been shown that the metabolic or free fatty acids are highly dependent on diet. In contrast, the bound fatty acids show only a minor connection to distribution and diet. The major thrust of this study has been to develop an approach to rapidly analyze the bound fatty acids and obtain the same results as those from a commercial fatty acid analyzer.

Curie-point pyrolysis mass spectrometry was conducted on fatty acid methyl ester (FAME) extracts from 20 bacteria that were also analyzed on the Microbial ID, Inc. (MIDI) fatty acid analyzer. The extracts had been prepared from classical saponification and methylation reactions. The study showed that similar results were obtained using the two systems and suggested that mass spectrometry could be used for rapid profiling of FAMEs. The study also differentiated Gram negative and positive bacteria using their fatty acid content.

Because the conventional FAME preparation require up to an hour, rapid approaches for preparing the FAMEs had to be developed for compatibility with the CBMS specifications. It was reported in the literature that tetramethyl ammonium hydroxide when mixed with bacteria and then heated produced FAMEs *in situ*. A study using *Bacillus anthracis, Francisella tularensis, Yersinia pestis,* and *Brucella melitensis* showed that similar results were obtained from the multivariate statistical analysis of the *in situ* pyrolysis-mass spectrometry data set and a data set from the mass spectrometric analysis of the conventional FAME extracts. The time required for the two types of analysis are vastly different. As previously mentioned, sample preparation for the traditional FAME extracts was one hour. In contrast, the *in situ* procedure requires about four minutes to complete the FAME preparation and analysis. Clearly, this approach meets the demands presented in the CBMS protocol and provides the known information capability of fatty acid profiling.

2. Peptides

A paucity of literature existed for the pyrolysis of peptides and its application for identifying bacteria. Dipeptides had been studied and were known to form diketopiperazines upon pyrolysis. The effect of increasing the number of amino acids in the peptide on formation of the diketopiperazine (DKP) was investigated in this study using Curie-point pyrolysis mass spectrometry. It was found that oligopeptides essentially depolymerized via the diketopiperazine structure. In this study, some peptides were observed not to form all of the expected DKPs which suggested that selected amino acids could prevent DKP formation. Two series of dipeptides, one containing a fixed N-terminal glycine with the C-terminal varied among the other 20 amino acids and a second series with a variable N-terminal and a fixed C-terminal, were

investigated to understand the formation of the DKPs. The results from this study clearly showed that 17 of 20 common amino acids formed DKPs. Only aspartic acid, glutamic acid, and arginine prevented formation.

Peptides containing up to 30 amino acids have been pyrolyzed. Bovine insulin produced six distinct sets of DKPs out of a possible 15 sets. The lack of formation of some of the DKPs can be explained based on the three amino acids that prevented DKP formation. However, some unknown factor also must play a role in preventing the DKP formation. This is presently being investigated.

3. Nucleic Acids

The ratios of the nucleic acid bases has been successfully used for classifying bacteria. The use of Curie-point pyrolysis-mass spectrometry to determine the guanine/cytosine molar ratios (G/C) has been evaluated. A standard curve based on G/C molar ratios of 100%, 75%, 67%, 58%, 46%, 33%, 25%, and 0% was prepared from guanosine-5'-monophosphate (GMP), cytidine-5'-monophosphate (CMP), adenosine-5'-monophosphate (AMP), and thymidine-5'-monophosphate (TMP). The 0% and 100% used AMP + TMP and GMP + CMP, respectively. The curve showed a clear correlation between the mass spectral ratio and the known G/C molar ratio. Further work using DNA cellular extracts and PCR products will continue over the next funding period.

4. Biomarkers

A series of mass spectral ions, m/z 67, 81, 82, 91, 95, 102, 103, 105, 115,117, 128, 129, 131 and 135, used in the 1992 and 1993 Dugway CBMS tests have been investigated by tandem mass spectrometry. Identification of the fragment ions and the precursor ions have been

determined for a number of the listed ions. However, many of the ions can not be identified with low resolution MS because of identical fragmentation spectra for two entirely different precursor ions. High resolution mass spectrometry will be required for identification of a portion of the listed ions.

TABLE OF CONTENTS

INTRODUCTION 1

EXPERIMENTAL 6
Pyrolysis/mass spectrometry 6
Samples 9
biological samples 9
peptides 10
chemicals 12
Fatty Acid Extraction Procedures 13
In-situ Fatty Acid Derivatization 13

RESULTS AND DISCUSSION 15
Fatty Acids 15
FAME pyrolysis-mass spectra of Gram-negative and Gram-positive bacteria 18
Multivariate analysis of FAMEs pyrolysis-mass spectra 24
Conclusions on mass spectrometry fatty acid analysis 34
Validation of Py-MS bacterial lipid analysis with the MIDI system 35
In situ Pyrolytic Methylation/Mass Spectrometry of Whole Bacteria 49
In situ Pyrolytic Lipid Methylation of Whole Bacteria using the CBMS . . 51
Proteins 59
Oligopeptides 61
Tripeptides 61
Phenylalanyl-Leucyl-Methionine 61
Other tripeptides 71
Tetrapeptides 71
Alanyl-Phenylalanyl-Leucyl-Methionine 71
Alanyl-Methionyl-Leucyl-Phenylalanine 73
Pentapeptides 74
Alanyl-Phenylalanyl-Leucyl-Methionyl-Tyrosine 74
Alanyl-Tyrosyl-Leucyl-Methionyl-Phenylalanine 78
Hexapeptides 81
Large Oligopeptides 81
Derivatized Oligopeptides 88
Conclusions on Oligopeptides 88
Dipeptides 90

Biomarker Identification 118
m/z 67 120
m/z 81 120
m/z 91 120
m/z 103 123
m/z 115 123
m/z 117 123
m/z 128 123
m/z 129 125
m/z 131 125
m/z 135 125
Conclusions on biomarker study 129
DNA Studies 129
Construction of the Standard Curve 130

CONCLUSIONS 133

REFERENCES 135

INTRODUCTION

The concept of using bacterial biomarkers to differentiate bacteria in complex environmental backgrounds has been demonstrated by Voorhees *et al.* (1). The mass spectral ions, m/z 79, 113, 117, 126, and 135, were found to be representative of major biomaterials contained in bacteria. Table I summarizes the ions and corresponding biomaterials used in

Table I. Summary of Marker Ions and Corresponding Biomaterial.

Ion	Material
79	Pyridine (Dipicolinic acid)
113	Diketopiperazine (protein)
117	Indole (Tryptophan)
126	Thymine (DNA)
135	Adenine (DNA)

this investigation. Dipicolinic acid (2,6-pyridine dicarboxylic acid) was known to be produced when certain bacteria such as *B. anthracis* sporulate. In the pyrolysis and electron ionization processes, dipicolinic acid produces pyridine which serves as the marker for dipicolinic acid. The daughter-ion spectrum of m/z 79 of pyridine shows m/z 52 as the only major fragmentation ion.

The materials listed in Table II were pyrolyzed at 510°C and the daughter-ion spectra of m/z 79 recorded. Figure 1 shows Py-mass spectra of three of the materials. The sporulated bacterial spectra all contained an intense m/z 52 fragment ion from the m/z 79 peak, while samples such as fog oil and diesel smoke showed virtually no m/z 52 peak.

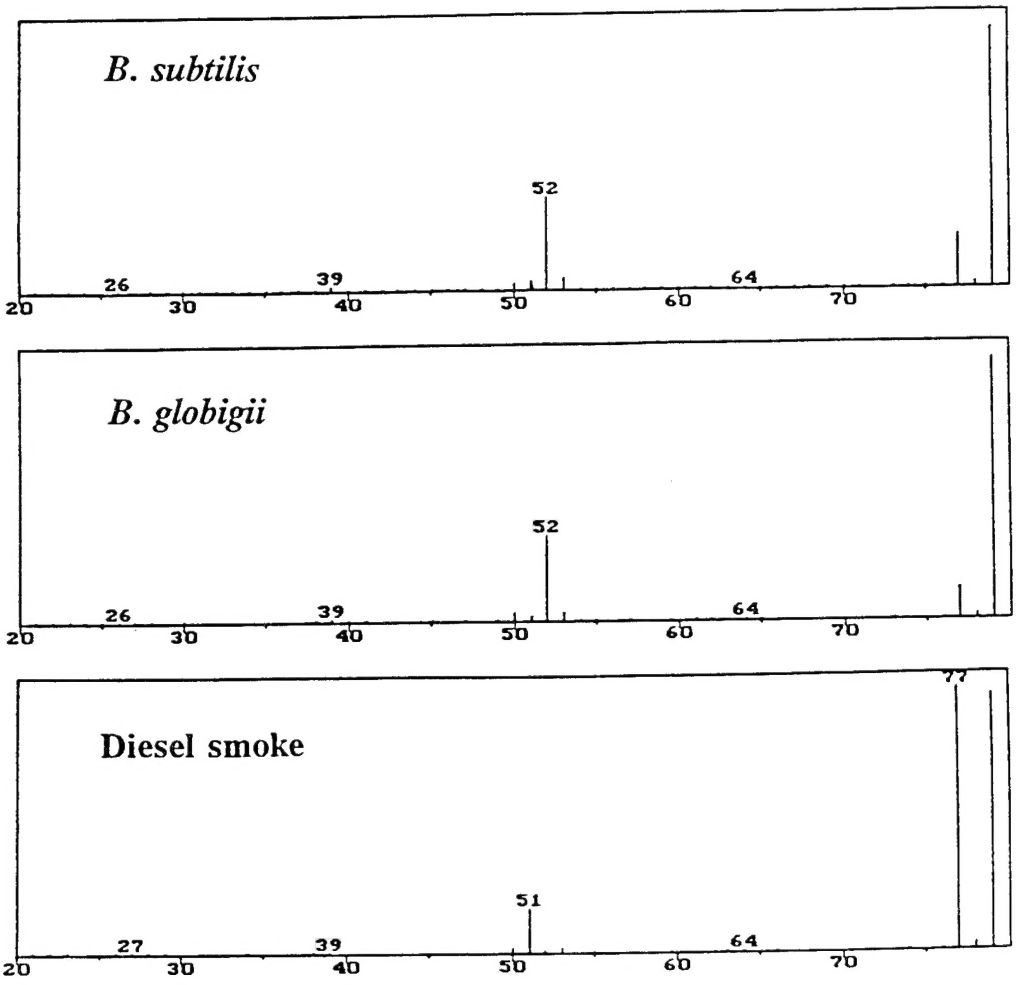

Figure 1. Daughter-ion Spectra of m/z 79 for Three Selected Materials.

The principal components plot (Figure 2) of the m/z 79 daughter-ion spectra separates the *B.g.* spores and *B. subtilis* from the remainder of the samples. The factor spectrum (Figure 3) generated for component 2 shows that m/z 52 and 79 are correlated for the *B.g.* spores and

Table II. Samples used in the study.

Substance	Category
Fog oil	f
Wood smoke	w
Diesel smoke	d
Grass pollen (Secale cerale)	p
Dry yeast	y
Aldolase	a
MS-2 coliphage	m
E. coli	e
B. Subtilis (sporulated)	b
B. globigii spores	g

B. subtilis, while peaks at m/z 51 and 77 are correlated in the negative direction with the remainder of the samples. This investigation showed for the samples studied that the daughter-ion spectra of m/z 79 can be used as a marker to differentiate the sporulated bacteria.

The above data indicate that the m/z 79 peak by itself was not unique for pyridine since almost all spectra showed a m/z 79 peak. In order to determine the compounds producing the m/z 79 peak in the non-bacterial samples, parent-ion scans of the m/z 79 peak were run for all the samples. At least three compound classes were found in the 10 samples that produce a m/z 79 peak. These included alkylcyclodienyl hydrocarbons, alkyl phenols, and alkylbenzaldehydes. All three of these compound classes showed a strong m/z 79 peak as well as a significant m/z 77 peak.

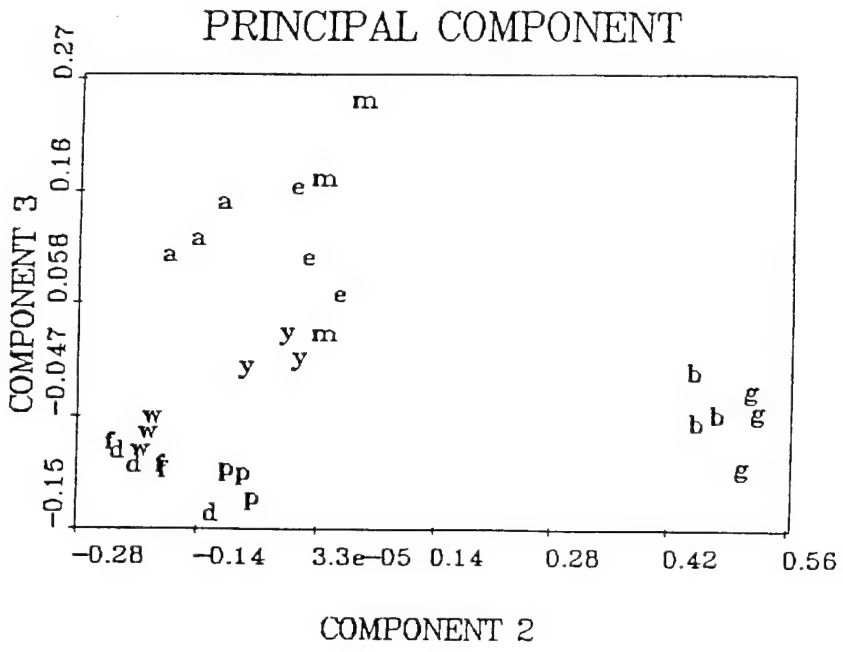

Figure 2. Factor-Factor Plot of Daughter-ion Spectra of m/z 79 (see Table III for Identification Codes for the Various Samples).

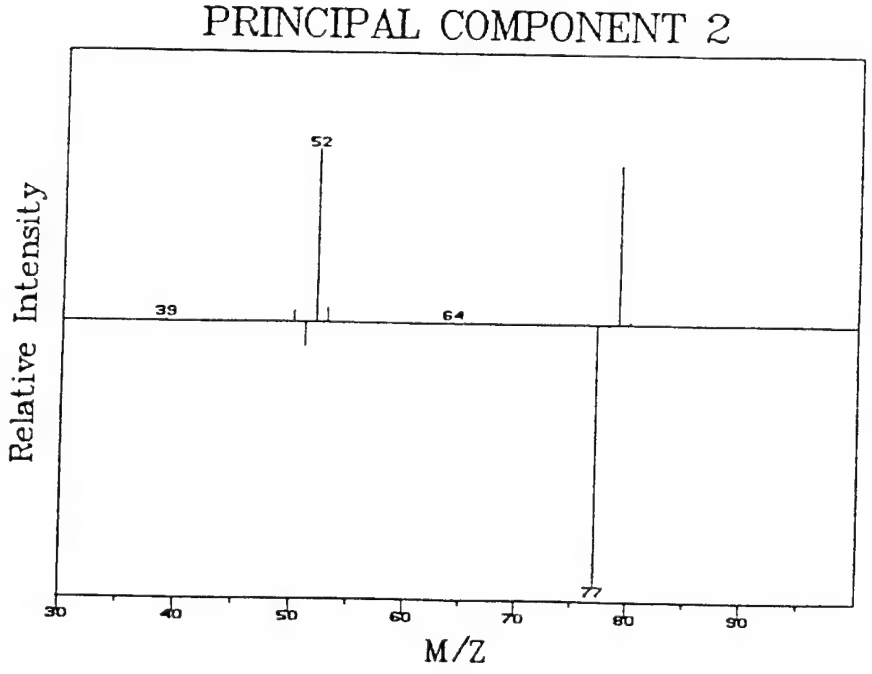

Figure 3. Factor Spectrum of Component 2 Shown in Figure 2.

The other four biomarker peaks (m/z 113, 117, 126, and 135) reported in Table II were studied with a similar approach and were found to differentiate materials containing protein and nucleic acids. The daughter-ion spectra of m/z 126 peak were the most complex of the five ions. It was found that this ion had thymine, carbohydrates and cyclic alkenes as the major contributors. Overall, this study demonstrated that pyrolysis-tandem mass spectrometry could be used to identify biomarkers in complex backgrounds.

The list of biopolymers and biochemicals that were proposed for investigation during this 1992-94 CSM/ARO contract is summarized in Table III. Also, listed in this table are the pertinent publications on Py-MS of biomarkers published by CSM over the last three years. All of the materials listed in Table III have been studied with varying degrees of success. Carbohydrates have provided the least amount of data from electron ionization Py-MS which could be used for classification purposes. This observation had been previously reported; however, because of the short transfer line in the CSM triple quadrupole MS (3), it was speculated that higher molecular weight carbohydrate species would be detected. All carbohydrates studied produced similar spectra that consist of dehydration products (i.e. levoglucosenone, hydroxymethylfurfural, and furfural) (15). No fragments for dimer or trimer species were detected from any of the polymeric carbohydrates investigated.

Table III. Biopolymers and Biochemicals in March 1992 Proposal.

Materials	References
Fatty Acids	2,3,4
Di-and Triglycerides	5
phospholipids	5
proteins and amino acids	6,7,8,9,10,11
carbohydrates	
nucleic acids	12
poly(3-hydroxyalkonates)	13
ubiquinones	14
porphyrins	
hydroxysteroids	
teichoic acids	
lipopolysaccarides	3
B vitamins	

EXPERIMENTAL

II. Pyrolysis/mass spectrometry

Most pyrolysis-tandem mass spectra were obtained using an Extrel Model EL-400 triple quadrupole mass spectrometer, fitted with a Fischer Model 0310 (1 kw) rf-generator to supply power to a Curie-point pyrolysis coil (16). The transfer line was heated to 375°C and the ion source to 250°C. All spectra were generated using 70 eV electron ionization. Three scan modes: full scan, parent ion scans, and daughter ion scans, were used in the study. Full scan spectra were generated by scanning quadrupole 1 (Q1) and setting quadrupole 2 (Q2) and quadrupole 3 (Q3) to pass all ions. In parent ion mode, Q1 was scanned while Q3 was set to a selected daughter, and in daughter ion mode, Q1 was set to a selected parent while Q3 was scanned. Argon was used as the collision gas for the daughter ion and parent ion scans.

The Curie-point wires were coated by the direct application of the selected biological solutions (1 mg organic to 1 ml methanol) onto 510°C wires (610°C and 358°C as options). Each sample required 5-10 μl of solution to obtain an adequate mass spectral signal. The methanol was evaporated under a stream of hot air prior to analysis. After introduction into the mass spectrometer, the glass sample holder (17) was preheated to 250°C. Triplicate pyrolysis-mass spectra were collected for each oligopeptide in the mass range of m/z 35 to 500, as well as daughter-ion and parent-ion scans for selected ions. The pyrolysis conditions were: rise time-100 ms, final hold- 9.9 sec, and transfer line temperature- 325°C.

A schematic of the chemical and biological mass spectrometer (CBMS) used in this investigation is shown in Figure 4 . This instrument is composed of a pyrolyzer, a transfer line, a valving system which contains a silicon membrane, and an ion trap mass spectrometer. The pyrolysis station used infrared radiation to heat a microgram sample to 550°C. The transfer line is a heated fused silica capillary approximately two meters in length heated to 230°C. The membrane present in the valving system (230°C) operates similarly to the early GC/MS membranes to remove the carrier gas and transmit the organics into the vacuum manifold. A low capacity ion-getter pump was used on the system without a roughing pump. Samples are introduced to the pyrolyzer either as aqueous solutions ($\sim$10mg organic/Ml) or bulk samples coated onto the Curie-point wires described above. The pyrolysis conditions were: final temperature-500°C, rise time- 41 sec, final hold-42 sec, and pyrolysis atmosphere-air.

Multivariate statistical analyses of data were carried out with the RESOLVE program (18). All spectra (full scan and daughters) were individually normalized to constant length and then subjected to principal components analysis with and without autoscaling. The resulting

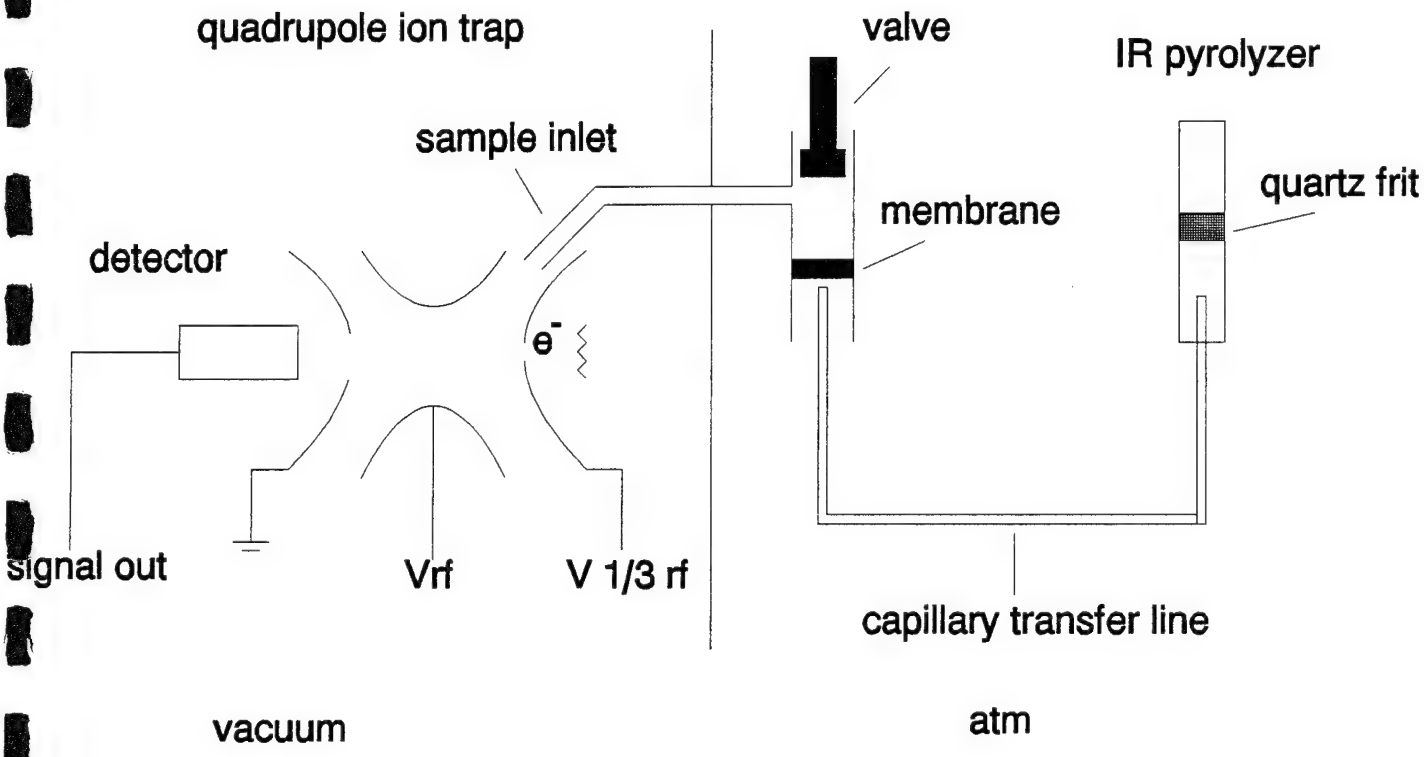

Figure 4. Chemical-Biological Mass Spectrometer (CBMS, Bruker-Franzen, Bremen, Germany) instrument diagram.

Karhunen-Loeve (K-L) or principal components plots were used to show the distribution of the samples in the multivariate mass spectral space. Loading plots, or factor spectra, were also used to show the correlations (positive and negative) of mass spectral peaks with the score axes values of the K-L plots. The principal components calculated for the full scan spectra were subjected to supervised rotation (19). The rotations were obtained by maximizing the Fisher distance between scores of a given category and the other spectra. At this point, an oblique linear discriminant was calculated for each bacterial class. The results of the procedure were displayed as factor score and loading plots. The factor spectrum associated with each rotation operation displays the peaks responsible for the separation of a particular sample from the remainder of the samples.

II. Samples

a. biological samples The microorganisms used in this study were chosen at random and are listed in Table IV. All microorganisms were grown on a tryptic soy agar at 37°C for 18 hours.

Table IV. Microorganisms used in this study

Index[1]	Gram-type	Microorganism
A	+	*Bacillus cereus*
B	+	*Bacillus circulans*
C	+	*Bacillus ficheniformis*
E	+	*Bacillus subtilis*
F	+	*Bacillus thuringiensis*
G	+	*Enterococcus (Streptococcus faecalis*
H	+	*Listeria monocytogenes*
I	+	*Staphylococcus aureus subsp. aureus*
i	+	*Staphylococcus epidermidis*
K	+	*Streptococcus pyogene*
L	-	*Enterobacter aerogenes*
N	-	*Proteus mirabifis*
0	-	*Providencia stuartii*
P	-	*Pseudomonas aeruginosa*
Q	-	*Pseudomonas cepacia*
R	-	*Pseudomonas fluorescens*
S	-	*Pseudomonas putrefaciens*
T	-	*Pseudomonas stutzeri*
U	-	*Serratia marcescens*

[1] This index is used in subsequent fatty acid results Figures.

A sample of gamma-killed *B. neotomae* for the biomarker investigation was obtained from the Armed Forces Institute of Pathology, Washington, D.C., Ted L. Hadfield.

b. peptides The oligopeptides used in the study were synthesized by Dr. Craig Miles, Biochemistry Department, Colorado State University (Fort Collins, CO). These included:

Tripeptides:

Phenylalanyl-leucyl-methionine (PHE-LEU-MET)
Methionyl-leucyl-phenylalanine (MET-LEU-PHE)
Phenylalanyl-methionyl-leucine (PHE-MET-LEU)
Tyrosyl-tyrosyl-phenylalanine (TYR-TYR-PHE)
Leucyl-leucyl-leucine (LEU-LEU-LEU)

Tetrapeptides:

Alanyl-phenylalanyl-leucyl-methionine (ALA-PHE-LEU-MET)
Alanyl-methionyl-leucyl-phenylalanine (ALA-MET-LEU-PHE)

Pentapeptides:

Alanyl-phenylalanyl-leucyl-methionyl-tyrosine
(ALA-PHE-LEU-MET-TYR)
Alanyl-tyrosyl-leucyl-methionyl-phenylalanine
(ALA-TYR-LEU-MET-PHE)

Hexapeptides:

Alanyl-tyrosyl-leucyl-methionyl-phenylalanyl-phenylalanine
(ALA-TYR-LEU-MET-PHE-PHE)
Alanyl-phenylalanyl-leucyl-methionyl-tyrosyl-phenylalanine
(ALA-PHE-LEU-MET-TYR-PHE)
Phenylalanyl-alanyl-phenylalanyl-leucyl-methionyl-tyrosine
(PHE-ALA-PHE-LEU-MET-TYR)

Tyrosyl-tyrosyl-tyrosyl-tyrosyl-tyrosyl-tyrosine
(TYR-TYR-TYR-TYR-TYR-TYR)

The derivatized oligopeptides used in this study included:

Seryl-phenylalanyl-phenylalanyl-arginine(TFA)
(SER-PHE-PHE-ARG)(TFA)
Phenylalanyl-seryl-phenylalanyl-phenylalanyl-arginine(TFA)
(PHE-SER-PHE-PHE-ARG)(TFA)
Glycyl-phenylalanyl-seryl-phenylalanyl-phenylalanyl-arginine(TFA)
(GLY-PHE-SER-PHE-PHE-ARG)(TFA)

Samples of derivatized oligopeptides were obtained from Dr. Paul Fennessey, University of Colorado Medical Center.

Of the dipeptides studied, most were obtained from Sigma Chemical, St. Louis MO. The remaining were synthesized by Macromolecular Resources, Colorado State University, Fort Collins, CO. Table V summarizes the dipeptides investigated.

Table V. Dipeptides Studied, Abbreviations and Sources

Dipeptide	Abbreviation
Alanyl-Glycine	Ala-Gly[1]
Arginyl-Glycine	Arg-Gly[1]
Asparagyl-Glycine	Asn-Gly[2]
Asparticyl-Glycine	Asp-Gly[1]
Cystyl-Glycine	Cys-Gly[1]
Glutamyl-Glycine	Gln-Gly[2]
Glutamicyl-Glycine	Glu-Gly[1]
Glycyl-Glycine	Gly-Gly[1]
Histadyl-Glycine	His-Gly[1]
Isoleucyl-Glycine	Ile-Gly[2]
Leucyl-Glycine	Leu-Gly[1]
Lysyl-Glycine	Lys-Gly[2]
Methionyl-Glycine	Met-Gly[1]
Phenylalanyl-Glycine	Phe-Gly[1]
Prolyl-Glycine	Pro-Gly[1]
Seryl-Glycine	Ser-Gly[1]
Threonyl-Glycine	Thr-Gly[2]
Tryptophanyl-Glycine	Trp-Gly[2]
Tyrosyl-Glycine	Tyr-Gly[1]
Valyl-Glycine	Val-Gly[1]
Glycyl-Alanine	Gly-Ala[1]
Glycyl-Arginine	Gly-Arg[2]
Glycyl-Asparagine	Gly-Asn[1]
Glycyl-Aspartic Acid	Gly-Asp[1]
Glycyl-Cysteine	Gly-Cys[2]
Glycyl-Glutamic Acid	Gly-Glu[1]
Glycyl-Glutamine	Gly-Gln[2]
Glycyl-Histadine	Gly-His[1]
Glycyl-Isoleucine	Gly-Ile[1]
Glycyl-Leucine	Gly-Leu[1]
Glycyl-Lysine	Gly-Lys[2]
Glycyl-Methionine	Gly-Met[1]
Glycyl-Phenylalanine	Gly-Phe[1]
Glycyl-Proline	Gly-Pro[1]
Glycyl-Serine	Gly-Ser[1]
Glycyl-Threonine	Gly-Thr[1]
Glycyl-Tryptophan	Gly-Trp[1]
Glycyl-Tyrosine	Gly-Tyr[1]
Glycyl-Valine	Gly-Val[1]

[1] From Sigma Chemical
[2] From Macromolecular Resources

c. chemicals All standard straight chain saturated, unsaturated, and hydroxy fatty acids (Aldrich) and branched iso- and anteiso-fatty acids (Ultra Scientific) were used without further purification. All fatty acid (FA) standards were dissolved in glass-distilled methanol (10 mg/Ml). Lipid A, monophosphorylated, from *E. coli*-F583 Rd-Mutant (Fluka Chemika) was also dissolved in glass-distilled methanol before analysis. Tetramethyl ammonium hydroxide was purchased from Fluka. The samples of TMP, GMP, CMP, and AMP were obtained from Sigma. Stock solutions of a 1:1 mole ratio were made up of GMP + CMP and AMP + TMP. Aliquots of the 1:1 stocks solution were taken to make solutions of varying G/C ratios which included 100%, 75%, 67%, 58%, 46%, 33%, 25%, and 0%.

III. Fatty Acid Extraction Procedures

Cells were isolated by washing with distilled water, and the fatty acids extracted and methylated as described by Miller (20). FAME samples were redissolved in 1: 1 ether-hexane as needed due to solvent evaporation. A 1 μL aliquot of this solution was applied to the Curie-point wire and air dried at room temperature. The total mass of FAMEs deposited on the wire was estimated to be in the low microgram range.

IV. In-situ Fatty Acid Derivatization (21)

For experiments in which TMAH was added, the sample was first dried onto the Curie-point wire. Then, approximately 10 μl, of a 0.1 M solution of tetramethyl ammonium hydroxide (TMAH) in methanol was applied to the sample, followed by evaporation of the methanol under a hot air stream. The sample was pyrolyzed as previously described in the Curie point pyrolysis

mass spectrometer procedure. For the derivatization experiments with the CBMS, the coated wire was dropped into the ir-pyrolyzer, followed by a regular pyrolysis cycle.

RESULTS AND DISCUSSION

II. Fatty Acids

Application of instrumentation-based techniques in microbiology to perform conventional procedures for the identification and differentiation of microorganisms has increased during the last decade. Gas chromatography (GC) (22,23), fast atom bombardment mass spectrometry (24), Curie-point pyrolysis mass spectrometry (2), pyrolysis-GC/mass spectrometry (25), Fourier transform infrared spectroscopy (26), UV resonance Raman spectroscopy (27), flow cytometry (10), and laser-based enzyme profiling (29,30) have all been used to differentiate microorganisms. These techniques apply established analytical methods to measure a distinct biochemical property and/or chemical distribution of taxonomic significance. Pyrolysis-mass spectrometry (Py-MS) has been used widely for the rapid identification and differentiation of whole bacteria. Moreover, Py-MS has identified useful chemical constituents in bacteria or biomarkers for the differentiation and identification of microorganisms in the presence of an environmental background (1).

The correlation between bacterial lipid composition and taxonomic classification has been extensively used for the identification of bacteria. The bacterial classifications based on fatty acid profiles have compared well with classifications based on nucleic acid homology (31). Improvements in lipid analysis methodology have extended this correlation to many bacteria. Gas chromatography of lipid extracts is commonly employed to determine cellular fatty acids in microorganisms (22,32). This commercialized method (33) is based on the hydrolysis and extraction of bacterial lipids, methylation of the carboxylic group to produce a fatty acid methyl ester (FAME), and subsequent gas chromatography analysis (32). Overall sample preparation

time is about 60 to 70 min. The chromatographic analysis of the FAME extracts takes about 20 min/sample, making the total turn-around time for this assay about 1.5 hours/sample. In addition, a standard FAME mixture is needed prior and at intervals along with the samples, increasing the total analysis time. The success of the procedure to identify individual fatty acid components relies on the judicious selection of this standard FAME mixture.

Pyrolysis-mass spectrometry rapidly heats and vaporizes the sample in vacuo, followed by ionization of the gas-phase molecules, and mass analysis. A histogram of the signal intensity versus mass-to-charge ratio (m/z) represents the mass spectrum of the compound or mixture of compounds. When Py-MS is performed on a microorganism, the resulting mass spectrum is a profile or chemical signature characteristic of the sample. Sample preparation and data collection (not including FAME extract preparation) is fast, taking about 5 min/sample. The instrument is calibrated once at the beginning of the day with a standard compound. Replacing the chromatographic run of the FAME extracts with Py-MS provides a faster assay for the identification and differentiation of bacteria, with the FAME extract preparation as the limiting step. Simple staining techniques can yield Gram-type information; however, automated, instrumentation-based techniques must be developed to perform *in situ* bacterial analysis in hostile environments. Toward this goal, the use of pyrolysis as a rapid sample processing/preparation step has proven very successful (25,34,35). Before replacing time consuming, extraction and separation steps with Py-MS, the feasibility of Py-MS to provide information useful for the differentiation and identification of microorganisms comparable to the GC/FAME approach must be proven. Pyrolysis-mass spectrometry (single quadrupole instruments) distinguishes compounds based on their mass-to-charge ratio, hence, isomer

differentiation is not always possible in a mixture containing iso-anteiso, *cis-trans* unsaturation and unsaturation position isomers. Therefore, the information content in a FAME extract Py-mass spectrum will be always lower than a FAME extract gas chromatogram (when only looking at the FAMEs molecular ion region). The lower information content of the mass spectrum, however, does not imply that a minimum amount of information required for successful differentiation and identification of microorganisms at the species level is not present.

In this study, Curie-point Py-MS of bacterial FAME extracts and pattern recognition have been used to differentiate Gram-positive and Gram-negative microorganisms. This differentiation was based solely on fatty acid distributions. With the aid of pattern recognition (principal components analysis, PCA), these differences were attributed to the presence of fragment ions of palmitoleic, oleic, 3-hydroxymyristic acid, branched pentadecanoic fatty acids, and a greater signal intensity of palmitic acid relative to pentadecanoic acid in the Gram-negative microorganisms studied. These ions were confirmed by either pyrolysis-tandem mass spectrometry (Py-MS/MS) or by comparison to the mass spectrum of a standard compound.

a. FAME pyrolysis-mass spectra of Gram-negative and Gram-positive bacteria

The spectra of three FAME extracts of Gram-negative microorganisms are shown in Figure 5: *Pseudomonas fluorescens, Proteus mirabilis,* and *Enterobacter aerogenes*. These mass spectra contain a pattern of straight-chain FAME molecular ions varying by one carbon, from C14:0 methyl ester (C14:0 ME) to C21:0 ME, with the palmitic ME signal (C16:0 ME, $M^{+\cdot}$ m/z 270) being the most intense. Along with the molecular ions, fragment ions due to electron ionization-fragmentation are present. These include the homolytic cleavage of the methoxy bond of C16:0 ME giving rise to the M-31 fragment ion at m/z 239, and the carbomethoxy series at m/z's 185, 199, 213, 227, etc., with the general formula $CH_3OCO(CH_2)_n^+$ (35). In the Py-mass spectra shown in Figure 5, additional peaks arising from unsaturated FAME are observed. For example, in the Py-mass spectrum of *P. fluorescens*, several other peaks corresponding to mono-unsaturated (even and odd chain length) FAME molecular ions and their fragment ions were identified by comparison to mass spectra of pure standards or by Py-MS/MS studies.

Most mono-unsaturated FAMEs studied in our laboratory (C16:1-C20:1) yielded, along with their molecular ions, fragment ions at M-32 (loss of CH_3OH) and M-74. Oleic ME (C18:1 ME, $M^{+\cdot}$ m/z 296) fragment ions appear at m/z 264 and m/z 222, and palmitoleic ME (C16:1 ME, $M^{+\cdot}$ m/z 268) fragment ions are found at m/z 236 and m/z 194. The M-32 and M-74 fragment ions of the unsaturated FAME C17:1 ME ($M^{+\cdot}$ m/z 282) and/or cyclopropaneC17:0 ME (cyC17:0 ME, $M^{+\cdot}$ m/z 282)

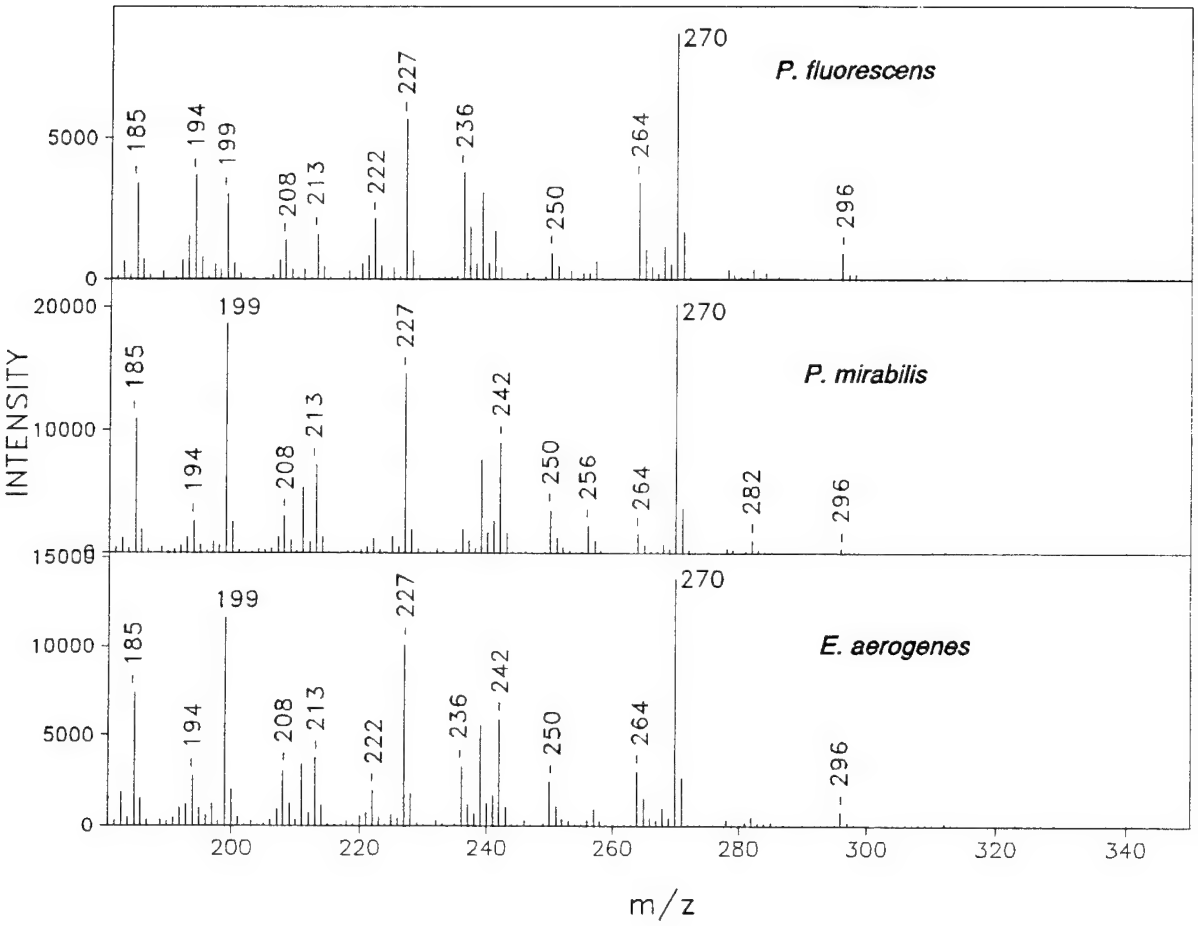

Figure 5. Pyrolysis-mass spectra of Gram-negative bacterial FAME extracts.

appear at m/z 250 and 208 respectively. The ion at m/z 208 may also correspond to the M-50, possibly $[M-(CH_3OH + H_2O)]^{+\cdot}$, fragment ion of 3-hydroxymyristic ME (3OH C14:0 ME) which is observed in the mass spectrum of a known standard. Molecular ions from the hydroxy FAMEs, 2- and 3-hydroxylauric (2OH, and 3OH C12:0 ME, $M^{+\cdot}$ m/z 230) and 3-hydroxymyristic (3OH C14:0 ME, $M^{+\cdot}$ m/z 258) were not observed. Branched fatty acids were not detected by Py-MS/MS scans in any of the Gram-negative bacteria investigated in this work. These observations agree with the known fact that most Gram-negative microorganisms contain mostly straight-chain saturated and unsaturated fatty acids (36,37,1).

Figure 6 shows the Py-mass spectra of FAME extracts of three Gram-positive bacteria: *Bacillus cereus, Listeria monocytogenes,* and *Staphylococcus aureus*. The C15:0 ME to C21:0 ME series of molecular ions is observed in these spectra. These mass spectra are generally less complex than mass spectra of Gram-negative bacteria. A smaller relative palmitic ME signal intensity ($M^{+\cdot}$ m/z 270) is observed in the Gram-positive mass spectra when compared to Gram-negative bacteria mass spectra (Figure 5). In the *B. cereus* mass spectrum in Figure 6, the presence of mono-unsaturated FAMEs C16:1 ME, and C17:1 ME (and/or cyC17:0 ME) is indicated by fragment ions corresponding to M-32 and M-74 (m/z 236, 194, 250, and 208 respectively). The M-31 fragment ion for the molecular ion at m/z 256 (C15:0 ME) is observed at m/z 225.

The presence of branched isomers at m/z 256 (C15:0 ME) and 284 (C17:0 ME) in the Py-mass spectra of the Gram-positive microorganisms *B. thuringiensis* and

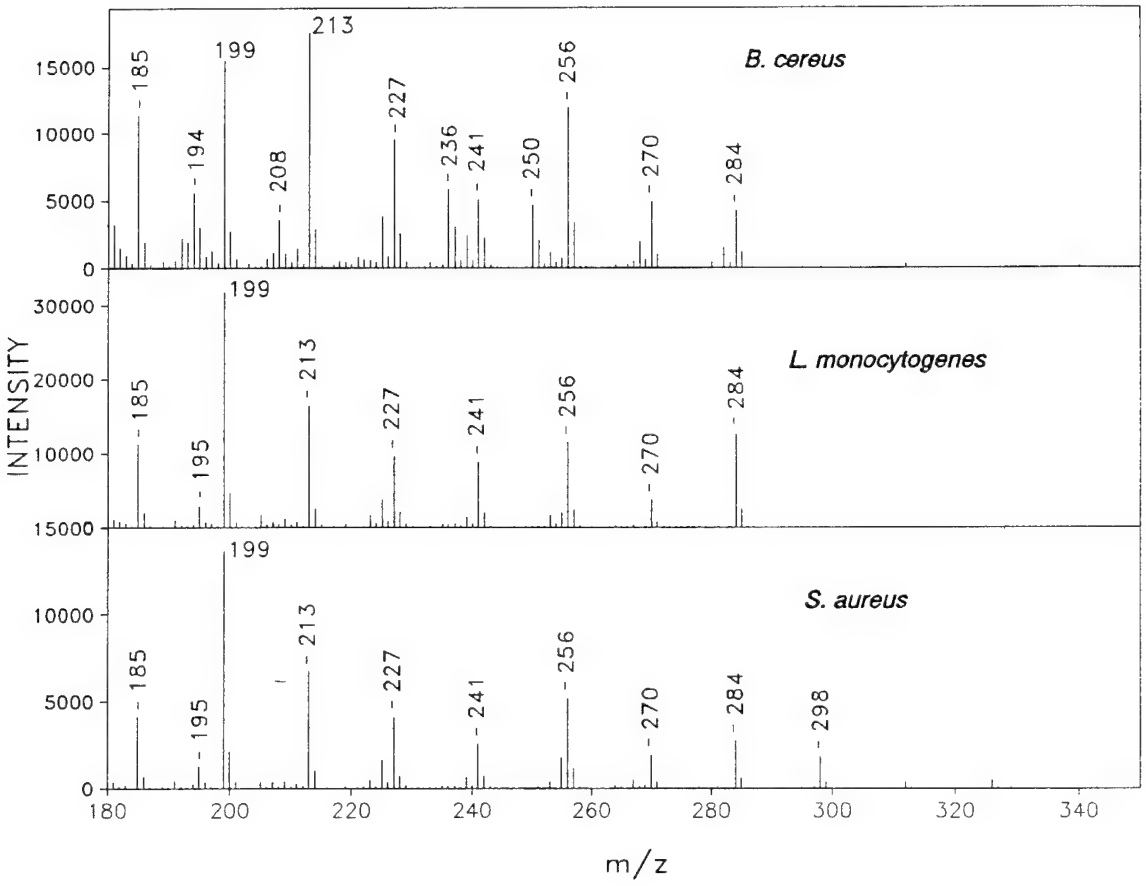

Figure 6. Pyrolysis-mass spectra of Gram-positive bacterial FAME extracts.

S. aureus were further studied by Py-MS/MS. For *B. thuringiensis*, the Py-daughter ion spectrum of m/z 256 (Figure 7, top spectrum) was characteristic of isoC15:0 ME (M-46 base peak, m/z 213). In the case of *S. aureus*, the m/z 256 ion was identified as anteisoC15:0 ME from the Py-daughter ion spectrum shown in Figure 7. This spectrum is very similar to that of anteisoC15:0 ME (M-57 base peak, m/z 199) standard, also shown in Figure 7. This similarity suggests that the anteiso branched isomer is more abundant than either the straight chain and/or iso-branched isomer C15:0 ME, even though mixtures of anteiso- and isoC15:0 ME (about 4:1 anteiso:iso-C15:0) are known to be present in *Staphylococcus* (38). The Py-daughter ion mass spectrum of C15:0 ME is also shown in Figure 7 for comparison. Measurements in our laboratory have shown that mixtures of branched:normal FAME isomers with varying ratios from 1:1 to 4:1 can be differentiated from either pure isomer by Py-MS and/or Py-MS/MS measurements. The ion at m/z 284 was determined from Py-MS/MS experiments to be a mixture of isoC17:0 ME and its straight chain C17:0 ME isomer (39). These findings are in agreement with previous studies that showed branched fatty acids to be widely present in Gram-positive bacteria (36,37,38). The presence of branched fatty acids, however, solely is not indicative of a Gram-positive type bacteria since there are exceptions as Gram-negative microorganisms in the genera *Xanthomonas*, *Legionella*, *Thermus*, *Desulfovibrio* and some *Pseudomonas* (i.e., *P. maltophilia*, and *P. pictorum*), among many, have significant amounts of branched and hydroxy-branched fatty acids (1,41).

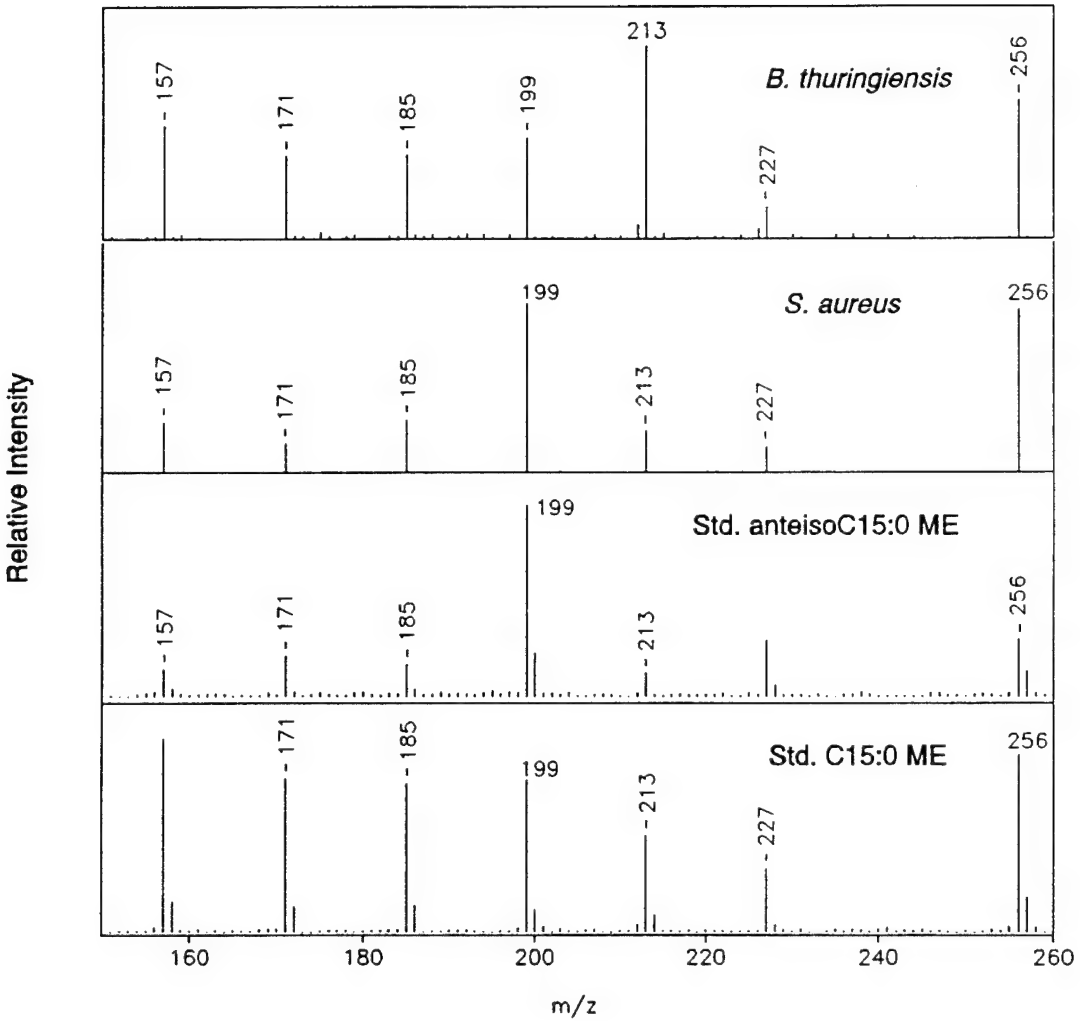

Figure 7. FAME Pyrolysis-product ion mass spectra of m/z 256.

b. multivariate analysis of FAMEs pyrolysis-mass spectra

Differentiation of Gram-positive and Gram-negative microorganisms can be accomplished by visual inspection of their mass spectra in Figures 5 and 6. The prominent C16:0 ME peak at m/z 270 relative to C15:0 ME at m/z 256 is a clear indication of a Gram-negative type bacteria. Conversely, the Py-mass spectrum of Gram-positive microorganisms are characterized by a larger branched-C15:0 ME (iso and/or anteiso) peak relative to C16:0 ME. Visual analysis of large data sets (comprising several replicates) can be tedious, and computer-based data analysis simplifies this task (41,42,26). Principal components analysis was performed with all the peaks of the mass spectrum. Figure 8 shows the score plot of principal components 1 and 3. Each similar letter or index corresponds to a replicate Py-MS analysis of that microorganism's FAME extract (see Table VI). A total of three groups or clusters are observed in the data plot.

Two main clusters are differentiated along the Component 1 axis and have been related to bacterial gram-type. Microorganisms with positive values for Component 1 axis are Gram-positive (clusters II and III), and microorganisms with negative values are mostly Gram-negative (cluster I). Note that only three Gram-positive microorganisms gave a false gram-type in this study (C, K, and G), that is, they were differentiated as Gram-negative bacteria. The mass spectra of these microorganisms showed a higher abundance of C16:0 ME over branched/normal-C15:0 ME and characteristic unsaturated FAME molecular ions and fragment ions (i.e., C18:1 ME).

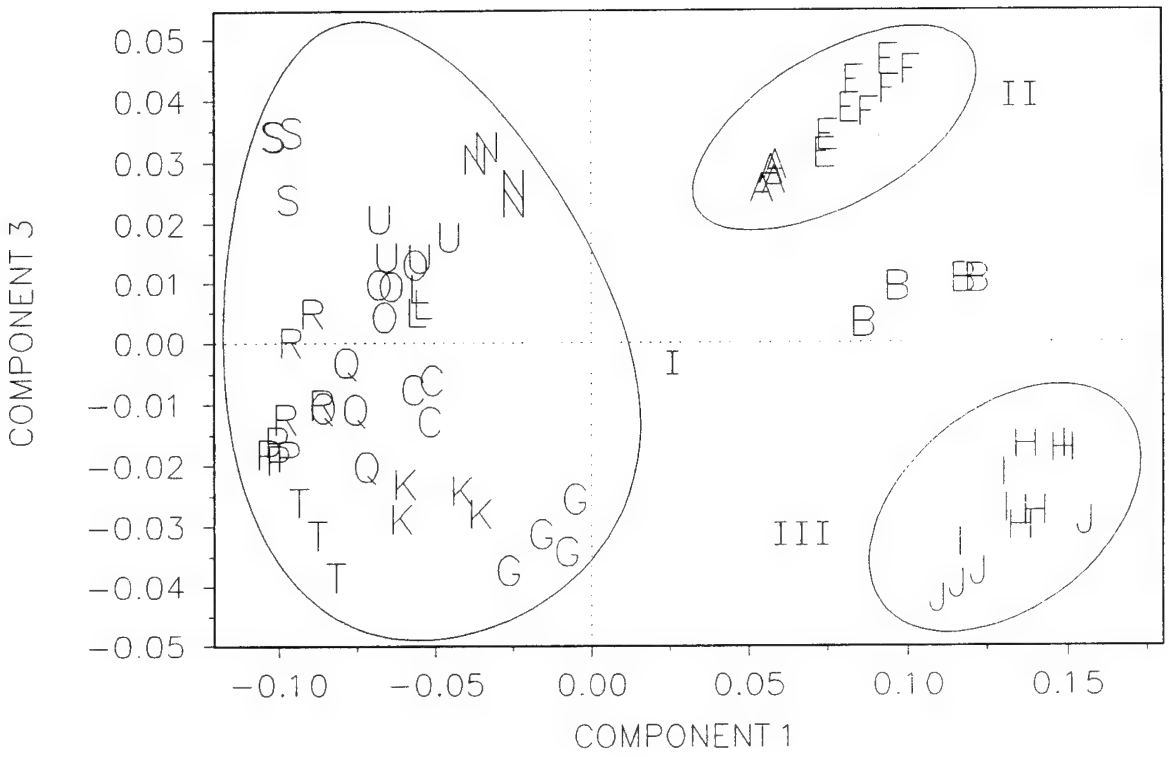

Figure 8. Score plot of Py-mass spectra of FAME extracts with principal components 1 and 3.

Table VI. Microorganisms used in this study

Index	Gram-type	Microorganism
A	+	*Bacillus cereus*
B	+	*Bacillus circulans*
C	+	*Bacillus licheniformis*
E	+	*Bacillus subtilis*
F	+	*Bacillus thuringiensis*
G	+	*Enterococcus (Streptococcus) faecalis*
H	+	*Listeria monocytogenes*
I	+	*Staphylococcus aureus subsp. aureus*
J	+	*Staphylococcus epidermidis*
K	+	*Streptococcus pyogene*
L	-	*Enterobacter aerogenes*
N	-	*Proteus mirabilis*
O	-	*Providencia stuartii*
P	-	*Pseudomonas aeruginosa*
Q	-	*Pseudomonas cepacia*
R	-	*Pseudomonas fluorescens*
S	-	*Pseudomonas putrefaciens*
T	-	*Pseudomonas stutzeri*
U	-	*Serratia marcescens*

Figure 9a shows the loading 1 plot or the mass spectral peaks responsible for differentiation along the Component 1 axis in Figure 8. Peaks in the positive direction are characteristic of Gram-positive microorganisms, and the negative peaks are characteristic of Gram-negative microorganisms. The peaks at m/z 256 and m/z 270 are again responsible for differentiating the two groups along Component 1 axis. The peaks in the positive direction in Figure 9a correspond to molecular ions and fragment ions of odd-numbered straight chain and branched fatty acids (iso and anteiso). Peaks from anteisoC15:0 ME are at m/z 256 ($M^{+\cdot}$) and its major fragment M-57 at m/z 199; and for isoC15:0 ME, the M-43 peak is at m/z 213. The ion at m/z 284 corresponds to a mixture of C17:0 ME and isoC17:0 ME as established by Py-MS/MS measurements. The signal at m/z 241 is also the M-43 fragment ion of isoC17:0 ME.

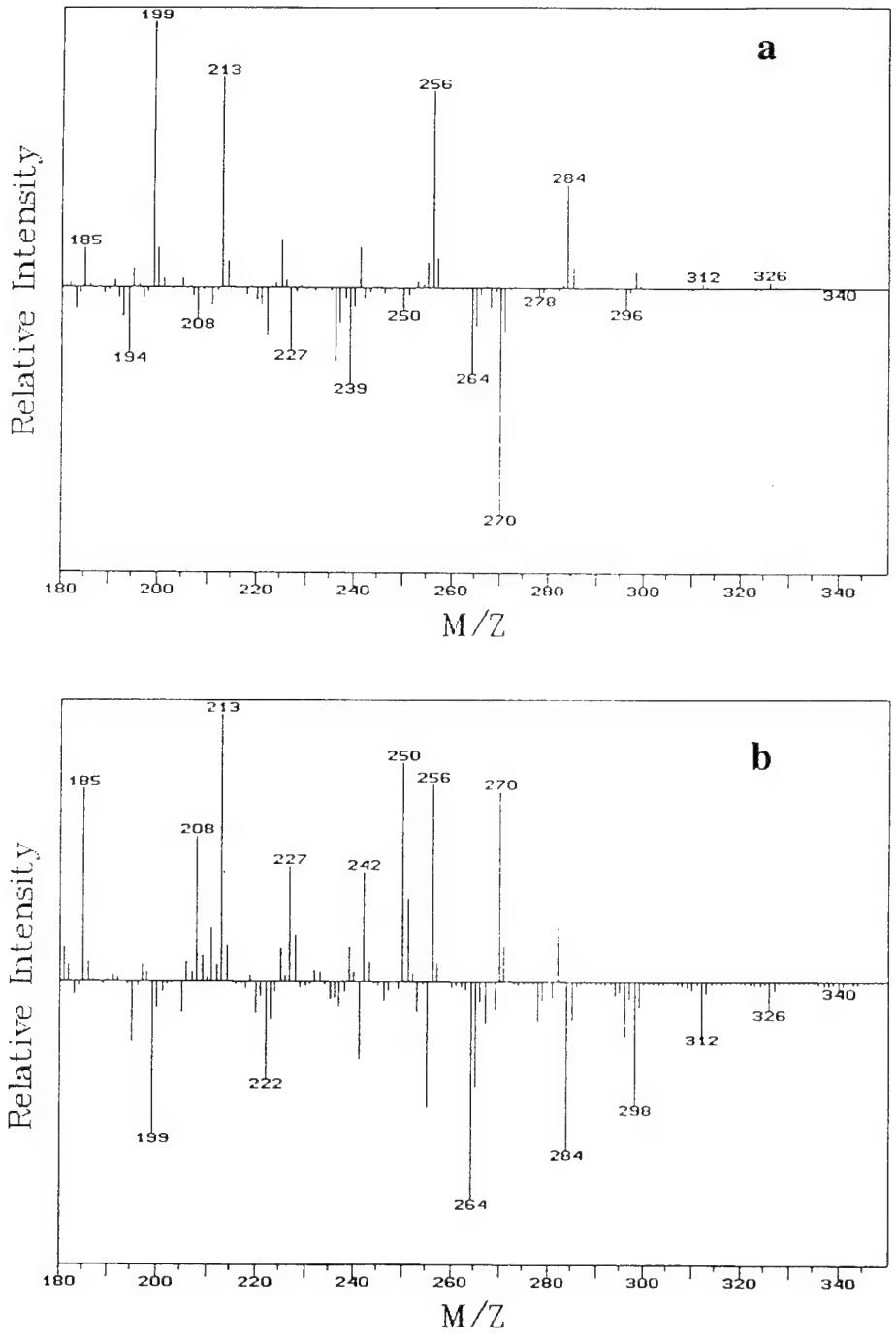

Figure 9. Loadings 1 (top) and loadings 3 (bottom) for score plot in Figure 8.

Also, higher molecular weight FAMEs C19:0 ME ($M^{+\cdot}$ m/z 312) and C20:0 ME ($M^{+\cdot}$ m/z 326) were observed in all Gram-positive microorganism Py-mass spectra. Peaks in the negative direction of the loading 1 spectrum correlate with molecular ions and fragment ions of even-numbered straight chain, 3-hydroxy, and unsaturated FAMEs. All Gram-negative bacteria Py-mass spectra contained a large C16:0 ME ($M^{+\cdot}$ m/z 270) signal. The ions at m/z 296 and 268 are C18:1 ME and C16:1 ME respectively with their fragments at M-74 and M-32. Also, the fragment ion at m/z 208, characteristic of 3-hydroxymyristic acid, indicates that this compound might be present.

Figure 9b shows the loading 3 plot or mass spectral peaks responsible for differentiation along the component 3 axis in Figure 8. These include high mass FAMEs (C18:0 ME and above), unsaturated, hydroxy, and iso and anteiso-branched FAMEs. In the positive direction, peaks corresponding to C16:0 ME, C17:1 ME, isoC15:0 ME, C14:0 ME are observed. All these ions are summarized in Table VII.

A better differentiation at the species level (i.e., a larger separation between replicates of *P. putrefaciens* (S) and *P. mirabilis* (N)) is observed for Gram-negative microorganisms over Gram-positive probably due to the presence of both unsaturated and hydroxy fatty acids (cluster I in Figure 8). Most of the microorganisms in the genus *Pseudomonas* (P, Q, R, S, T in Figure 8) are differentiated at the species level along Component 3. The genus *Proteus* (N) is distinguished from other genera; however, the genera *Serratia* (U), *Providencia* (O), and *Enterobacter* (L) can not be differentiated. Further PCA of Py-mass spectra from only Gram-negative

Table VII. FAME ions useful for Py-MS bacterial identification

FAME	m/z	FAME	m/z
C14:0 ME	242	C16:1 ME	268
M-31	211	M-32	236
3OH C14:0 ME, M-50	208	M-74	194
aC15:0 ME	256	C17:0 ME	284
M-31	225		
M-57	199	iC17:0 ME	284
		M-43	241
iC15:0 ME	256		
M-31	225	aC17:0 ME	284
M-43	213	M-57	199
C16:0 ME	270	C17:1 ME[2]	282
M-31	239	M-32	250
M-29[1] 241		M-74 208	
-14	227		
-14	213	C18:1 ME	296
-14	199	M-32	264
-14	185	M-74	236

[1] Fragments represent the carbomethoxy series.
[2] Also cyclopropyl-C17:0 ME.

microorganisms in Table VI differentiated all microorganisms at the species level with the exceptions of *P. aeruginosa* (P) and *P. fluorescens* (R). Based on results from GC/FAME analysis, improved differentiation of Gram-negative microorganisms at the species level could be achieved in this data set if the molecular ions of 2- and 3-hydroxy fatty acids, as well as, iso-branched 3-hydroxy fatty acids were detected (31).

On the positive side of the Component 1 axis of Figure 8, two clusters (II and III) containing only Gram-positive microorganisms are observed. Bacteria classified in cluster II (A, E, and F) are characterized by the presence of isoC15:0 ME (base peak m/z 213, M-43) and C14:0 ME (m/z 242) in their Py-mass spectra. The Py-mass spectra of microorganisms in this

cluster also show the presence of small amounts of C17:1 ME (or cyC17:0 ME, m/z 282), and corresponding fragments at m/z 250 (M-32) and m/z 208 (M-74). It is important to note that the microorganism *B. cereus* (A) in cluster II is genetically and pathogenically very similar to *B. anthracis*. Cluster III (H, I, J) is differentiated from cluster II in that the m/z 256 ion is anteisoC15:0 ME, yielding a base peak at m/z 199 (M-57). Moreover, segregation of microorganisms in Table VI into three clusters can be accomplished mainly by daughter ion spectra of their m/z 256 ion (see Figure 7).

Reproducibility of the FAME bacterial extract, Py-mass spectra was examined by comparing replicate Py-MS analyses for two different bacteria. The similarity between normalized Py-mass spectrum replicates, defined as the inverse of the Euclidian distance (40), was determined for *B. cereus* (A) and *S. pyogene* (K). For two identical mass spectra the similarity equals unity. Moreover, the average similarity for an ideal group of identical mass spectra is also unity. Hence, the difference in average similarity between an ideal group an the group of replicates for *B. cereus* (A) was calculated to be 0.007 (0.7 %). For *S. pyogene* (K) this value was 0.06 (6 %). These values correlate well with the spread of the letter indices (A and K) on the score plot in Figure 8. Reproducibility of FAME profiles obtained by MS varies, in part, due to the relative amounts of each FAME present in the mixture. The average similarity differences observed in this study ranged from 0.007 (0.7 %) to an upper limit of about 0.1 (10 %).

Exceptions to gram-type separation in Figure 8, *B. licheniformis* (C), *E. faecalis* (G), and *S. pyogene* (K), were further analyzed in order to classify correctly their gram-type. It is well known that a lipid moiety called Lipid A is exclusively present in Gram-negative bacterial

lipopolysaccharide (43). Lipid A is a complex molecule composed of glucosamine, phosphate and fatty acids of which there is a large proportion of 3-hydroxymyristic acid (3OH C14:0) (44). The Py-mass spectrum of *E. coli* Lipid A in the mass range of 50 to 400 amu shows a strong ion signal at m/z 89. This ion corresponds to a stable fragment of 3-hydroxy fatty acids (45) as confirmed by Py-MS/MS studies and comparison to a mass spectrum of a 3OH C14:0 standard. In 3-hydroxy FAMEs, this ion shifts 14 amu and it appears at m/z 103. Since only Gram-negative bacteria are known to have a Lipid A moiety and most Gram-positive bacteria lack hydroxy fatty acids (36,46), the presence of this stable fragment ion is indicative of a Gram-negative microorganism. For example, Figure 10 shows the low mass scan Py-mass spectra of *S. pyogene* (K) and a known Gram-negative microorganism *P. mirabilis* (N). The lack of this ion suggests that *S. pyogene* is not a Gram-negative bacteria (Figure 10a), and the presence of the m/z 103 ion assigns correctly *P. mirabilis* as Gram-negative (Figure 10b). The microorganism *B. licheniformis* could not be identified as a Gram-positive bacteria by this approach (its Py-mass spectrum showed the m/z 103 fragment ion) and remains the only exception encountered in this study.

A PCA of the same data set was performed with only peaks corresponding to FAME molecular and fragment ions identified in this study (Table VII). Figure 11

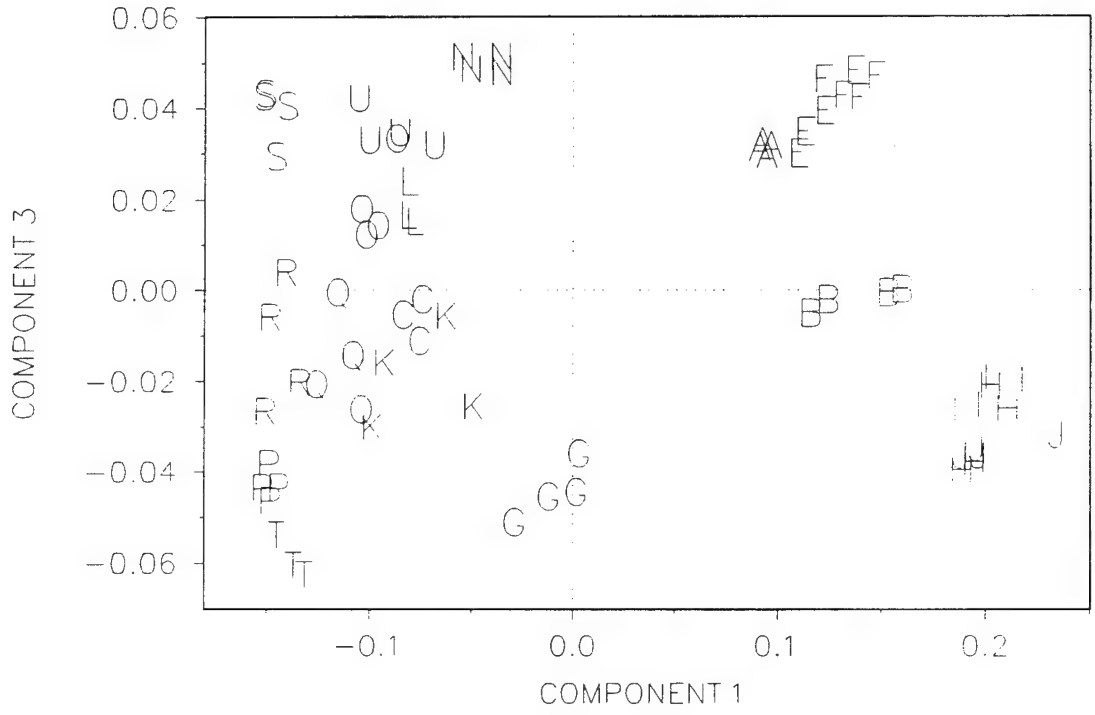

Figure 11. Score plot with principal components 1 and 3 obtained using only masses listed in Table VII.

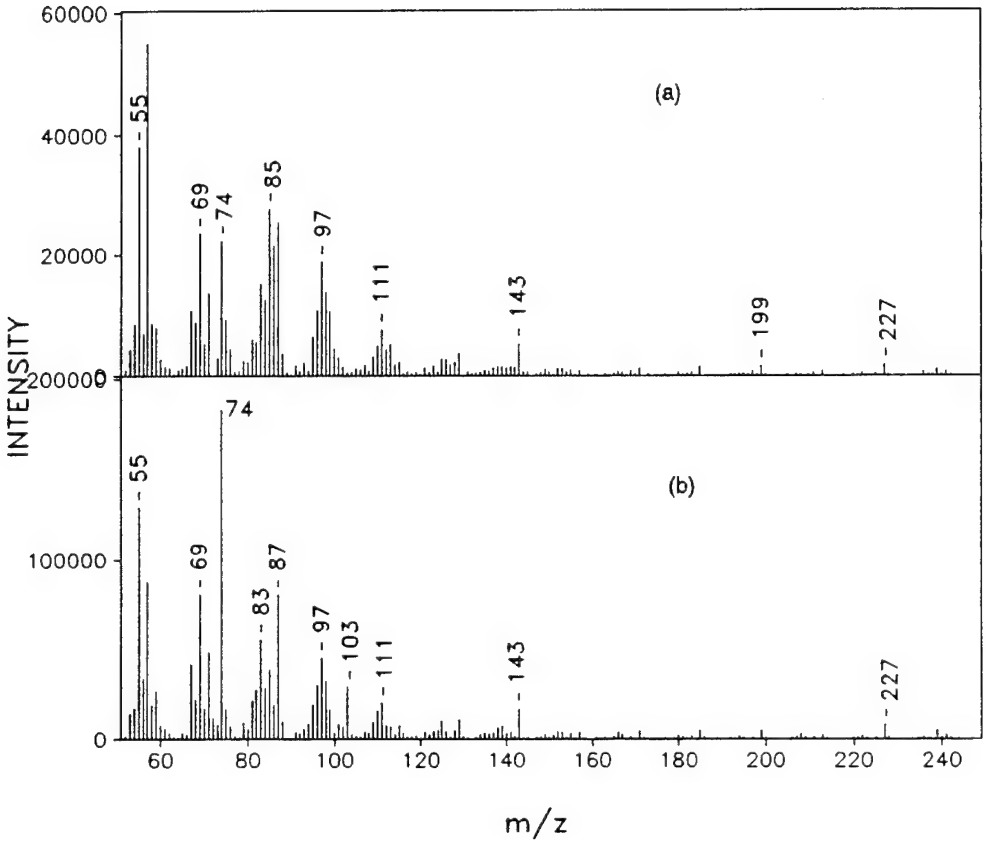

Figure 10. Low-mass, Py-mass spectra of FAMEs fron a Gram-positive bacteria, (a) *S. pyogene*, and a Gram-negative bacteria (b) *P. mirabilis*.

shows the normalized and mean centered score plot using principal components 1 and 3. This plot is similar to that obtained with PCA using all peaks in each mass spectrum (compare with Figure 8). The same number of clusters were obtained using only the 21 mass spectral peaks listed in Table VII. In addition, the degree of differentiation or distance between each cluster is larger based on the magnitude of the Component 1 axis . This is due to elimination of redundant information (signals common to all samples) and chemical noise (2). This approach can be useful in the data analysis of Py-mass spectra obtained in the presence of an environmental background.

c. Conclusions on mass spectrometry fatty acid analysis

The results presented in this study correlate differences in the fatty acid distribution, observed with Py-MS, in microorganisms with their Gram-type. Gram-negative microorganisms are characterized mainly by a high abundance of C16:0 in their Py-mass spectrum. On the other hand, Gram-positive microorganisms contained a high abundance of branched-C15:0 (iso or anteiso) in their Py-mass spectra. Three PCA clusters were identified in this study. Cluster I contained all Gram-negative microorganisms and some Gram-positive. These spectra were characterized by straight chain and unsaturated fatty acids and were rich in C16:0. Cluster II contains Gram-positive microorganisms only. The spectra in this group were characterized by straight chain, small amounts of unsaturated and cyclopropyl fatty acids and were rich in isoC15:0. Pathogenic *Bacilli* were grouped within this cluster. Cluster III was composed of Gram-positive microorganisms only. Their Py-mass spectra had high levels of anteisoC15:0. Furthermore, microorganisms investigated in this study can be assigned correctly to each cluster by obtaining only their Py-daughter ion spectra of m/z 256.

Differentiation and identification of Gram-positive microorganisms should take advantage of the higher abundance of branched and unsaturated fatty acids present in these microorganisms. Similarly, Gram-negative microorganisms can be differentiated mainly by their relative amounts of unsaturated fatty acids.

Future work will be aimed at the development of a whole bacteria, *in situ* lipid methylation, Py-MS protocol without the need of time consuming FAME extraction procedures and chromatographic separations (22). Preliminary work in our laboratory has shown that pyrolysis of whole cells and *in situ* methylation of their lipids can be accomplished with a total turn-around time of 10 minutes/sample (sample preparation and mass spectral analysis) (47,48). This will yield a bacterial lipid-based technique for the rapid and accurate differentiation and identification of microorganisms with simple Py-MS instrumentation.

d. Validation of Py-MS bacterial lipid analysis with the MIDI system

The overall goal of this phase of the project was to validate the use of whole bacterial cells with *in situ* lipid methylation and Py-MS analysis as the potential chemotaxonomic technique for the CBMS instrument. A secondary goal was to understand the effect of growth conditions on the bacterial lipid profile. The overall task has been done step wise by comparison to a well established technique like the MIDI system. Experimental conditions in the Py-MS assay were such as to analyze the same range of FAME detected (C12:0 to C20:0) in the MIDI system. Two sets of bacteria were analyzed and compared. The first set of bacteria, listed in Table VI, consisted of representative bacteria of Gram positive and Gram negative type. Microorganisms in Table VI were grown under MIDI system-standard pathogen growth conditions. Table VIII lists the second set of bacteria that included 6 pathogens (comprising 4

genera) all grown at different growth conditions: *Bacillus anthracis, Francisella tularensis, Yersinia pestis, Brucella abortus, Brucella suis, and Brucella neotomae.* Data analysis of both Py-MS data sets included principal components analysis and then a comparison to the MIDI system assay and algorithm. The MIDI system algorithm is a proprietary package based on a feature array and it calculates a similarity index based on the unknown's distance in n-dimensional space from the mean profiles of the closest library entries (49).

Pyrolysis-MS/FAME/RESOLVE and GC/FAME/MIDI analyses of FAME extracts from bacteria listed in Table VI resulted in similar segregation of the bacteria studied into three discrete clusters in the PCA plot (Figure 12). Moreover, the same fatty acids were responsible for this segregation in both assays as confirmed by the loading plots. Also, Py-MS/FAME/RESOLVE yielded the same results as GC/FAME/RESOLVE, (Figure 13) confirming the retention of the taxonomic information by both the data generation (Py-MS) and the data analysis (RESOLVE) in the former assay. However, GC/FAME in general gave larger Euclidian distances between clusters than the Py-MS approach when both data sets were analyzed with the same pattern recognition software (RESOLVE). This translates to better differentiation between clusters based on phenotypic trends like Gram-type.

Table VIII. Different Growth Condition for Pathogenic Bacteria.

Index	Bacteria	Media	Growth Stage
A	Bacillus anthracis	TSA-1	
A	Bacillus anthracis	CAD	top of bottom
A	Bacillus anthracis	CAD	mid-log
A	Bacillus anthracis	TSA-2	
A	Bacillus anthracis	CAD	COB-VEG?
A	Bacillus anthracis	mid-log	
B	Brucella abortus, S-19	Bruc. agar	
B	Brucella abortus	Bruc. broth	stationary
B	Brucella abortus, S-19	Bruc. broth	mid-log
B	Brucella abortus, 2308	Bruc. broth	stationary
B	Brucella abortus, 2308	Bruc. broth	mid-log
B	Brucella melitensis	Bruc. broth	
B	Brucella melitensis		stationary
B	Brucella melitensis	Bruc. broth	mid-log
B	Brucella neotomae	Bruc. agar	37 °C
B	Brucella neotomae	Bruc. broth	stationary
B	Brucella neotomae		mid-log
B	Brucella neotomae	TSA	
B	Brucella suis	Bruc. broth	stationary
B	Brucella suis		mid-log
B	Brucella suis	Bruc. agar	
F	Francisella tularensis	MH broth	stationary
F	Francisella tularensis	MH agar	mid-log
F	Francisella tularensis	MH broth	mid-log
F	Francisella tularensis	MH agar	
F	Francisella tularensis	chocolate	
Y	Yersinia pestis-EV76	TSA	
Y	Yersinia pestis-EV76	Bruc. agar	
Y	Yersinia pestis	TSB	stationary
Y	Yersinia pestis	TSB-1	mid-log
Y	Yersinia pestis	TSB-2	mid-log

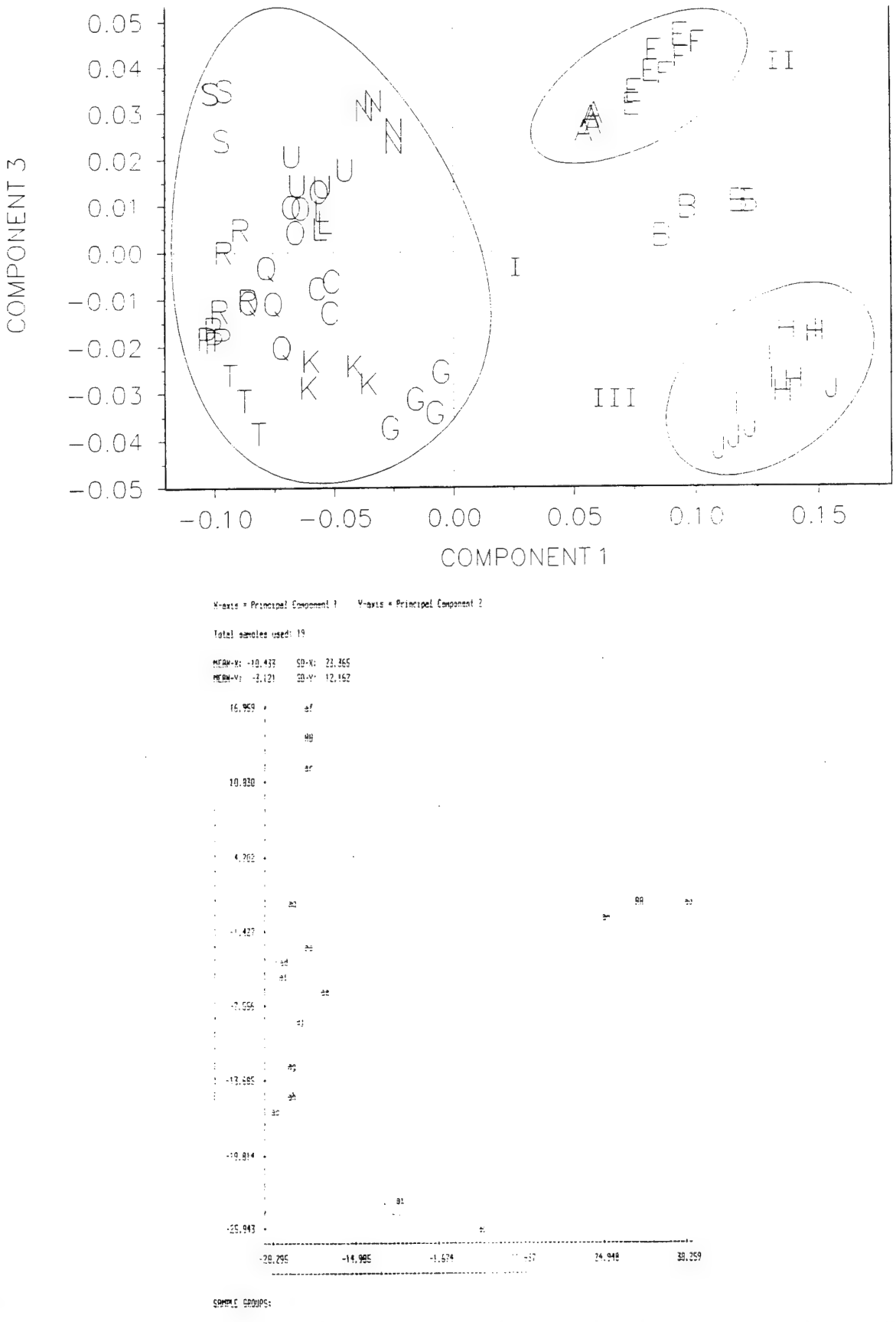

Figure 12. PCAs of Py-MS (top) and MIDI (bottom) analyses of FAME extracts from bacteria listed in Table VI.

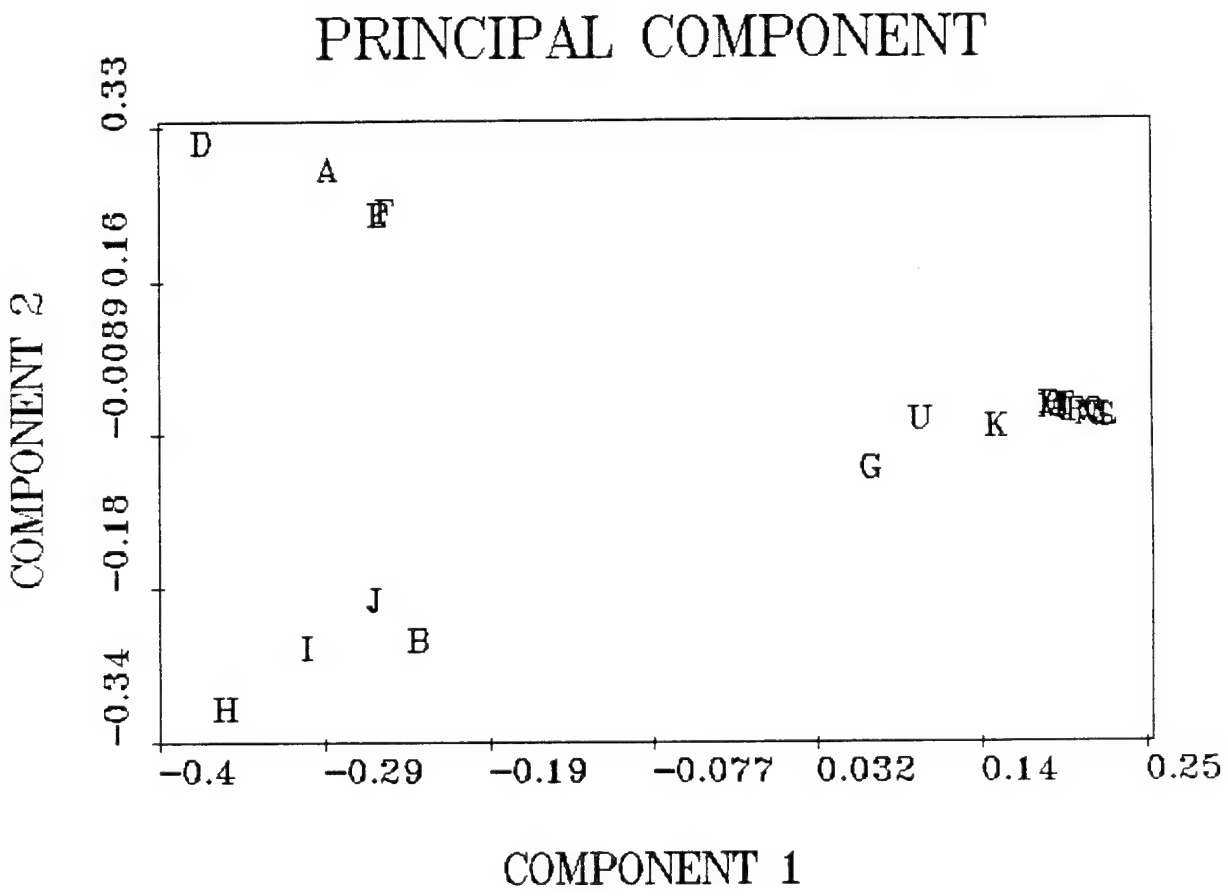

Figure 13. PCA of GC/FAME/RESOLVE analysis of bacteria listed in Table VI.

In the second set of bacteria studied (Table VIII), pathogens were grown at different growth conditions and harvested at different growth stages. The analysis of this set also had the purpose of determining the effect of growth conditions on the bacterial lipid profile. Representative Py-mass spectra of FAME extracts from these bacteria are shown in Figure 14. Again, Py-MS and MIDI GC analyses of the FAME extracts yielded equivalent PCA patterns (Figure 15). It is well know that bacterial lipid profiles depend on growth factors like the type of media, age of culture, and incubation temperature. The wide spread of each cluster in the PCA plot is a direct consequence of the effect of a wide range of growth conditions on the lipid distribution in bacteria and does not reflect the reproducibility of the assay (calculated to be between 1-10%) (50). With equivalent experimental conditions, both approaches failed in differentiating *F. tularensis* and *Brucella spp.* *Bacillus anthracis* and *Yersinia pestis* were separated from all other bacteria.

The presence of unique cellular monounsaturated fatty acids in *F. tularensis* is well known in the microbiology literature. Included in order of abundance (percentage of total fatty acid composition) are C24:1ω15c (9.9 %), C18:1ω9c (8.1 %), and C22:1ω13c (3.2%) These fatty acids, with the exception of C18:1, were not detected since the Py-MS experimental parameters were set to match those of the MIDI system. The MIDI system only detects fatty acids below 20 carbon atoms. A representative FAME sample of *F. tularensis* was analyzed with a mass range of 200 to 450 amu and is shown in Figure 16. Table IX shows the high mass FAMEs and their fragment ions.

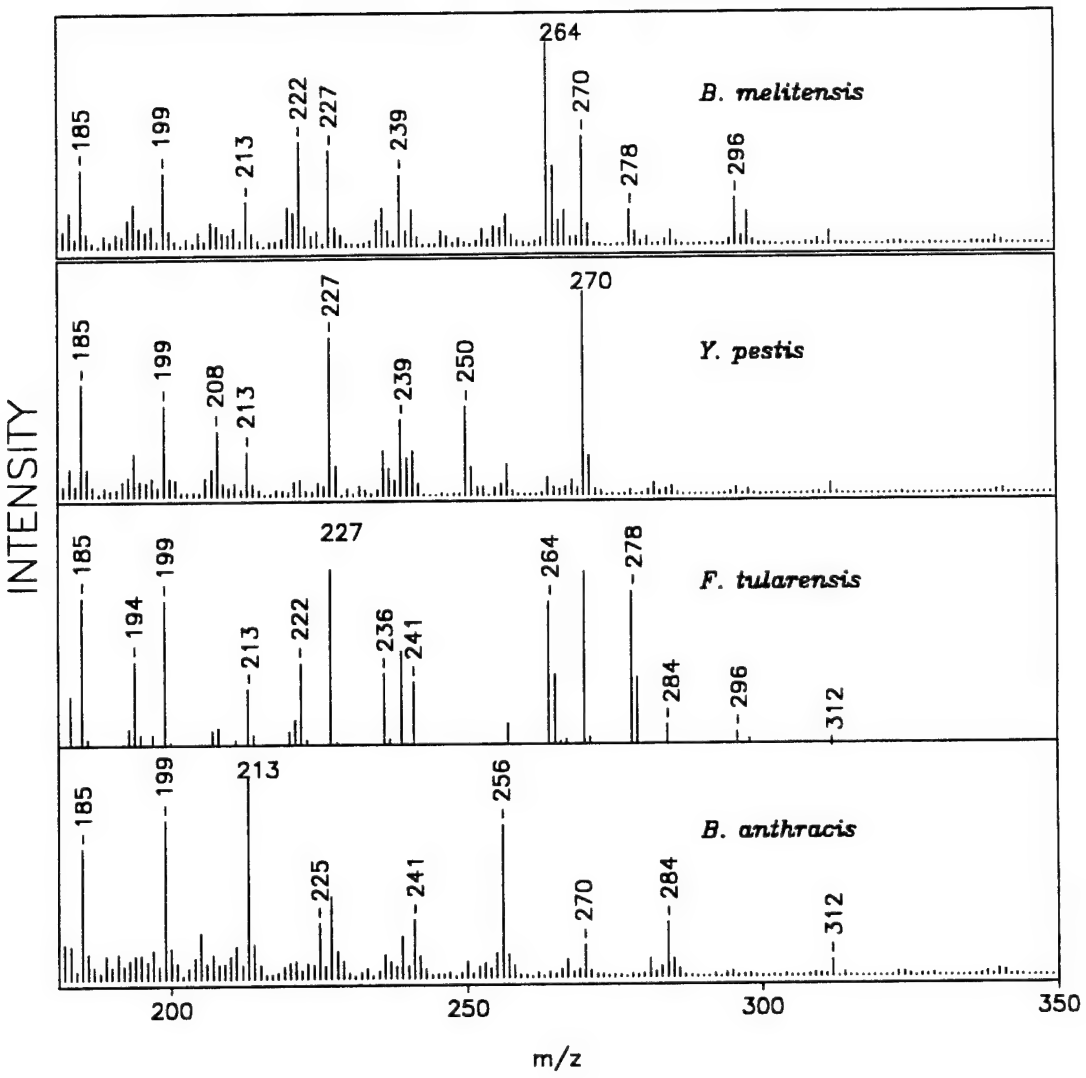

Figure 14. Py-mass spectra of FAME extract from pathogenic bacteria.

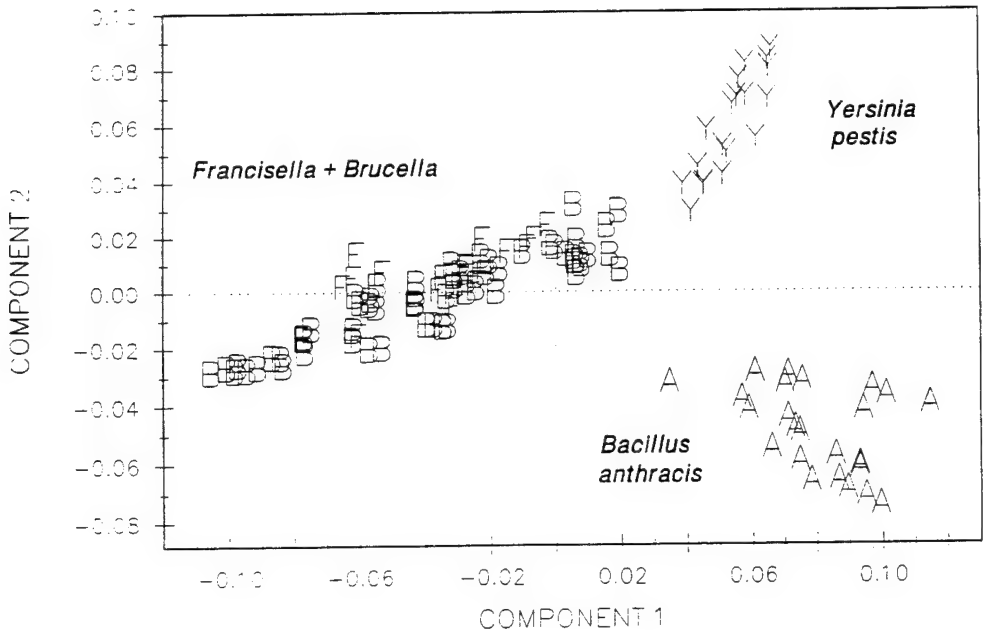

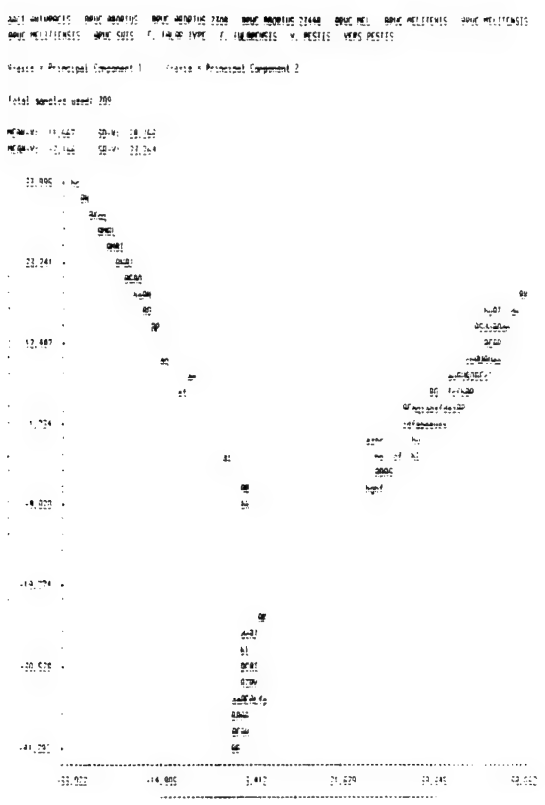

Figure 15. PCAs of Py-MS (top) and MIDI (bottom) analyses of FAME extracts of pathogenic bacteria. Mass range of 180-350 amu.

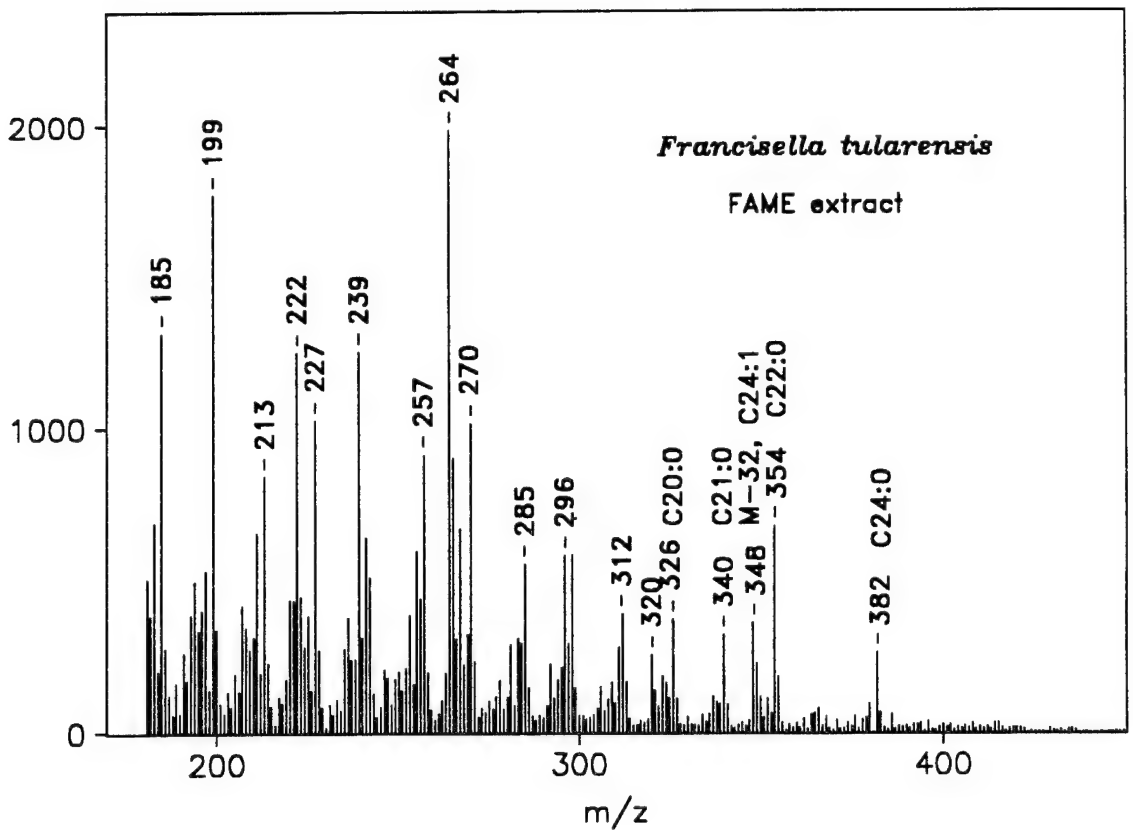

Figure 16. Py-mass spectrum of FAME extract from *Francisella tularensis*.

Table IX. FAME Ions above C20:0 ME in *F. tulerensis*.

FAME	m/z
C24:0 ME	382
C24:1 ME	380 (trace)
M-32	348
C22:0 ME	354
C22:1 ME	352 (trace)
M-32	320*
C21:0 ME	340
C20:0 ME	326

*No evidence of C20:3 ME (M+.; m/z 320; and fragments at m/z 289, 277, 263, 249, 235, 222) was observed, even though the MIDI system identified about 25 % of the total FA composition as this FA in a sample of *F. tularensis*.

Increasing the mass range in a linear instrument reduces the duty cycle of the measurement, hence a compromise must be established in selecting the upper mass range for this analysis. The electron ionization Py-mass spectrum of monounsaturated FAMEs was characterized by a prominent M-32 and M-74 fragment ions. These two EI fragment ions were detected even before the molecular ion was detected with a reasonable signal-to-noise level (for C18:1 ME, the intensity of the fragment ion at M-32, m/z 264, was about 4 times larger than the intensity of the molecular ion, m/z 296). This fragmentation pattern was also observed in cyclopropyl-FAMEs. Therefore, it was decided that increasing the mass range by ten amu, or 180 to 360 amu, would not only detect these monounsaturated FAMEs, but would also avoid increasing the chemical noise and decreasing the duty cycle of the measurement.

The Py-MS/FAME analysis of pathogenic bacteria in Table X was repeated with this new parameter. Complete differentiation of the four genera listed in Table VIII and X was achieved and is shown in Figure 17. *B. anthracis* was separated from the other bacteria on the basis of Gram-type differentiation, mainly the presence of branched-C15:0 (iso and anteiso) and C17:0 fatty acids. Distinct biomarkers present in the remaining pathogens include: C20:0, C22:0 and C24:1 in *Francisella tulerensis*, cyclopropyl-C17:0 in *Yersinia*, and cyclopropyl-C19:0 in *Brucella*. Differences in growth conditions in *B. anthracis* mainly changed the ratio of intensities of peaks at m/z 199 and m/z 213 (Figure 18). These peaks have been correlated to the presence of isoC15:0 ME (M-43 @ m/z 213) and anteisoC15:0 ME (M-57 @ m/z 199) (50). Based on this observation/knowledge, one may conclude that the relative amounts of these two FAMEs have changed with different growth conditions. However, MS/MS measurements (Figure 19) of the m/z 256 ion revealed that the iso-to-anteiso ratio remained relatively unchanged (branched fragmentation is enhanced in CID). This last observation agrees with results obtained with the MIDI system where the isoC15:0 ME FAME remained the most abundant isomer regardless of growth conditions. In the Gram-negative pathogens, different growth conditions (from standard MIDI system) induced the production of monounsaturated fatty acids like C18:1 and cyclopropylC19:0 (*Francisella* and *Brucella*). In samples of *Francisella tularensis*, the unsaturated fatty acid C24:1ω15c was present regardless of growth conditions. In samples of *Yersinia* and *Brucella*, the relative abundances of cyC17:0 and cyC19:0 changed with different growth conditions. Lipid profiles of *Yersinia pestis* were affected the least by changing growth conditions.

Table X. Second Study of Pathogenic Bacteria.

Index	Bacteria	
A	Bacillus anthracis-Ames	
A	Bacillus anthracis-Ames	
A	Bacillus anthracis-Ames	
A	Bacillus anthracis-Ames	
A	Bacillus anthracis-Sternes	
A	Bacillus anthracis-Sternes	
A	Bacillus anthracis-Sternes	
A	Bacillus anthracis-Sternes	
A	Bacillus anthracis-Vollum	
A	Bacillus anthracis-Vollum	
A	Bacillus anthracis-Vollum	
A	Bacillus anthracis-Zimbabwe	
A	Bacillus anthracis-Zimbabwe	
A	Bacillus anthracis-Zimbabwe	
A	Bacillus anthracis-Zimbabwe	
B	Brucella melitensis (VAC)	Bruc. broth
B	Brucella melitensis (VAC/REV1)	Bruc. broth
B	Brucella melitensis	Bruc. agar
B	Brucella melitensis	Bruc. broht
B	Brucella melitensis-16w	Bruc. broth
B	Brucella melitensis-Suis (wild)	Bruc. agar
B	Brucella melitensis-Suis (wild)	Bruc. broth
B	Brucella melitensis-Suis (wild)	Bruc. broth
B	Brucella melitensis-abortus (VAC S19)	
B	Brucella melitensis-abortus (wild)	
B	Brucella melitensis-abortus (wild)	
B	Brucella melitensis-abortus (VAC S19)	Bruc. broth
B	Brucella melitensis-abortus (VAC S19)	Bruc. agar
B	Brucella melitensis-melitensis (VAC/REV1)	
F	Francisella tularensis (Live Vaccine Strain)	
F	Francisella tularensis-LVS	
F	Francisella tularensis-LVS	
F	Francisella tularensis-Palaeartica Type B	
F	Francisella tularensis-Palaeartica Type B	
F	Francisella tularensis-Utah Type A, 2173	
F	Francisella tularensis-Utah Type A, 2173	
F	Francisella tularensis-Utah Type A, 2173	
F	Francisella tularensis-Utah Type A, 2173	
Y	Yersinia pestis-A1122	
Y	Yersinia pestis-California-A1122	
Y	Yersinia pestis-EV76	
Y	Yersinia pestis-EV76	
Y	Yersinia pestis-EV76	
Y	Yersinia pestis-India 195/p	Bruc. agar
Y	Yersinia pestis-India 195/p	TSB
Y	Yersinia pestis-India 195/p	TSB
Y	Yersinia pestis-La Paz	Bruc. agar
Y	Yersinia pestis-La Paz	TSB
Y	Yersinia pestis-La Paz	TSB
Y	Yersinia pestis-Nair Kenya	Bruc. agar
Y	Yersinia pestis-Nair Kenya	TSB

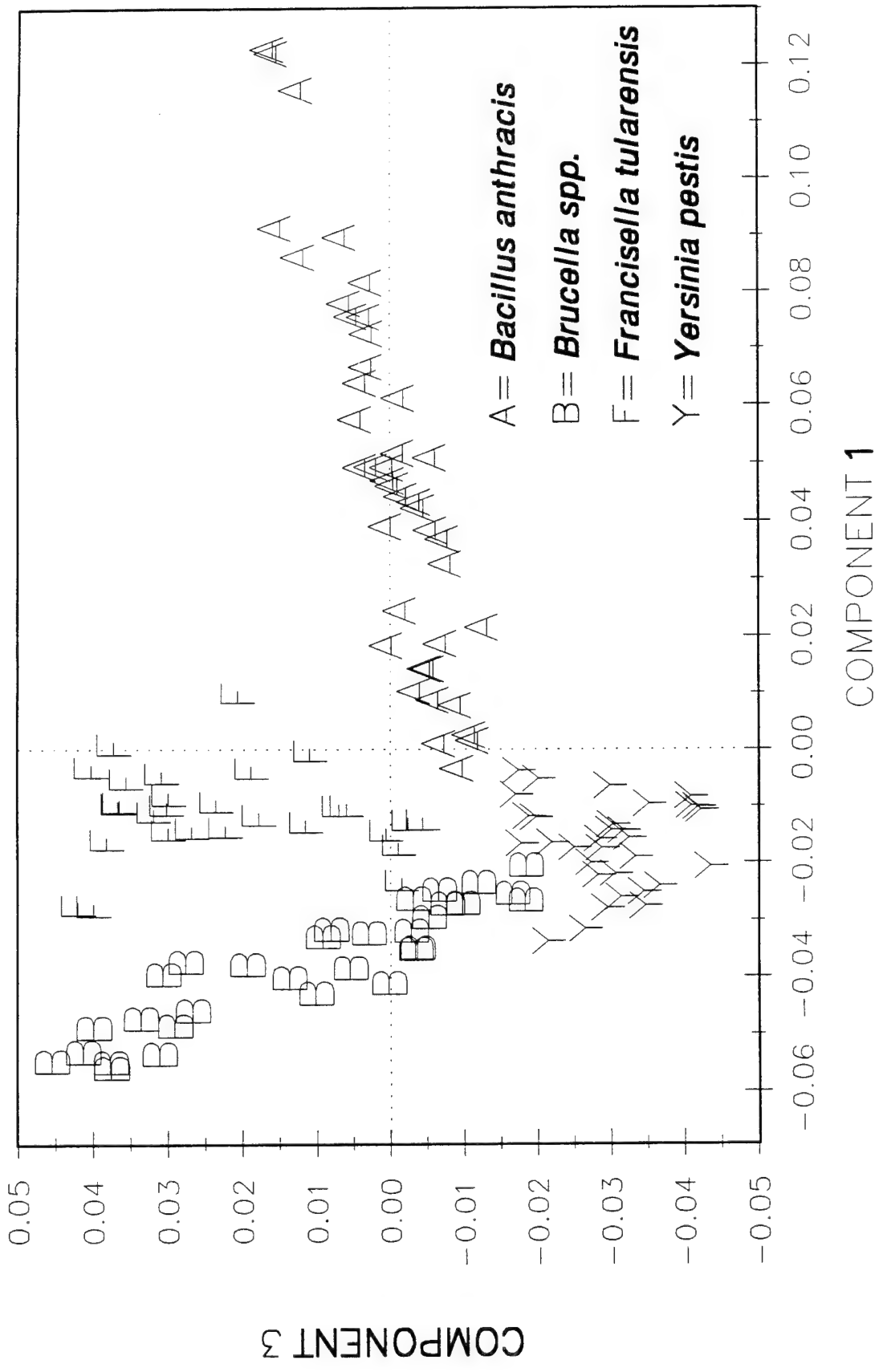

Figure 17. PCA of Py-MS/FAME analysis of bacteria listed in Table X. Mass range of 180-360 amu.

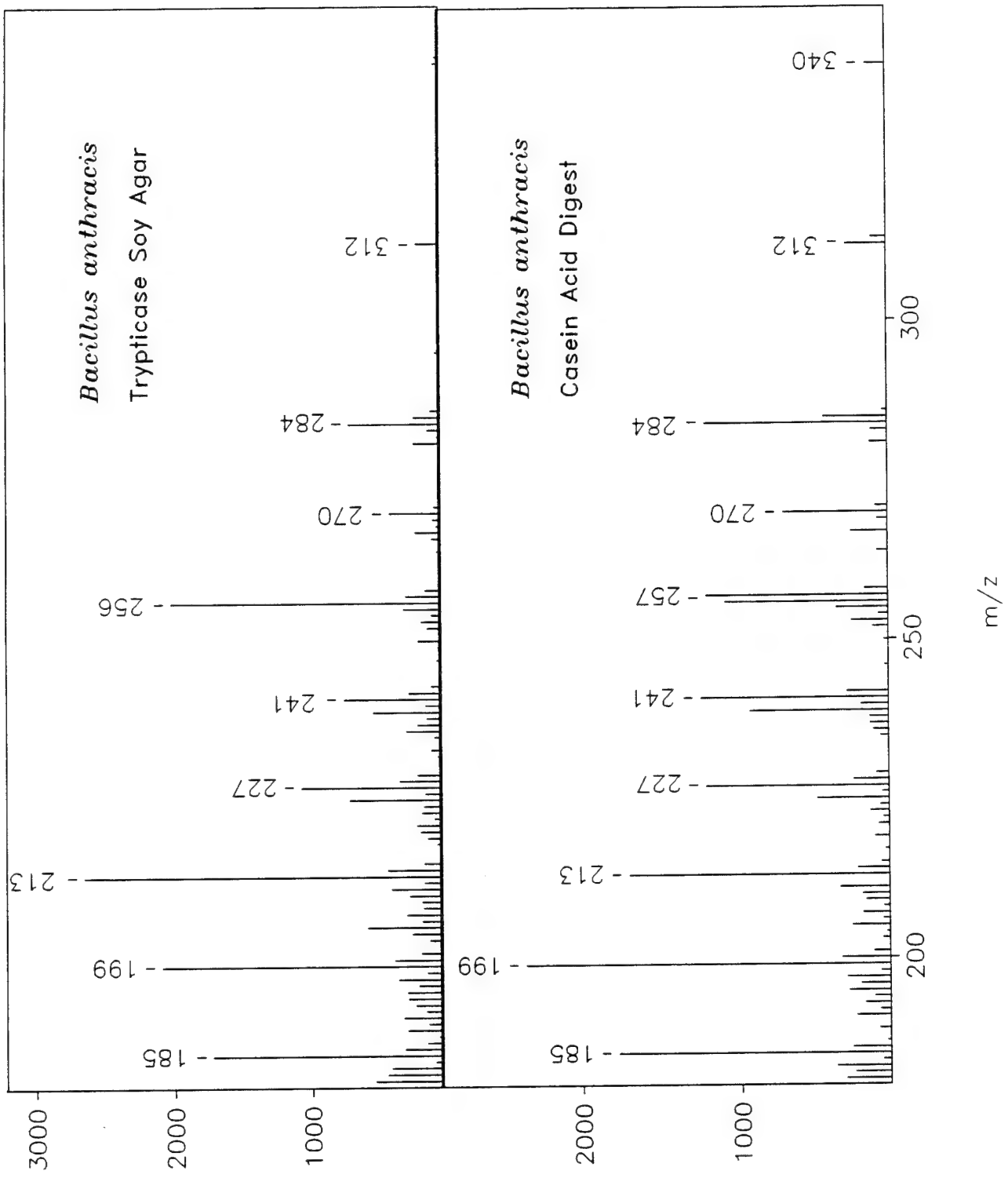

Figure 18. Py-mass spectra of FAME extracts from *B. anthracis* grown in two different media.

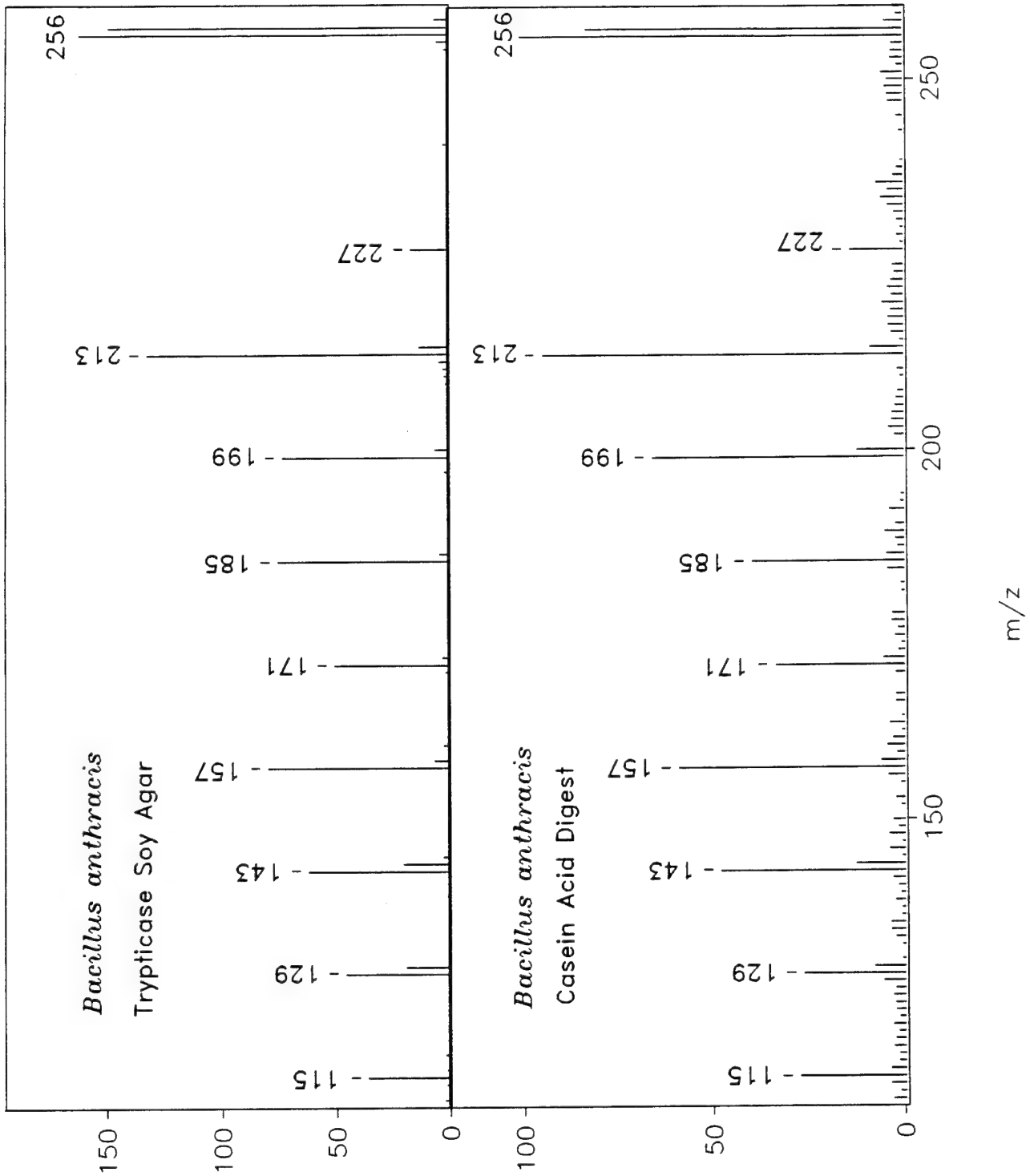

Figure 19. Py-daughter ion spectrum of the ion at m/z 256 of FAME extracts from *B. anthracis* grown in two different media (same samples as in Figure 18).

Based on these results, a decision tree can be constructed for the detection and differentiation of these four pathogens based on fatty acid biomarkers (Figure 20). This decision tree is not robust, since some included biomarkers are not specific to a particular pathogen. For example, the presence of isoC15:0 is not specific to *B. anthracis*, but it is also present in other Bacilli (50). Also, *B. anthracis* grown under different conditions may produce more anteisoC15:0 than the isoC15:0. However, these fatty acids (branched-C15:0) remain excellent biomarkers for Gram-positive typing in this group of pathogens. Other non-specific biomarkers are seen in samples of *Yersinia* and *Brucella* as both show the FAMEs cyC17:0 and cyC19:0, but in different abundances. So far, the only specific and unique biomarker in this group of pathogens remains C24:1 in *Francisella tularensis*.

e. *In situ* Pyrolytic Methylation/Mass Spectrometry of Whole Bacteria

The data presented above resulted from samples requiring an hour of preparation time. Controlled cell hydrolysis, methylation time and temperature as well as pH are crucial for reproducible bacterial fatty acid extraction and methylation. Moreover, this procedure is not amenable to automation or field operation. Clearly, for the Army's application, a methylation procedure that can be incorporated into a current detection technology and can be easily automated is required. The advantages of pyrolysis as a sample pretreatment and sample volatilization step prior to mass spectrometry or GC have been exploited successfully in a variety of problems (51). One of the sample pretreatment often used in analytical pyrolysis is the methylation of carboxylic functional groups prior to GC or MS analysis (36).

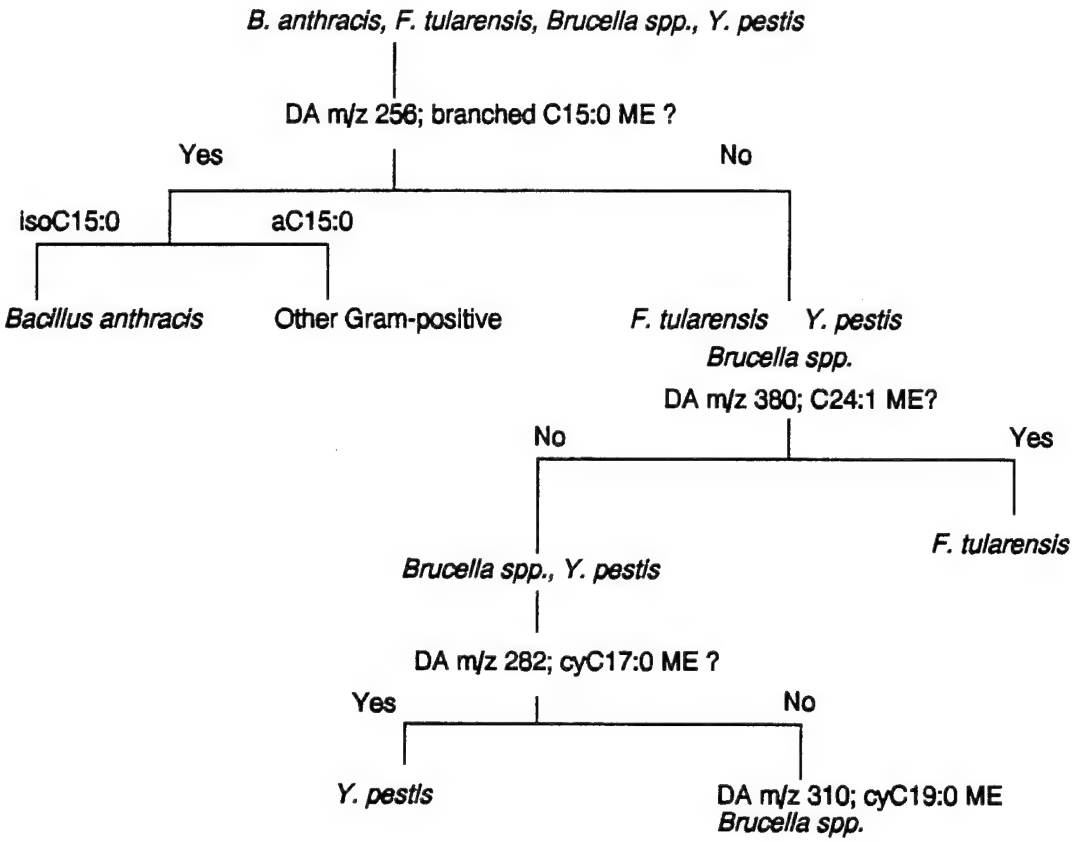

Figure 20. Decision tree for pathogen detection based on Py-MS/MS of FAME biomarkers.

In this procedure, the sample is mixed with a methylating reagent on the pyrolysis element (wire, foil, coil, etc.) and then pyrolyzed. At high temperatures, the methylating reagent (tetramethyl ammonium hydroxide) reacts with all ester-linked and free carboxylic functional groups producing methyl esters.

The *in situ* pyrolytic methylation of fatty acids has been applied in the analysis of lipids in whole bacteria by Py-GC (32,52). *In situ*-GC methylation has also been used to detect dipicolinic acid in spores of *Clostridium* species (53). Our laboratory has successfully applied this methodology to Curie-point Py-MS to obtain lipid profiles of whole bacteria. Moreover, these results correlated with previous results obtained in the Py-MS analysis of FAME bacterial extracts (See Figure 21).

f. *In Situ* Pyrolytic Lipid Methylation of Whole Bacteria using the CBMS

Our laboratory has been successful in implementing this methodology in the CBMS. As previously stated, the CBMS is equipped with an infrared pyrolyzer unit, a 3-meter heated transfer line, and a silicone membrane interface between the pyrolyzer an the ion trap. Four bacteria, *Bacillus anthracis, Francisella tularensis, Brucella melitensis,* and *Yersinia pestis*, were analyzed with the *in situ* methylation in the CBMS. Figure 22 shows mass spectra with lipid profiles for these four pathogens. Comparable taxonomic information is obtained in the CBMS as in the Curie-point, Py-MS/FAME extract procedure. Complete differentiation between the four genera of pathogens is achieved with *in situ* pyrolytic methylation-CBMS analysis of whole bacteria. This differentiation follows the decision tree previously shown (Figure 20).

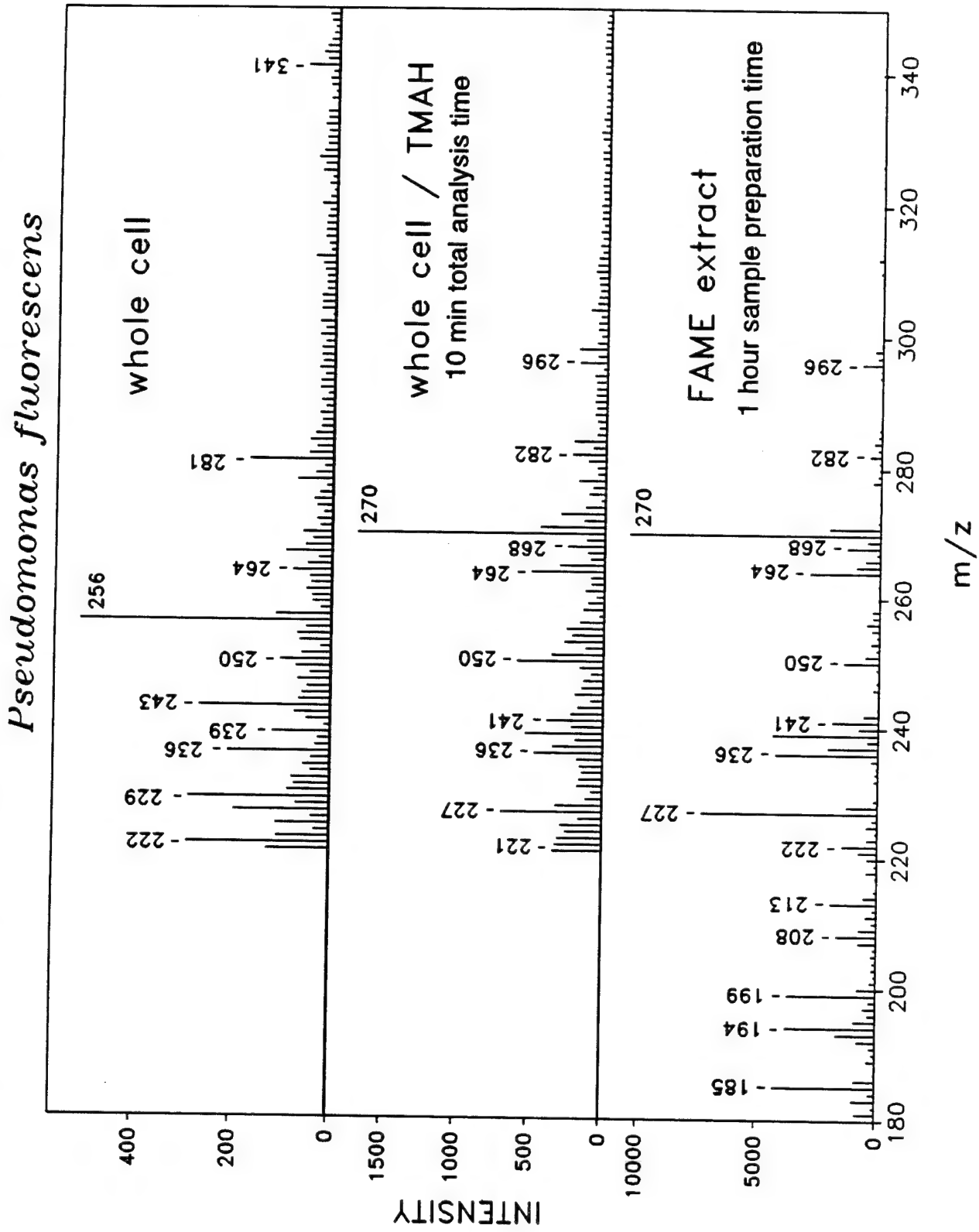

Figure 21. Curie point Py-MS of *Pseudomonas fluorescens* showing advantage of the *in situ* pyrolytic methylation methodology.

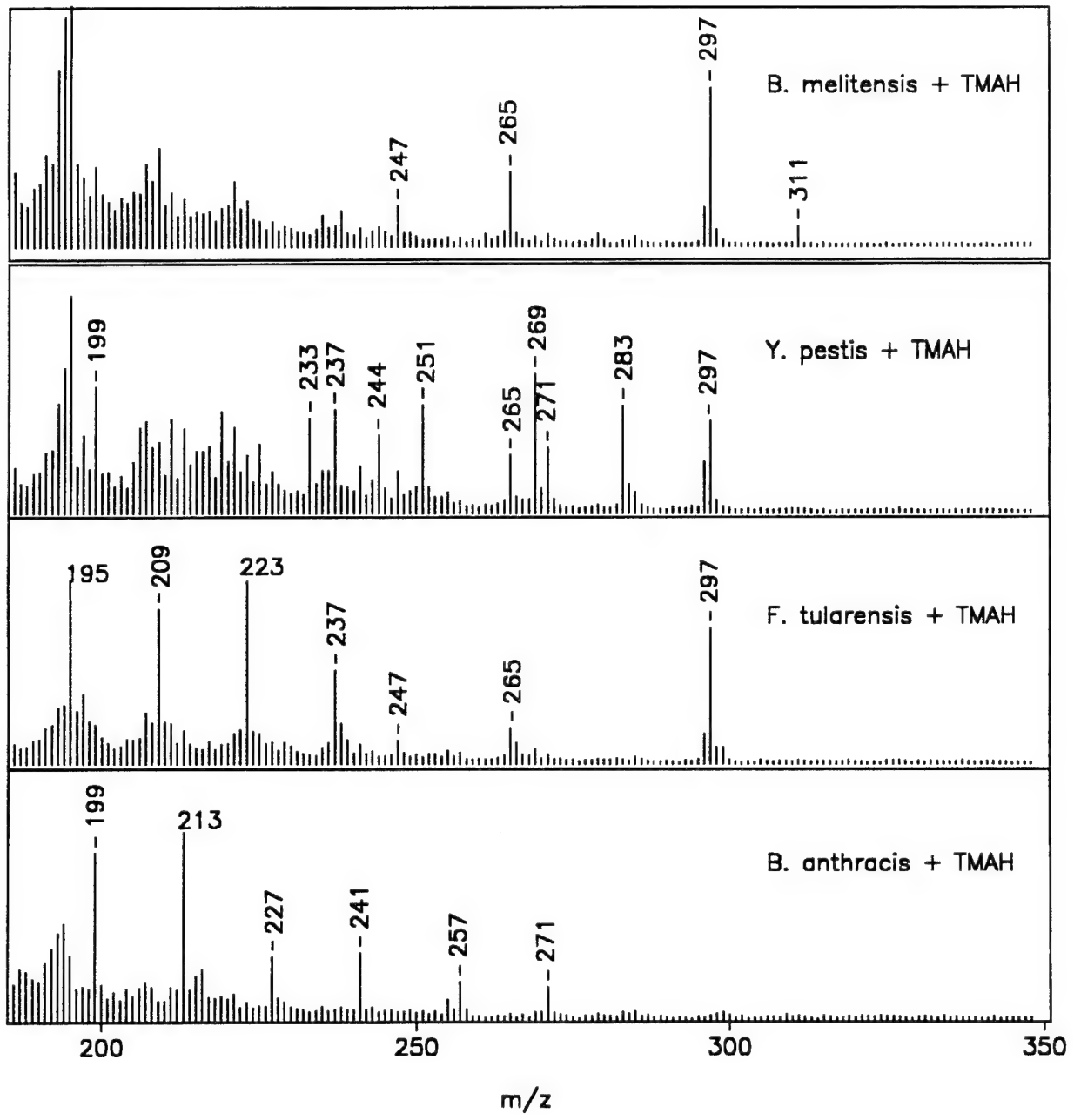

Figure 22. Mass spectra obtained by *in situ* IR-pyrolytic methylation of fatty acids from whole bacteria with the CBMS.

The extent of molecular ions (M+1) and fragmentation is dependant on the amount of FAME produced during the *in situ* methylation. This in turn is dependant on the number of cells pyrolyzed. In this case, it is estimated that about $5x10^7$ to $5x10^8$ cells produced the above lipid profiles.

In the future, pyrolysis conditions and sample introduction into the IR-pyrolyzer must be optimized. There is strong evidence that Py-temperature and transfer line temperature play an important role in the methylating efficiency and in the discrimination of the blank signal from the FAME signal (FAMEs are retained in the CBMS transfer line). Also, ionization mechanisms and fragmentation pathways of FAMEs in the ion trap must be characterized before reliable FAME profiles can be obtained. In the CBMS, FAMEs are initially ionized via EI+. However, because of the high analyte partial pressures during ionization inside the trap, self-chemical ionization takes place (50,54). This process yields almost 100% of the $[M+1]^+$ ion (see Figure 23). The ratio of abundances of the ions at M+1 and M, or (M+1)/M, depends on the amount of sample introduced and the total ion storage time in the ion trap (ionization time + scan delay + scan time). Figure 24 shows this effect for a standard C16:0 ME injected through a GC interface in the CBMS (271/270 trace). The FAME fragmentation in the CBMS is a result of a "mixed process", where both EI+ (m/z 74, McLafferty rearrangement ion) and collision induced dissociation (CID) fragment ions (characteristic base peak at m/z 101) are observed. It is likely that CID fragmentation takes place because air (mostly nitrogen) is the buffer gas. The unique configuration of CM7 (turbomolecular pump and extra gas inlets in the manifold) will allow confirmation of this hypothesis by measurement of FAME mass spectra

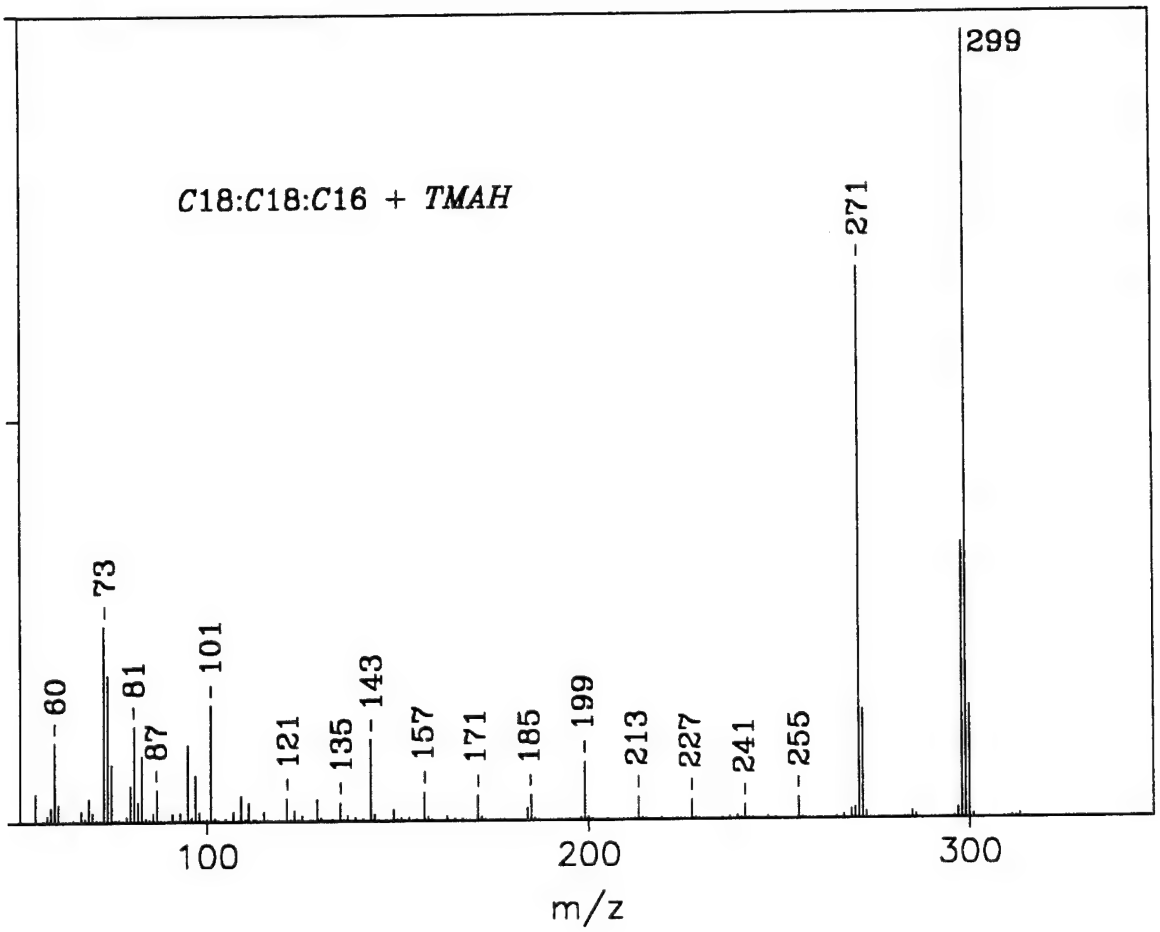

Figure 23. Electron ionization-mass spectrum obtained by *in situ* pyrolytic methylation of the triglyceride C18:C18:C16 in the CBMS showing different ionization and fragmentation pathways.

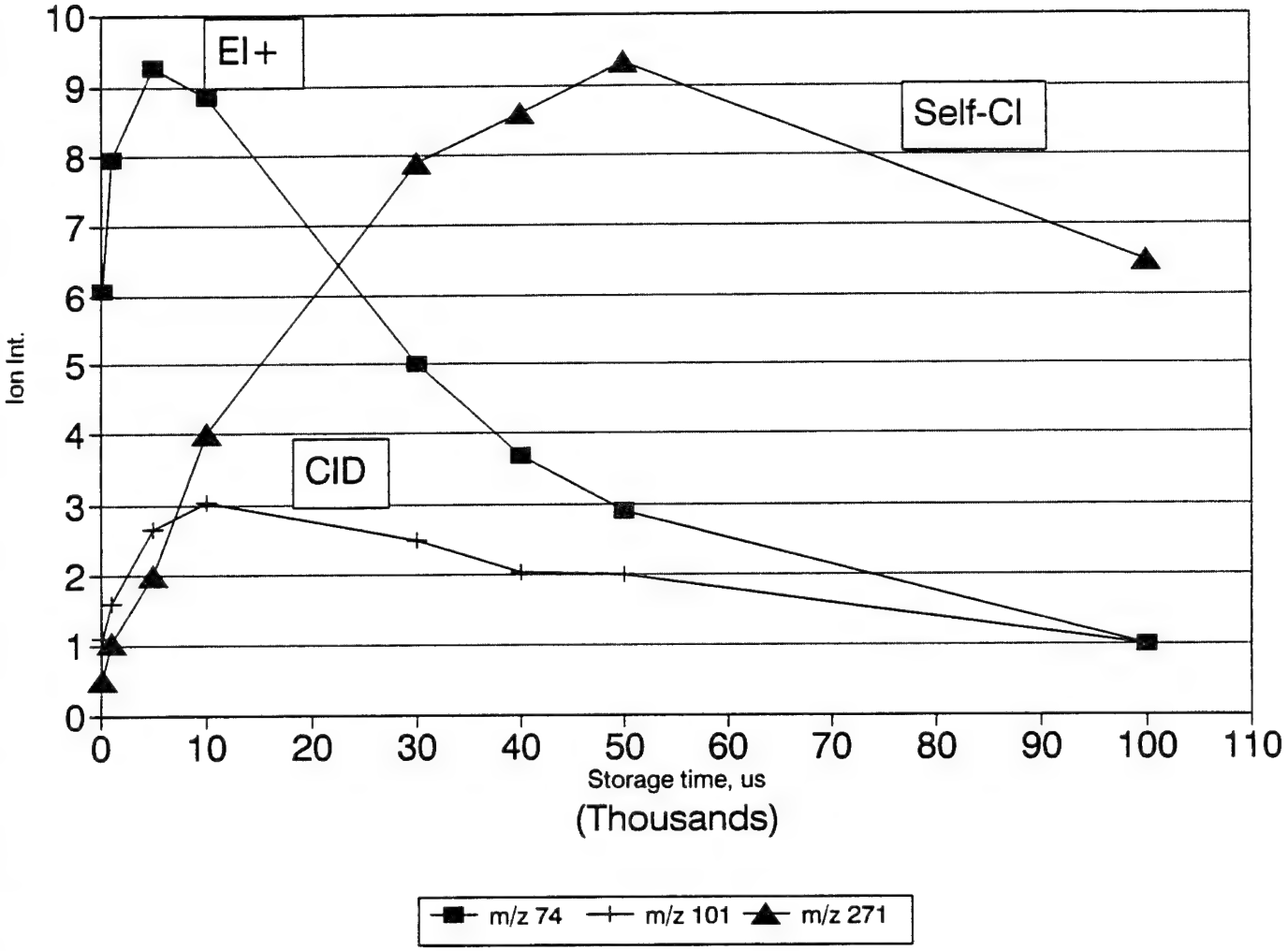

Figure 24. Dependance of C16:0 ME ion intensities on total ion storage time in the ion trap (CBMS-12).

with He as the buffer gas. The contribution from each fragmentation pathway mainly depends on the total ion storage time in the trap (49,55). The differential sensitivity or detection limits between polar (unsaturated FAMEs) and non-polar (saturated FAMEs) compounds in the CBMS remains an issue to be solved.

Reduction in the number of whole cells detected with the CBMS will require two approaches. First, the optimization of the parameters that affect the efficiency of the *in situ* pyrolytic methylation process. These include pyrolysis temperature, heating temperature profile, transfer line temperature, and reagent concentrations (cell density and methylating agent). Second, the optimization of the FAME detection limits with the quadrupole ion trap. There is a fundamental limit in the number of ions that can be stored in the ion trap before space-charge effects take place. Since we are only interested in detecting FAME ions between 180 and 360 amu, utilizing a scan function that traps ions between 50 and 360 amu will decrease the signal-to-blank ratio (S/B) of the measurement. Changing the scan range of the measurement, in this case "scan_begin" to 180 amu in the CBMS, will decrease the ionization efficiency (56) of the ions of interest by approximately a factor of 40 (see Figure 25). Hence, the implementation of non-linear resonance waveforms to eliminate low-mass ions (from 2 to 180 amu) while maintaining a low q_z value (low V_{RF}-high trapping efficiency) during ionization is a logical step. Moreover, with the ability to create notch-filters in the range of the secular frequency of the trapped ions, detection of multiple ions (as the ones listed in the decision tree

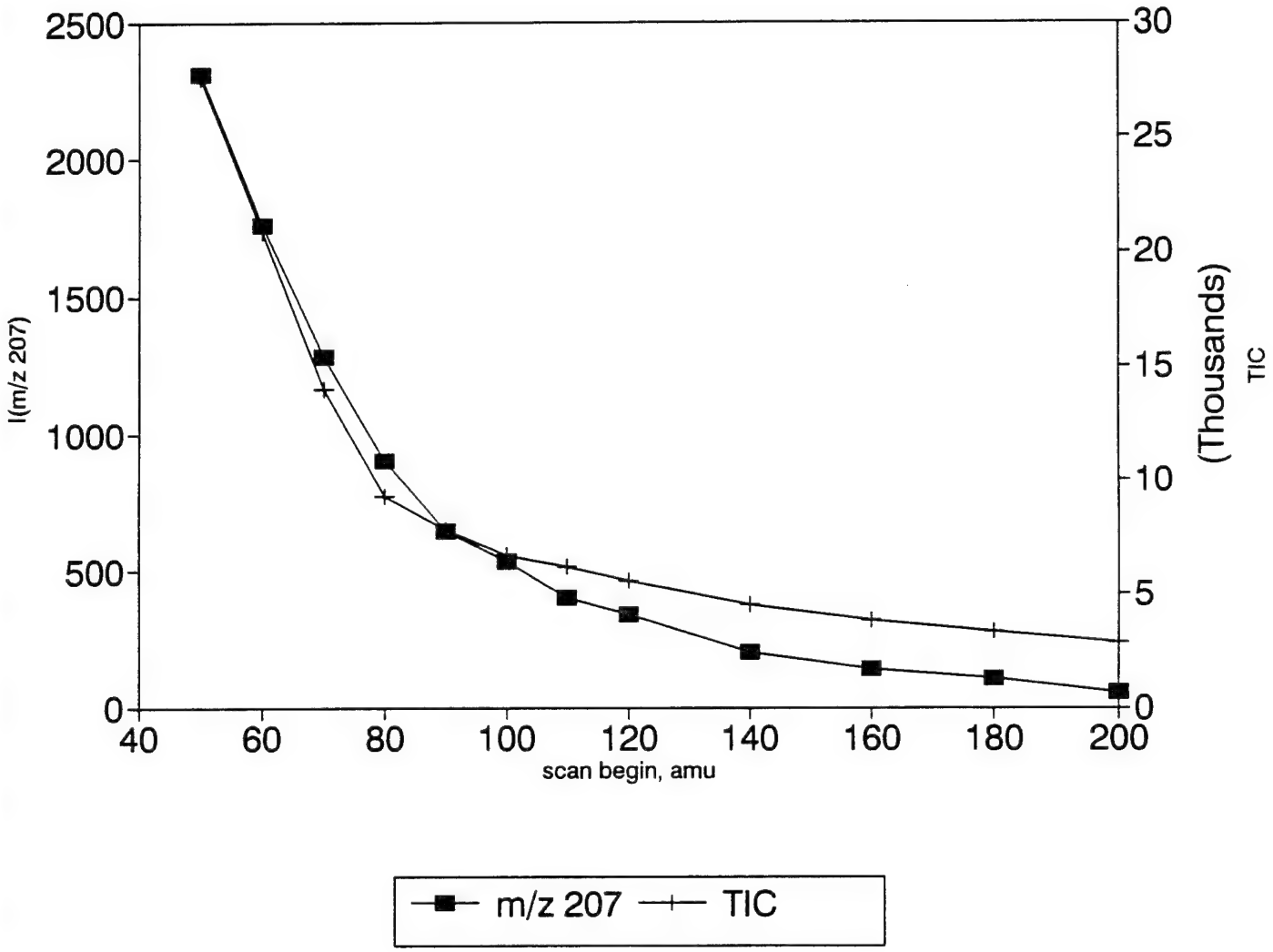

Figure 25. Dependance of ion m/z 207 intensity on "scan_begin" in the CBMS-12. Increasing "scan_begin" increases V_{RF} (q_z) during ionization. End mass 400 amu; ionization time 20 ms; scan delay 15 ms.

in Figure 20) in a single measurement can be possible. This technology is currently present in commercially available instruments like the Teledyne 3DQ instrument (known as the FNF or Multiple Ion Monitoring option) and in the Finnigan GCQ (known as the Ultra-SIM). This technology has proven to be a very efficient way to improve not only the S/B, but the overall sensitivity of the measurement.

II. Proteins

Studies on the formation of 2,5-diketopiperazines (DKP), **1**, from the pyrolysis of peptides have been primarily limited to dipeptides. Svec and Junk (57) found that sublimation

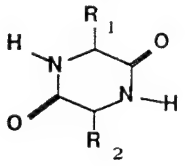

1

of alanyl-alanine and glycyl-glycine into a mass spectrometer between 120° and 160°C produced DKPs. They noted that the DKP ring fragmented prior to cleavage of the ring substituents. Noguerola *et al.*(58) recently reported on a detailed pyrolysis mechanistic study of 12 dipeptides using Curie-point pyrolysis-tandem mass spectrometry. Results from this investigation showed that dipeptides decomposed by two general fragmentation pathways, one involved the direct cleavage of the dipeptides while the other involved the DKP formation. In the case of the DKP formation, most of the ring substituents were cleaved from the ring to produce the ions m/z 113, 114, and 127 that were markers for the dipeptides. This study also provided evidence that the cyclization with loss of water to form the DKP occurred as a thermal event, while many of the other fragmentations occurred from the electron ionization processes.

Several researchers, primarily using pyrolysis-gas chromatography have also reported on the formation of the diketopiperazine (59-65). In contrast, other groups have not observed the DKPs in their work on the pyrolysis of various dipeptides (66-69).

Data on the formation of DKPs from the pyrolysis of larger peptides are limited. Lichtenstein (63) reported that DKPs were formed when peptides containing from 2 to 4 amino acids were heated in naphthol to an upper temperature of 150°C. For tripeptides, Lichtenstein observed the formation of the DKP and a C-terminal amino acid. Mauger pyrolyzed a series of actinomycins using a conventional pyrolysis-GC approach (64). He found at 400°C that each adjacent pair of amino acids contained in the actinomycin produced a diketopiperazine except for pairs that contained threonine.

Li and Lubman have also investigated pyrolysis of peptides using laser desorption mass spectrometry (69). In the resonance multiphoton ionization mass spectra, they observed DKPs in the laser-induced thermal decomposition process for oligopeptides and their derivatives whose N-terminal group was not blocked. The peptides TYR-GLY-GLY and TYR-GLY-GLY-PHE-MET produced intact molecular ions plus a number of thermal decomposition species. One interesting elimination that occurred during the cyclization was the loss of the glycine from the tripeptide and GLY-PHE-MET from the pentapeptide. These are similar reactions to those reported by Lichtenstein (63).

Two research groups have found in the pyrolysis of complex proteins cyclization reactions that lead to non-DKP products (70-72). Munson *et al.* postulated the formation of substituted diketoimidazolidines from hair pyrolysis (70,71) while Boon and DeLeeuw observed 3,5-dialkyl-3,4-dihydro-2H-pyrrole-2,4-dione and 3-alkenyl-5-alkyl-pyrrolidine-2,4-dione in the

pyrolysis of three biomaterials (72). Mauntado has also reported that synthetic polymers based on common amino acids decomposed by a series of β-cleavages (73). The following paper concentrates on the DKP formation produced during Curie-point pyrolysis of a series of oligopeptides and discusses this reaction as a mode of peptide depolymerization.

a. oligopeptides

1. Tripeptides

Phenylalanyl-Leucyl-Methionine

The mass spectrum of PHE-LEU-MET is shown in Figure 26. Much of this spectrum is an additive spectrum of the dipeptide PHE-LEU spectrum (Figure 27) and the amino acid methionine spectrum. Noguerola *et al.*(58) previously found that PHE-LEU thermally decomposes to produce a series of peaks at m/z 260, 204, 169, 141, 113, 103, 91, and 85. Peaks contained in a methionine spectrum (74), such as m/z 149, 131, 104, 61, and 56 are also prominent in the PHE-LEU-MET spectrum.

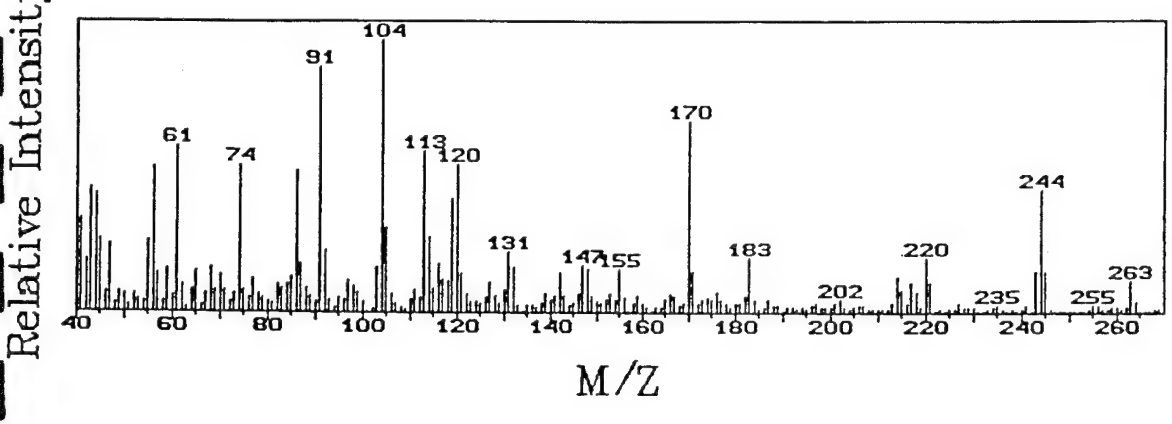

Figure 26. The Pyrolysis-Mass Spectrum of PHE-LEU-MET (Each Segment has been normalized separately).

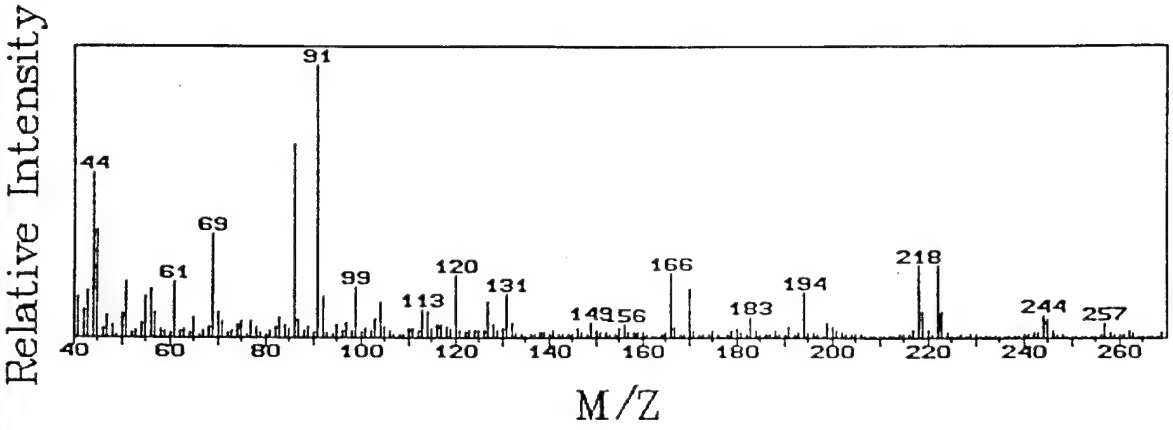

Figure 27. The Pyrolysis-Mass Spectrum of PHE-LEU.

The peak at m/z 260 was established as the PHE-LEU DKP by the daughter ion experiments. Examples of daughter ion spectra of some of the major peaks are shown in Figures 28-30. These studies showed that the peaks at m/z 204, 169, 141, 113, 103, 91, and 85 were all fragmentation ions of the DKP. The peaks at m/z 204 and 169 are due to the cleavage of benzyl or isobutene groups from the DKP while m/z 113 results from loss of both substituents. The other peaks at m/z 103, 91 and 85 were produced by fragmentation of the diketopiperazine skeleton, which is consistent with Noguerola's observation (58).

The common appearance of the same series of peaks corresponding to the DKP of PHE-LEU in both di- and tri-peptides suggests that the thermal and EI decomposition pathways are quite similar. The DKP formation occurs in dipeptides by the amino electron pair of the N-terminal amino attacking the carbonyl carbon of the C-terminal amino acid with subsequent loss of water. The DKP formation in tripeptides must occur by a similar mechanism to the original Swec mechanism (57) where the C-terminal amino acid losses an amino acid rather than water.

The full spectrum of PHE-LEU-MET also showed a weak molecular ion peak at m/z 409. The peaks at m/z 373, 335, and 318 were shown by daughter ion experiments of m/z 409 to be fragmentation of the side groups directly from the tripeptide backbone during electron ionization. In addition, the m/z 120 peak in the PHE-LEU-MET spectrum is postulated to occur from the N-terminal cleavage from the tripeptide molecular ion, Figure 31. Inspection of daughter and parent ion spectra provides strong evidence for this hypothesis,

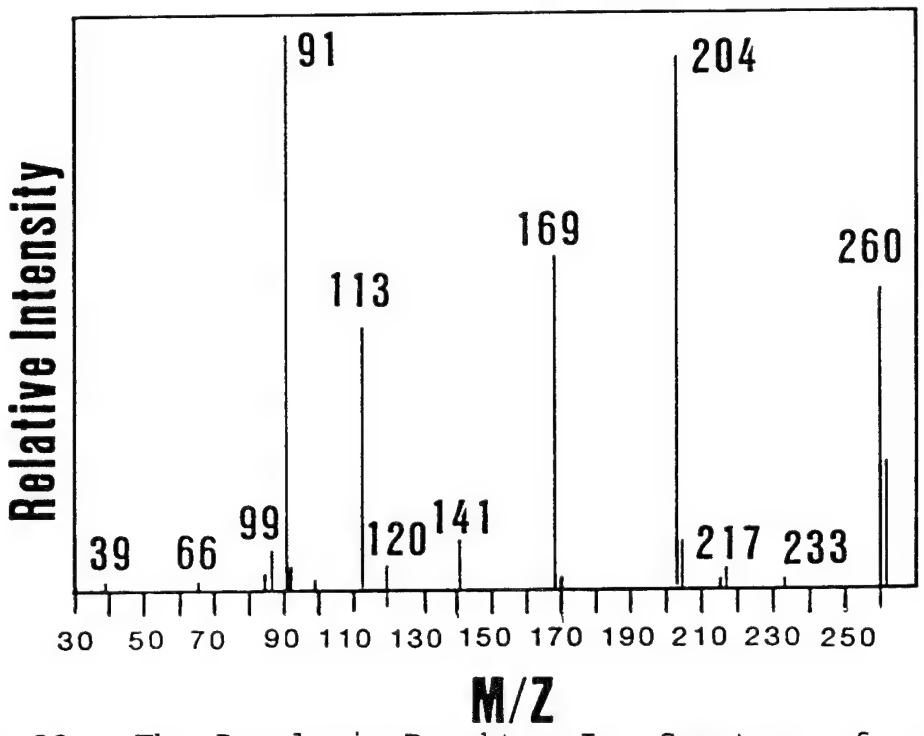

Figure 28. The Pyrolysis-Daughter Ion Spectrum of m/z 260 from PHE-LEU-MET.

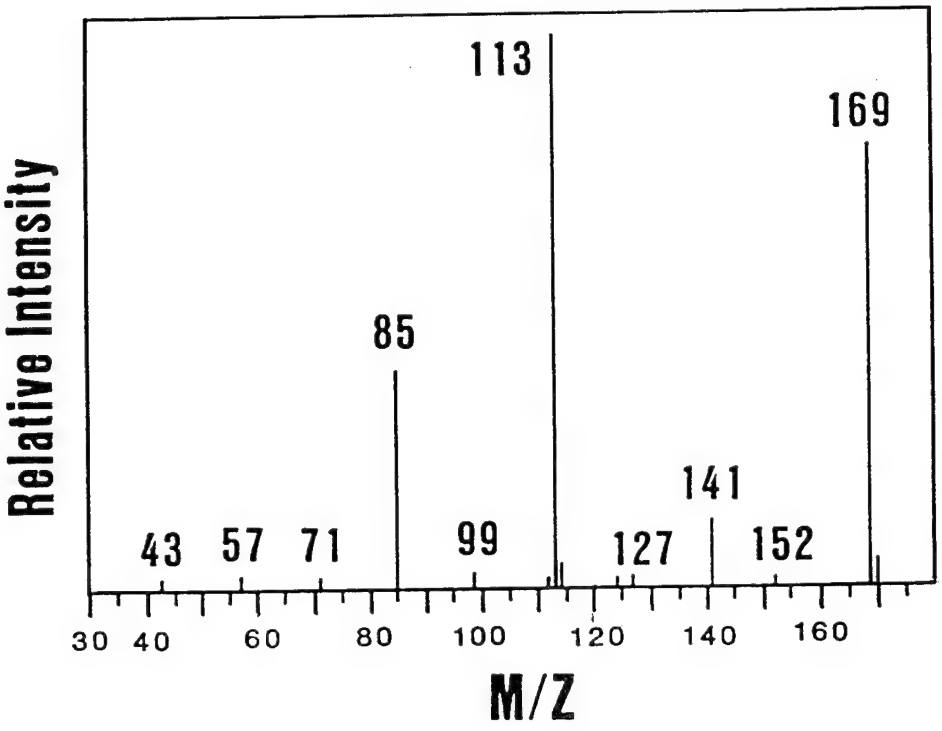

Figure 29. The Pyrolysis-Daughter Ion Spectrum of m/z 169 from PHE-LEU-MET.

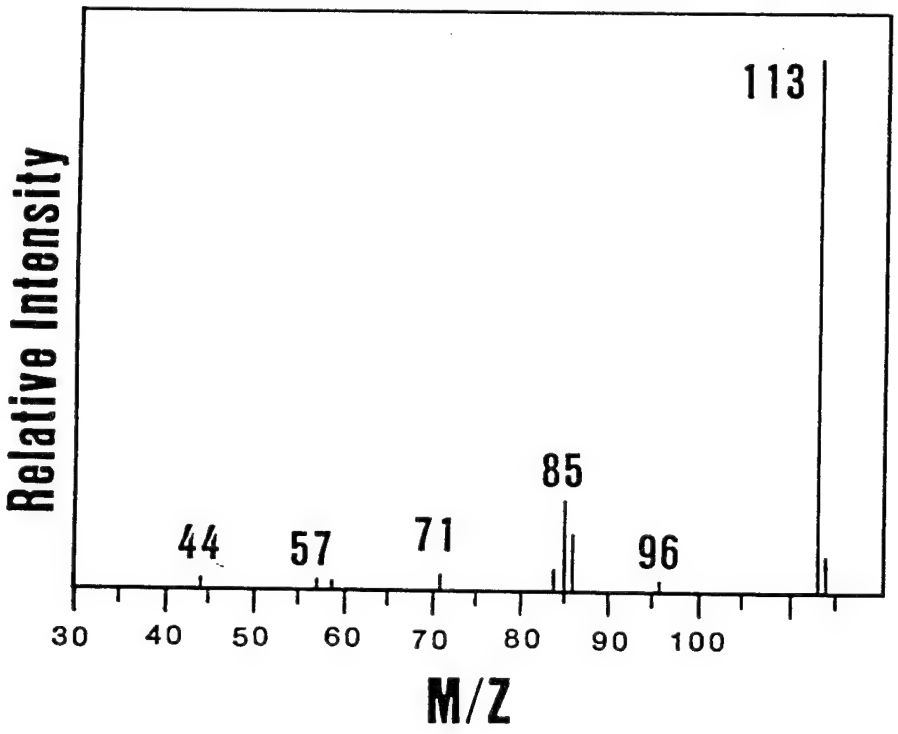

Figure 30. The Pyrolysis-Daughter Ion Spectrum of m/z 113 from PHE-LEU-MET.

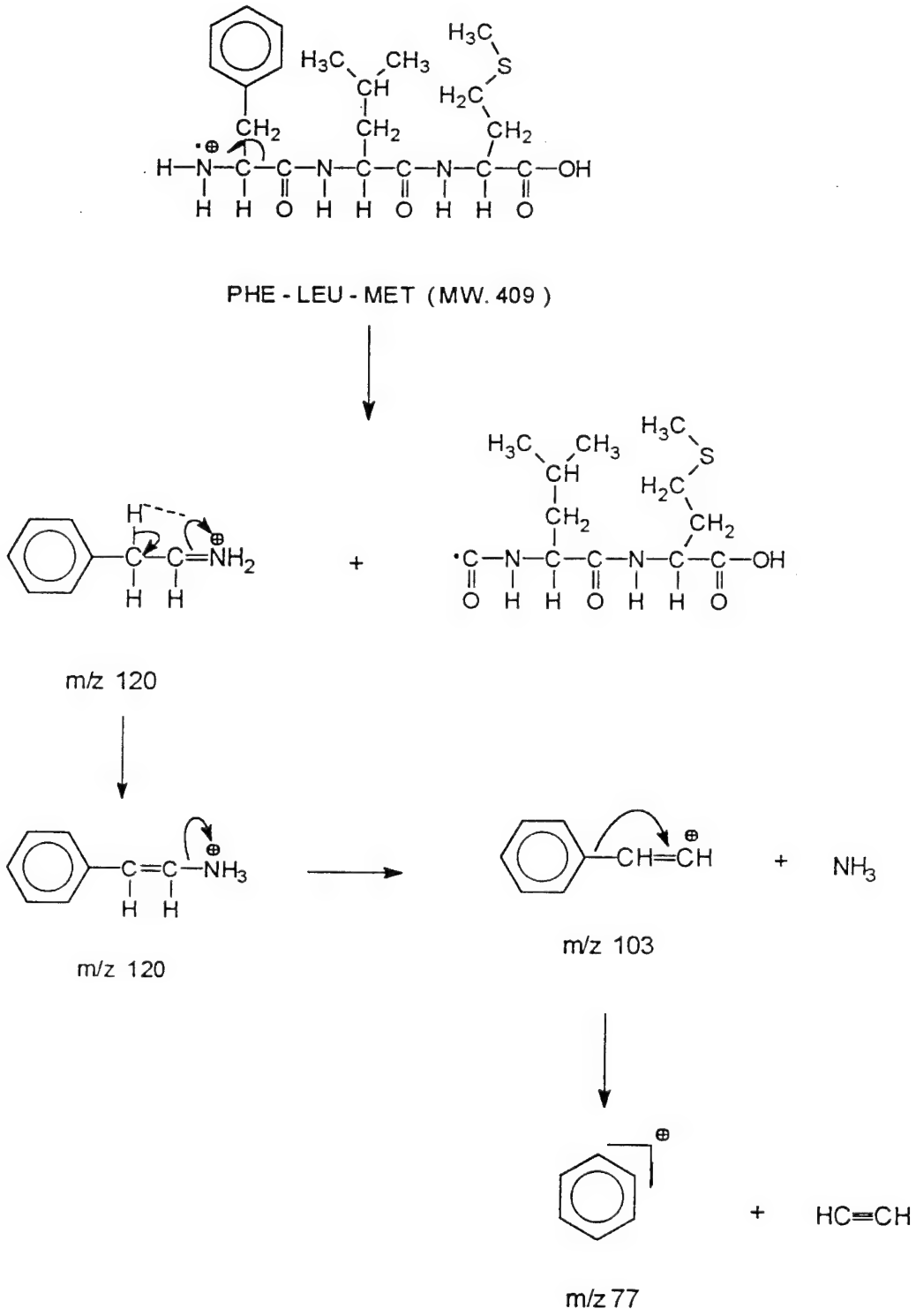

Figure 31. The N-Terminal Cleavage Mechanism of PHE-LEU-MET.

which is supported by the fact that (a) the molecular ion, m/z 409, was present in the parent ion spectrum of m/z 120, and (b) the daughter ion spectrum of m/z 409 had a prominent m/z 120 peak.

Methionyl-Leucyl-Phenylalanine

The dipeptide MET-LEU thermally decomposed to produced a series of peaks at m/z 244, 183, 170, 155, 127, 113, and 85 (58). Noguerola reported that the decomposition of this DKP occurred via two new pathways (Figure 32) (58). One was the initial loss of ethenyl methyl sulfide, which was followed by the loss of isobutene, both through an EI induced six-membered γ-hydrogen rearrangement. The other pathway was the radical cleavage of methyl methylene sulfide followed by two successive ethylene losses.

The tripeptide MET-LEU-PHE similarly undergoes many of the same reactions (Figure 33). Figure 33 shows the pyrolysis-mass spectrum of MET-LEU-PHE. A series of peaks common to both the dipeptide MET-LEU and the tripeptide MET-LEU-PHE spectra are observed. The daughter ion spectra of these peaks from the tripeptide provide data to support the mechanism for the formation and fragmentation of the MET-LEU DKP and the free C-terminal amino acid, phenylalanine. Peaks at m/z 147, 120, and 91 that appear in Figure 33 are from the phenylalanine lost in the formation of the DKP.

The base peak at m/z 104 in Figure 33 resulted from the EI cleavage of the N-terminal methionine residue from the intact tripeptide. This is supported by the presence of a significant m/z 104 peak in the daughter ion spectrum of the molecular

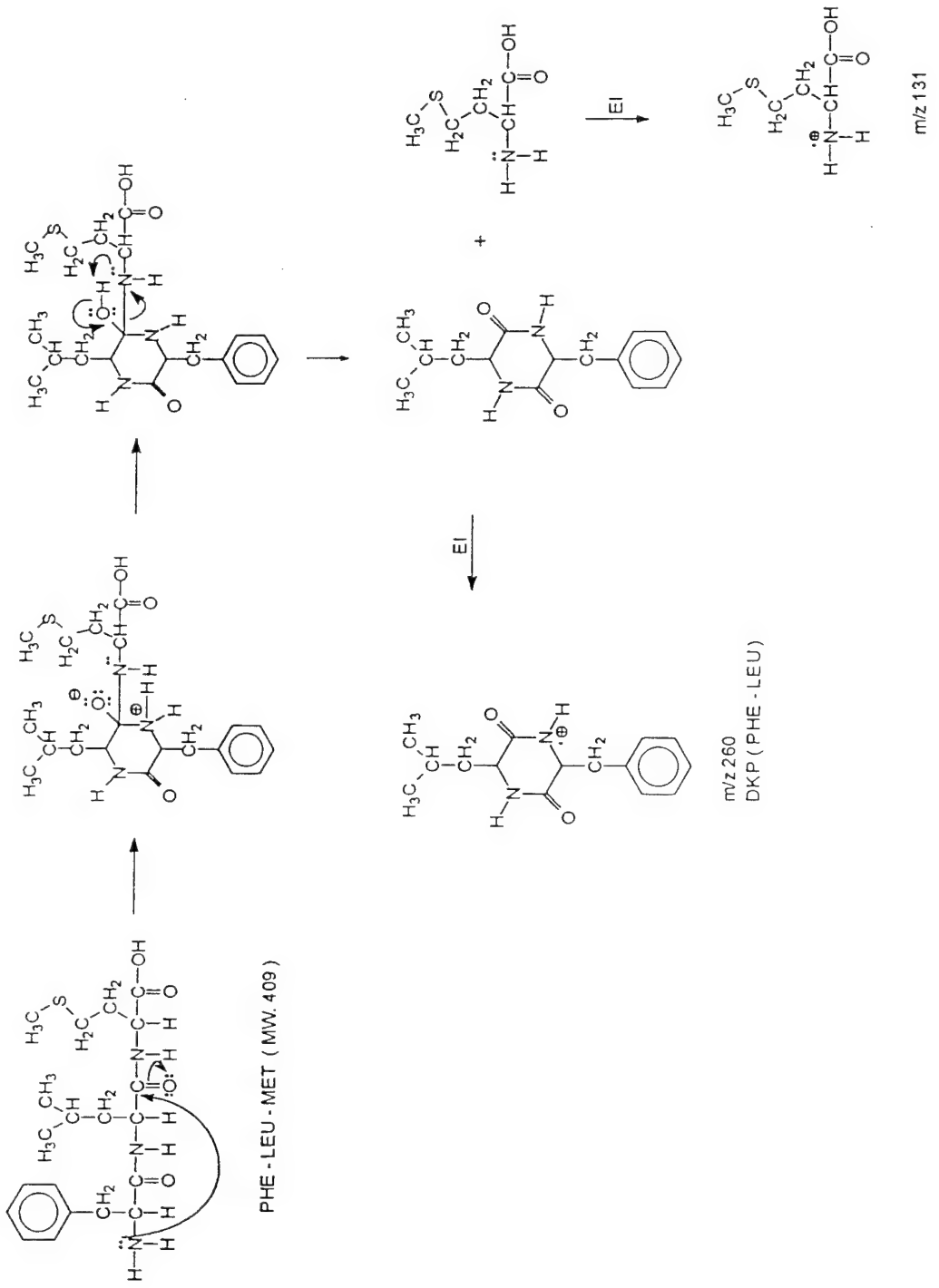

Figure 32. The DKP Formation Mechanism for Tripeptides.

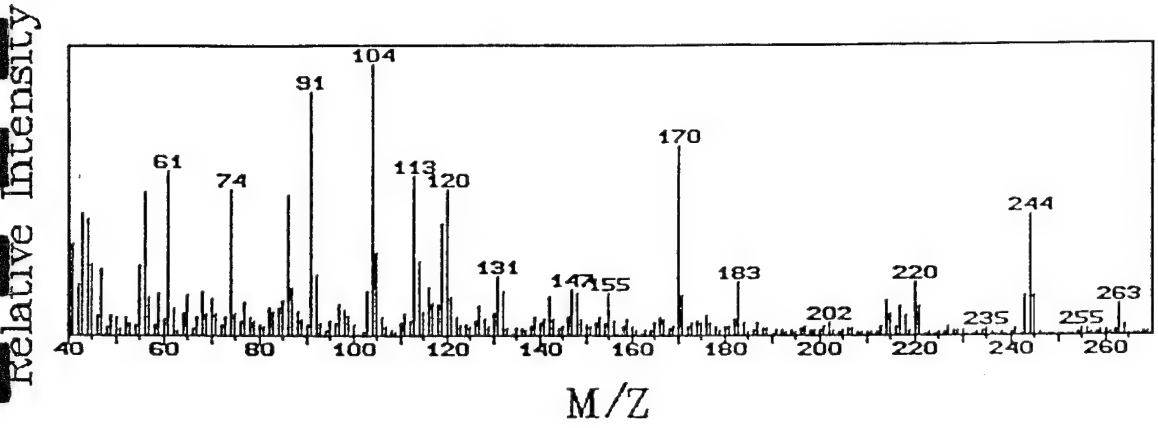

Figure 33. The Pyrolysis-Mass Spectrum of MET-LEU-PHE.

ion (m/z 409) and the absence of m/z 104 in the daughter ion spectrum of the MET-LEU DKP (m/z 244).

Other tripeptides

Pyrolysis-mass spectra of three additional tripeptides, PHE-MET-LEU, TYR-TYR-PHE, and LEU-LEU-LEU, were also obtained. The peaks in these spectra are explained based on the DKP formation and the EI induced fragmentations of the substituents from the intact peptide chain plus the N-terminal cleavage mechanism, similar to those previously postulated from di- and tri-peptide results.

2. Tetrapeptides

Alanyl-Phenylalanyl-Leucyl-Methionine

The pyrolysis-mass spectrum of ALA-PHE-LEU-MET (Figure 34) is more complex than the spectra observed for the tripeptides PHE-LEU-MET and MET-LEU-PHE. Two series of peaks based on dipeptide results (58) at m/z 218, 194, 166, 127, 99, 91, and 71 and m/z 244, 183, 170, 155, 127, 113, and 85 were expected and observed in the spectrum of ALA-PHE-LEU-MET. The first series of peaks can be assigned to the ALA-PHE DKP and its fragments. The second series of peaks correspond to the LEU-MET DKP and its fragments.

The daughter ion spectra of the ALA-PHE DKP (m/z 218), together with the parent ion spectra of m/z 91 and 127, verified the presence of the ALA-PHE DKP. The parent ion spectrum of m/z 91 showed a prominent peak at m/z 218, indicating the direct formation of a benzyl cation from the phenylalanine residue in the DKP. The peak at m/z 203 which

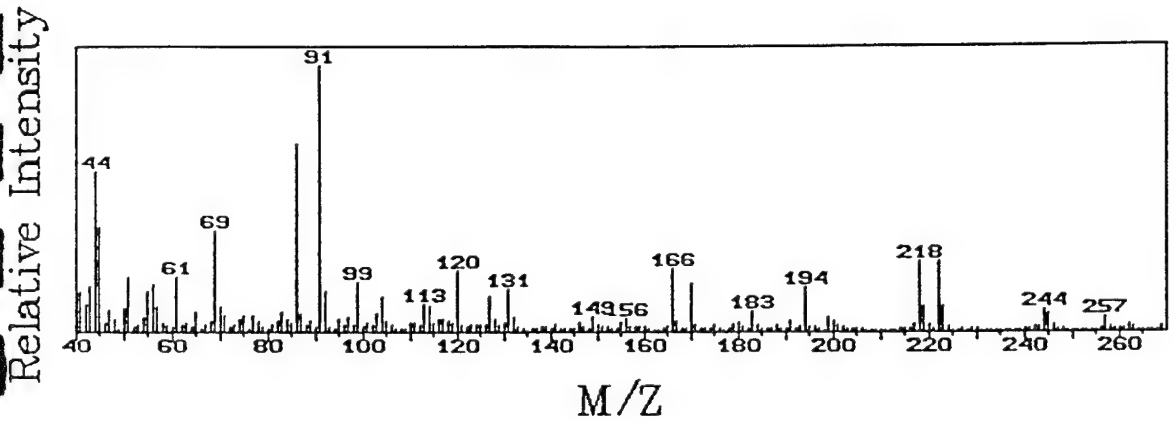

Figure 34. The Pyrolysis-Mass Spectrum of ALA-PHE-LEU-MET.

would correspond to a loss of a methyl radical from the ALA-PHE DKP was absent in the daughter ion spectrum of m/z 218. This is consistent with Noguerola's hypothesis (58), that the methyl group from the alanine residue is retained on the DKP. The parent ion spectrum of m/z 127 exhibits an intense peak at m/z 218 as well as smaller peaks at m/z 244, 183, 170, and 155. The peaks at m/z 183, 170, and 155 are known to be the fragments of the DKP of LEU-MET.

The presence of m/z 131 and 61 plus m/z 86 and 44 suggests the possibility that the free amino acids, methionine and leucine were also produced during cyclization. Parent-ion scans of m/z 86 from the pyrolysis of the tetrapeptide showed that this ion was produced by the fragmentation of m/z 183. This fragmentation had previously been postulated by Noguerola (58) as the product from the loss of the dimethyl sulfide radical from the cyclized LEU-MET DKP, m/z 244. The parent-ion scan of m/z 131 established that m/z 262 was the precursor to this ion. Although the possibility that free amino acids are produced cannot be totally eliminated, other sources for these peaks have been identified. In addition, some of the known peaks in the mass spectra of the two suspected amino acids were not observed in the pyrolysis-mass spectrum of the tetrapeptide.

The ALA-PHE-LEU-MET pyrolysis-mass spectrum yielded an intense peak at m/z 44. It is not certain whether this peak comes from the N-terminal cleavage of the alanine residue or from CO_2. Several attempts were made to obtain the molecular ion peak (m/z 480) with no success. Most likely, the molecular ion from the tetrapeptides was not observed due to insufficient volatility for direct detection prior to extensive thermal degradation.

Alanyl-Methionyl-Leucyl-Phenylalanine

The mass spectrum of ALA-MET-LEU-PHE as shown in Figure 35, shows the thermally cyclized DKPs of ALA-MET and LEU-PHE. The series of peaks for the LEU-PHE DKP, m/z 260, 204, 169, 141, 113, 103, 91, and 85 are analogous to those of the PHE-LEU DKP discussed above. The fragmentation of the ALA-MET DKP (m/z 202) observed in its daughter ion spectrum (Figure 36) supports cleavage of the substituents by six-membered EI-induced rearrangements occurs. For instance, the peak at m/z 128 corresponds to the elimination of the ethenyl methyl sulfide group, 74u. Another peak at m/z 187 was assigned as the loss of a methyl radical (15u) from the alanine residue in the DKP of ALA-MET. It is not apparent why the loss of methyl radical from the DKP of ALA-MET is more favorable than a methyl radical loss from the DKP of ALA-PHE as discussed for the tetrapeptide ALA-PHE-LEU-MET. The N-terminal cleavage was not observed. Daughter and parent-ion studies suggested that no C-terminal amino acid (phenylalanine) from ALA-MET-LEU-PHE was produced.

3. Pentapeptides

Alanyl-Phenylalanyl-Leucyl-Methionyl-Tyrosine

A comparison of the pyrolysis-mass spectrum of ALA-PHE-LEU-MET-TYR, Figure 37, with the spectrum of ALA-PHE-LEU-MET, Figure 35, shows them to be similar. One difference is the significant change in the relative intensities of m/z 91 and m/z 107. The base peak for ALA-PHE-LEU-MET, m/z 91, is lower in ALA-PHE-LEU-MET-TYR, while the base peak for ALA-PHE-LEU-MET-TYR, m/z 107, is very weak in ALA-PHE-LEU-MET. Another

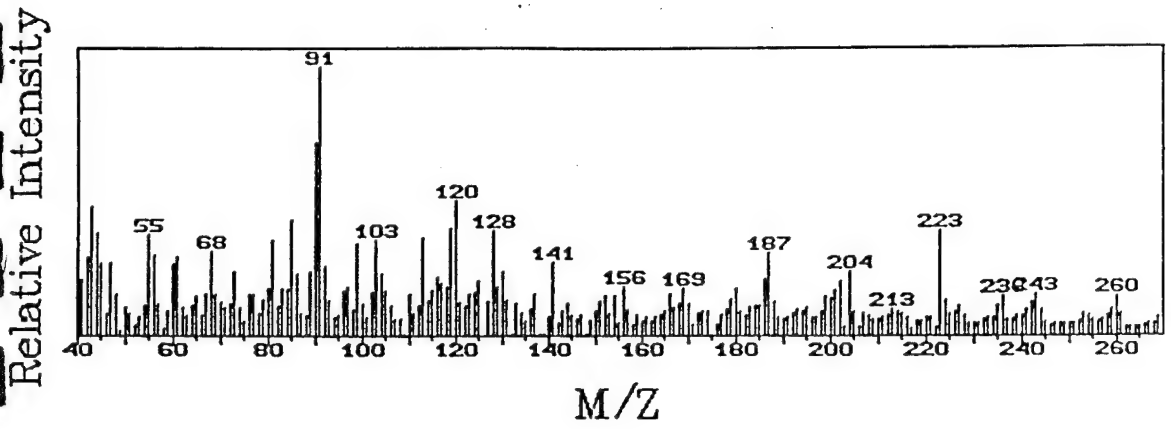

Figure 35. The Pyrolysis-Mass Spectrum of ALA-MET-LEU-PHE.

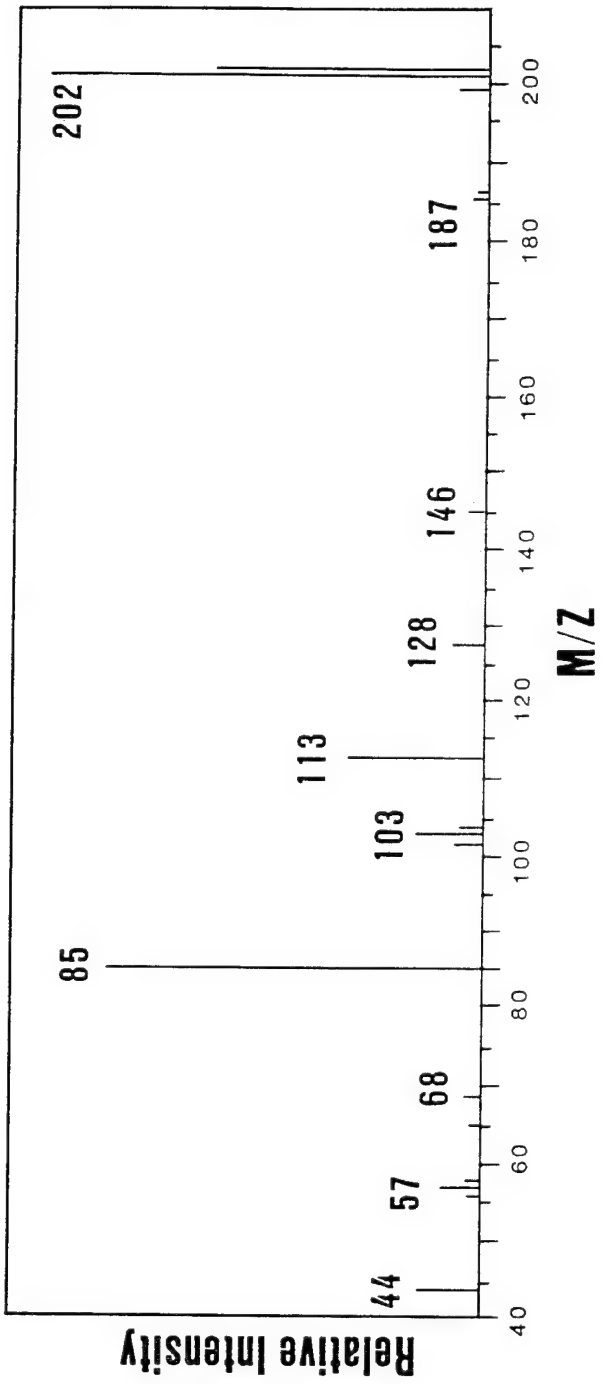

Figure 36. The Pyrolysis-Daughter Ion Spectrum Showing the Cleavage of m/z 202 from ALA-MET-LEU-PHE.

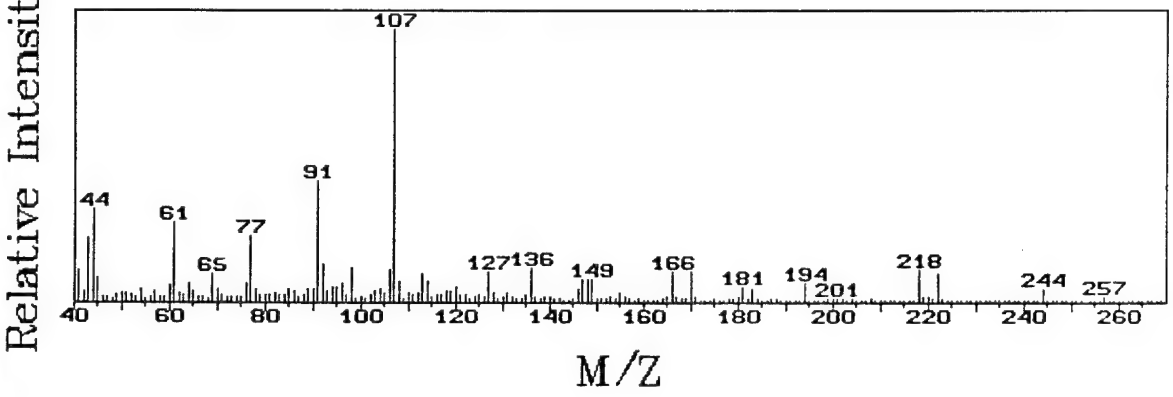

Figure 37. The Pyrolysis-Mass Spectrum of ALA-PHE-LEU-MET-TYR.

difference is the presence of m/z 136 and 77 in the ALA-PHE-LEU-MET-TYR spectrum. These two peaks correspond to tyrosine mass spectral fragments (74). Hence, the major differences between ALA-PHE-LEU-MET and ALA-PHE-LEU-MET-TYR can be attributed to the presence of the C-terminal amino acid tyrosine in the pentapeptide spectrum.

The assigned peaks in the ALA-PHE-LEU-MET-TYR pyrolysis-mass spectrum support the previously discussed cyclization pathway to form two DKPs plus a free C-terminal amino acid. The two series of peaks at m/z 218, 194, 166, and 127 and m/z 244, 183, 170, 155, and 127 are attributed to the DKPs of ALA-PHE and LEU-MET, respectively. Daughter ion spectra and previous dipeptide results were used to verify the assignments of all peaks.

Alanyl-Tyrosyl-Leucyl-Methionyl-Phenylalanine

The pyrolysis-mass spectrum of ALA-TYR-LEU-MET-PHE is shown in Figure 38. Peaks attributed to two consecutive DKP formations were observed. The molecular ion, m/z 234, for the ALA-TYR DKP is accompanied by both the cleavage of 4-hydroxybenzyl radical to produce an m/z 128 ion, and fragmentation to form an ionic hydroxybenzyl group, m/z 107. The daughter ion spectrum of m/z 234, Figure 39, supports this interpretation. A series of peaks for the LEU-MET DKP at m/z 244, 183, 170, 155, 127, and 113 also occurs in the pyrolysis-mass spectrum.(58) The peaks at m/z 91 and 147 in Figure 38 show that phenylalanine, the C-terminal amino acid, was cleaved from ALA-TYR-LEU-MET-PHE.

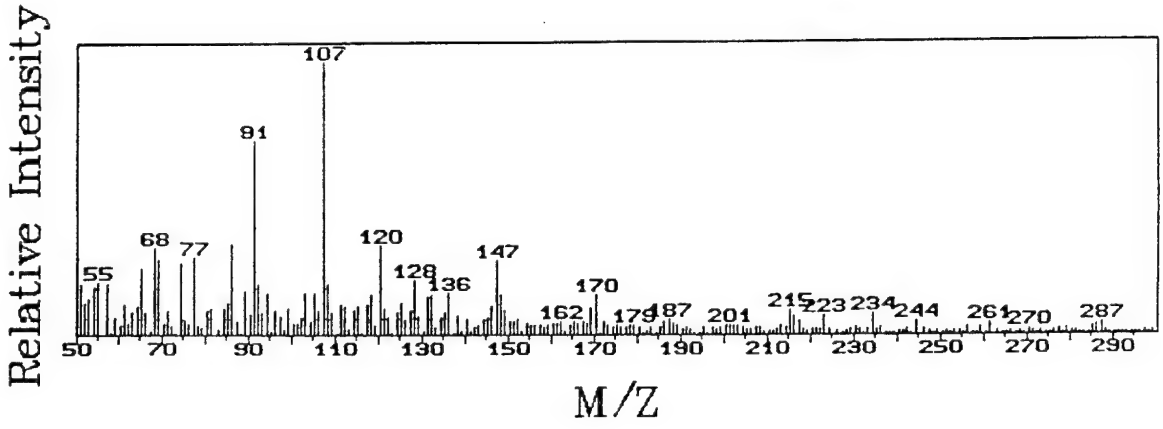

Figure 38. The Pyrolysis-Mass Spectrum of ALA-TYR-LEU-MET-PHE.

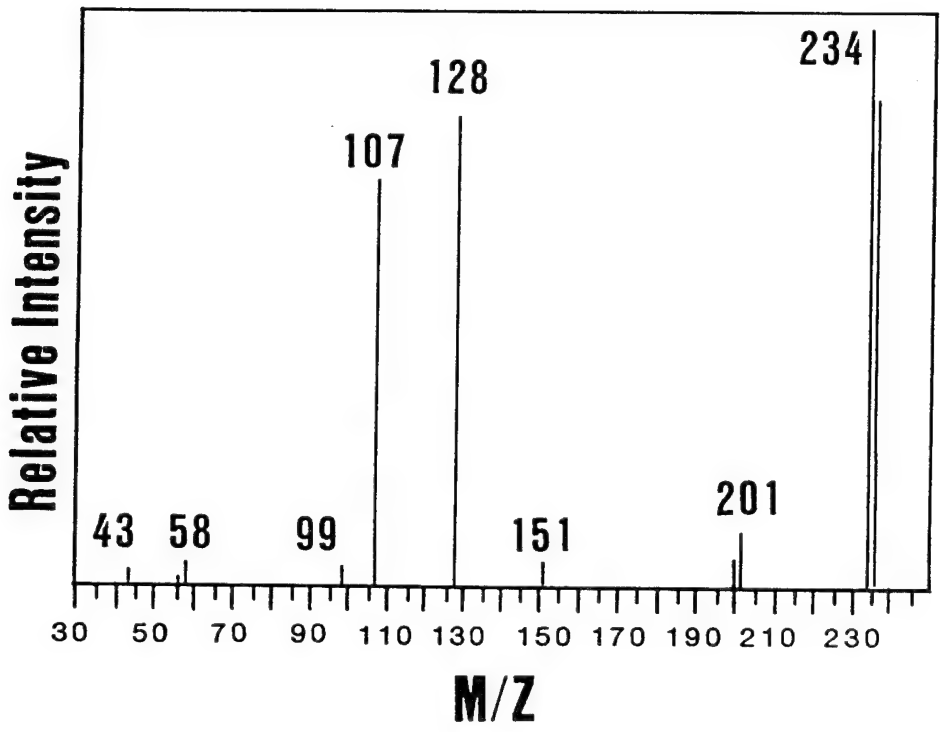

Figure 39. The Pyrolysis-Daughter Ion Spectrum of m/z 234 from ALA-TYR-LEU-MET-PHE.

4. Hexapeptides

It was postulated that the hexapeptides should thermally fragment by consecutive cyclization to produce three DKP units, A - B - C - D - E - F. ALA-TYR-LEU-MET-PHE-PHE, ALA-PHE-LEU-MET-TYR-PHE, PHE-ALA-PHE-LEU-MET-TYR and TYR-TYR-TYR-TYR-TYR-TYR have been analyzed to test this hypothesis. Table XI summarizes the major peaks corresponding to the related DKPs. The pyrolysis-mass spectra are shown in Figure 40a - c.

In some cases, pyrolysis of a hexapeptide produced many mass spectral peaks with low intensities, making assignments difficult. Lowering the Curie-point temperature from 510°C to 358°C enhanced the DKP peak intensities from the hexapeptides. The mass spectra of these oligopeptides had fewer peaks when pyrolyzed at 358°C.

b. Large Oligopeptides

The fingerprints generated from oligopeptides (6-30 AAs) analyzed via Curie-point pyrolysis mass spectrometry are similar to those generated from the pyrolysis of smaller peptides (2-6 AAs). A total of fifteen oligopeptides (Table XII) spanning this larger range were analyzed.

Peptides of two to six amino acid units in length have been noted to form diketopiperazines (DKPs) during pyrolysis mass spectrometry. Several pairs of DKPs

Table XI. Major Mass Spectral Peaks of Hexapeptides.

Hexapeptides	Diketopiperazines (DKP) (u)		Major Peaks (m/z)
	ALA-TYR	(234u)	128, 107
ALA-TYR-LEU-MET-PHE-PHE	LEU-MET	(244u)	183,170,155
	PHE-PHE	(294u)	203,112
	ALA-PHE	(218u)	127,99,91,77
ALA-PHE-LEU-MET-TYR-PHE	LEU-MET	(244u)	183,170,155
	TYR-PHE	(310u)	293,204,187,91
	PHE-ALA	(218u)	128,107,91
PHE-ALA-PHE-LEU-MET-TYR	MET-TYR	(260u)	204,187,169,141
	MET-TYR	(294u)	203,188,107
TYR-TYR-TYR-TYR-TYR-TYR	TYR-TYR	(326u)	310,220,203,107

Table XII. Larger Oligopeptides Studied and Their Length in Amino Acid Units

Phe-Ala-Phe-Leu-Met-Tyr (6)
Thr-Leu-Asn-Asp-Glu-Leu-Glu (7)
Asp-Glu-Leu-Glu-Ile-Ile-Glu (7)
Arg-Gly-Leu-Ile-Val-Phe-His-Thr-Ser (9)
Trp-Ala-Gly-Gly-Asp-Ala-Ser-Gly-Glu (9)
Phe-Ser-Trp-Gly-Ala-Glu-Gly-Gln-Arg (9)
Arg-Pro-Pro-Gly-Phe-Ser-Pro-Phe-Arg (Bradykinin) (9)
Pro-His-Pro-Phe-His-Phe-Phe-Val-Tyr-Lys (10)
Arg-Pro-Lys-Pro-Gln-Gln-Phe-Phe-Gly-Leu-Met (Substance P) (11)
Lys-Pro-Val-Gly-Lys-Lys-Arg-Arg-Pro-Val-Lys-Val-Tyr-Pro (14)
Gln-Ala-Thr-Val-Gly-Asp-Ile-Asn-Thr-Glu-Arg-Pro-Gly-Met-Leu-Asp-Phe-Thr-Gly-Lys (20)
Asn-Pro-Asn-Ala-Asn-Pro-Asn-Ala-Asn-Pro-Asn-Ala-Asn-Pro-Asn-Ala (16)
Insulin Chain A Oxidized (21)
Insulin Chain B Oxidized (30)
Histone Fragment 1-34 (34)

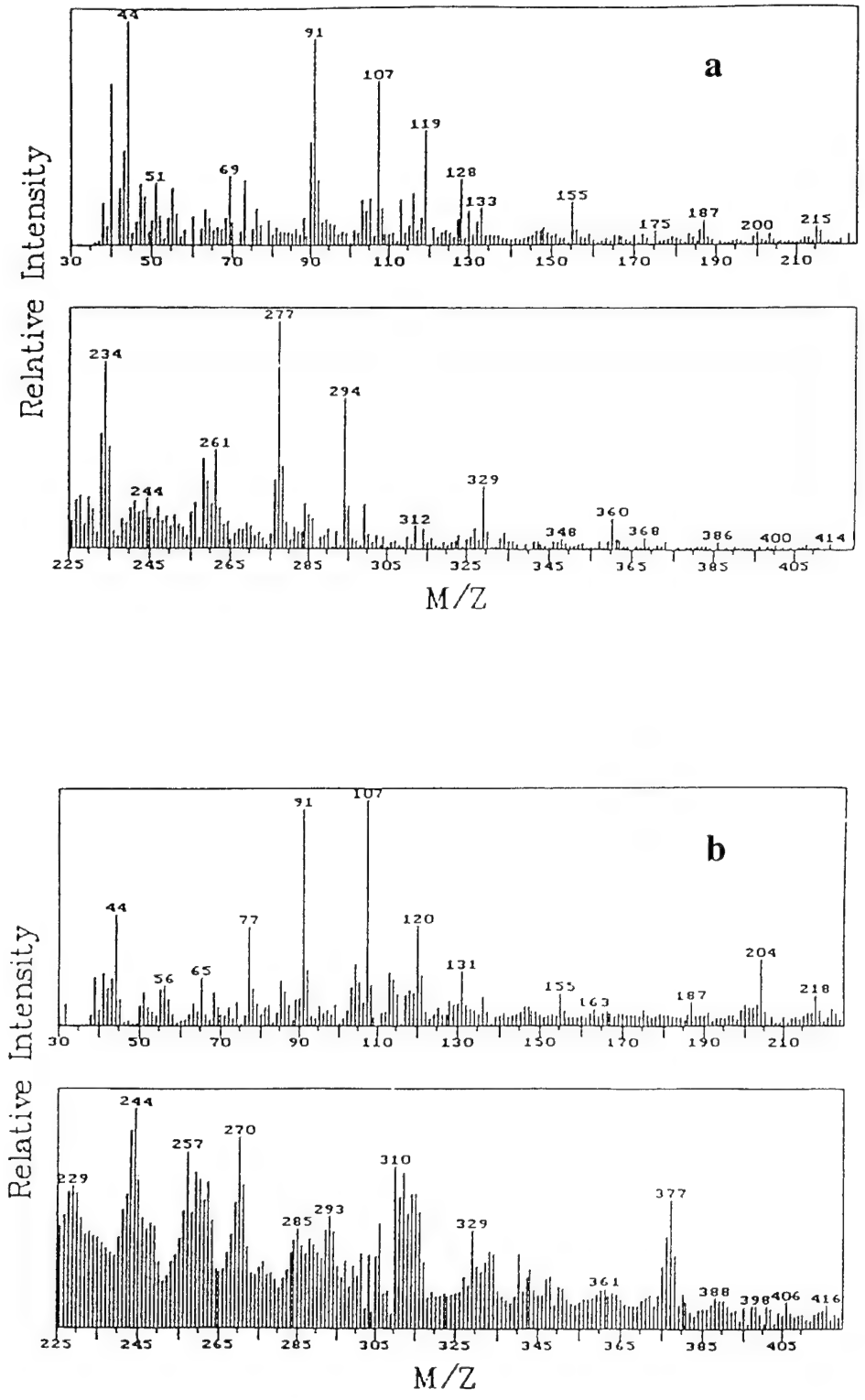

Figure 40. The Pyrolysis-Mass Spectra of Three Hexapeptides (Each Segment has been normalized separately).

a. ALA-TYR-LEU-MET-PHE-PHE

b. ALA-PHE-LEU-MET-TYR-PHE

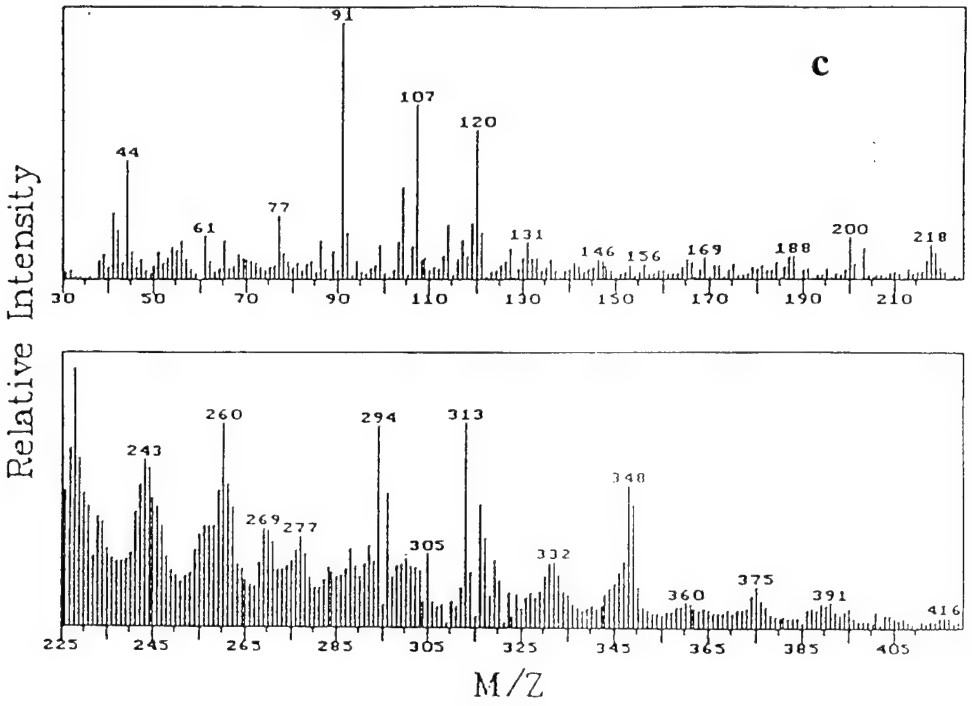

Figure 40. The Pyrolysis-Mass Spectra of Three Hexapeptides (Each Segment has been normalized separately).

a. ALA-TYR-LEU-MET-PHE-PHE
b. ALA-PHE-LEU-MET-TYR-PHE
c. PHE-ALA-PHE-LEU-MET-TYR

were formed for peptides with six amino acid units. In the larger peptides studied, several pairs of DKPs were also formed, depending on the positions in the peptides analyzed and the amino acids involved in the cyclization process. The first two amino acid units in the oligopeptide most readily formed the thermal cyclization products in the larger peptides. Certain amino acids (e.g. proline) were found to enhance the thermal cyclization products for the amino acids to which they were attached. Other markers for particular amino acids were noted. Alpha cleavage at the N-terminal is common and produces characteristic fragments for many amino acids (e.g. phenylalanine). Side group cleavages are prevalent in oligopeptides, producing characteristic markers for many amino acids (e.g. tyrosine, methionine, phenylalanine).

Oxidized chain B of bovine insulin was the largest peptide studied with 30 amino acid units. Six distinct sets of DKP markers were observed in the spectrum, accounting for the majority of the major peaks. DKPs were formed with the following amino acid:

Phe-Val (AAs 1 & 2)

His-Leu (AAs 5 & 6)

Val-Glu (AAs 12 & 13)

Tyr-Leu (AAs 16 & 17)

Gly-Glu (AAs 20 & 21)

Arg-Gly (AAs 22 & 23)

The pyrolysis-mass spectrum of the bovine insulin is shown in Figure 41.

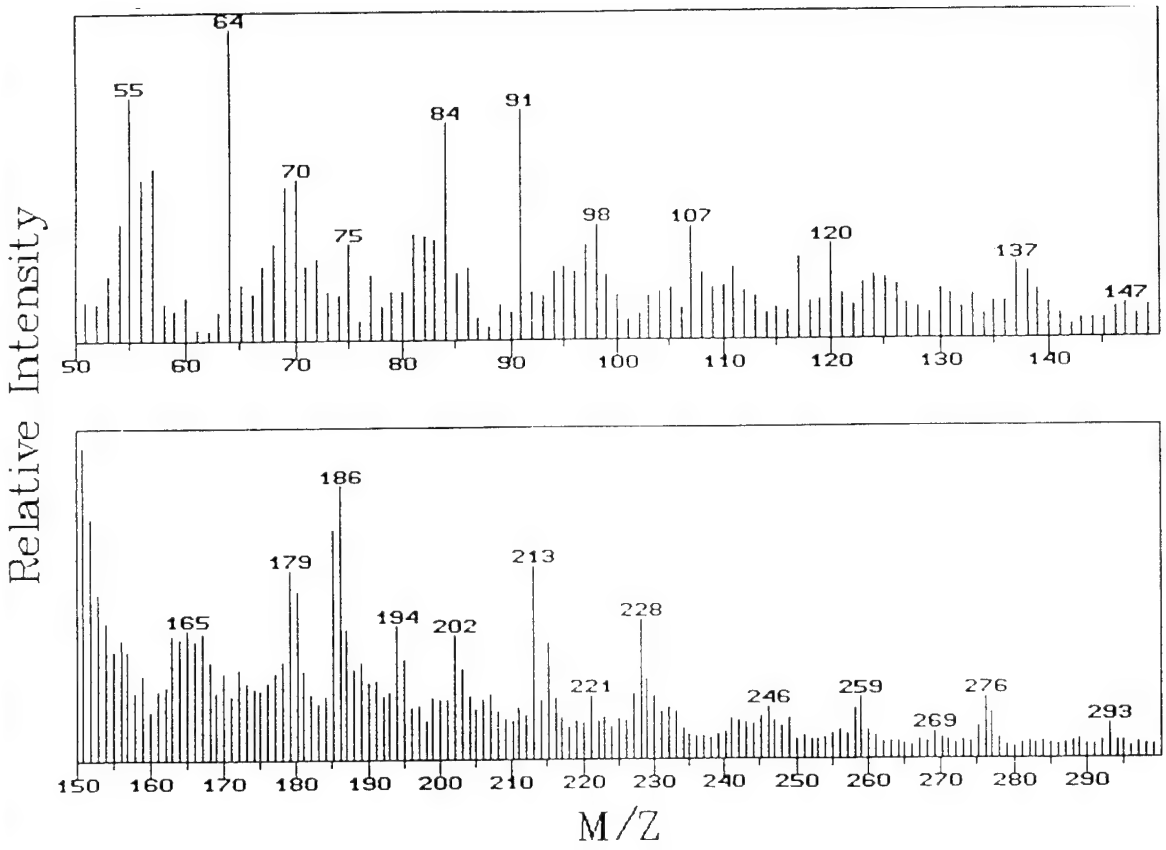

Phe-Val DKP mass 246 (AAs 1 & 2)
His-Leu DKP - Leu R group mass 194 (AAs 5 & 6)
Val-Glu DKP mass 228 (AAs 12 & 13)
Tyr-Leu DKP mass 276 (AAs 16 & 17)
Gly-Glu DKP mass 186 (AAs 20 & 21)
Arg-Gly DKP mass 213 (AAs 22 & 23)

Figure 41. Pyrolysis Mass Spectrum of Oxidized Bovine Insulin

Fragmentation processes of the ionized DKPs are limited. Mass spectral peaks due to the cleavage of side groups were prevalent in the daughter ion spectra of DKPs. Some ring fragmentation is also observed. Since unique molecular ions are formed for almost every DKP pair, daughter ion spectra allow for the determination of amino acid pairs in unknown oligopeptides. Similar results were obtained for the smaller oligopeptides studied.

c. Derivatized Oligopeptides

Several derivatized oligopeptides containing from four to six amino acids have also been examined. All of these peptides contained a trifluoroacetyl group (TFA) as an amide on the N-terminus. As a result of the lower basicity of the nitrogen on the N-terminus, these peptides showed no tendency to thermally cyclize. Absence of the peaks corresponding to any DKPs confirmed that an available electron pair on the nitrogen of the N-terminus of the oligopeptides is a fundamental requirement for cyclization to form a DKP from oligopeptides.

d. Conclusions on oligopeptides

Three levels of general electron ionization and thermal fragmentation pathways of underivatized linear oligopeptides have been established. First, cyclization to form 2,5-diketopiperazines (DKPs) takes place readily under pyrolytic conditions. Although the formation of DKPs has been reported by others (57-65), the occurrence has been limited primarily to the two amino acids residing on the N-terminal end of the oligopeptides, while the rest of the amino acid moieties were eliminated. Our experiments have revealed that the formation of DKPs can also occur during the depolymerization of oligopeptides. As a result, a DKP molecular ion

together with its fragment ions can be used to identify peptide pairs present in complex systems.

The second decomposition mode involves N-terminal cleavage. The ions from N-terminal cleavage have only been observed in the mass spectra of the di- and tri-peptides where molecular ions were also present. Based on this, the observed volatility and selected daughter ion spectra, N-terminal cleavage has been determined to be a result of electron ionization. Finally, C-terminal elimination from odd-numbered oligopeptides to produce a free amino acid was observed in peptides containing three and five amino acids.

e. dipeptides

The results from the previously discussed study showed a variability in the relative intensities of the various DKPs which depended on the amino acids involved in the cyclization process and their position in the peptide. This suggested that the substituents on the 2-carbon played an important role in DKP formation. Another observation from this investigation was that the basicity of the N-terminal amino group influenced cyclization. When the N-terminal amino acid was derivatized with trifluoroacetic acid, the cyclization was not observed during pyrolysis.

Due to the diversity of the naturally occurring amino acids, several factors which could be expected to influence thermal DKP formation. Cramer used a variety of factors to characterize 142 common organic compounds (75). Hellberg *et al.* included 29 categories in an attempt to relate and differentiate amino acids from one another by factor analysis (76). Three "principal properties", related to bulk, hydrophilicity and electronic factors were found to characterize the physiochemical properties of amino acids. Factors such as pK_a and pI (pH at isoelectric point) were included as electronic factors. The factors which can be used to describe amino acid and peptide behavior during pyrolysis mass spectrometry have not been explored. This paper details a thorough investigation into the molecular effects that influence DKP formation during the pyrolysis mass spectrometry of 39 dipeptides.

Two series of dipeptides have been studied to determine the various molecular effects on DKP formation. In the first series, 20 dipeptides were prepared with an N-terminus of glycine and a C-terminus that varied among the 20 naturally occurring amino acids. Each dipeptide in the second series had a C-terminus of glycine and an N-terminus that included the same 20

amino acids. A total of 39 dipeptides were studied, rather than 40, as the dipeptide Gly-Gly was redundant in the second series. As discussed earlier, two EI decomposition pathways have been observed for DKPs. The first involved cleavage of the substituents (R groups) prior to ring fragmentation. The second pathway, which described ring fragmentation prior to substituent cleavage, was made based on dipeptides containing only glycine and alanine. The results from the present study indicated that both pathways were operational and depended on the substituents of the amino acids composing the dipeptide. The DKP was found to fragment prior to loss of the two simplest substituents --H, in glycine and $--CH_3$ in alanine. However, for the other amino acids investigated in this study which formed DKPs, substituents were cleaved prior to DKP ring fragmentation.

1. Dipeptides with Glycine as the N-terminus

The first series that will be discussed is the series of 20 dipeptides studied with a fixed N-terminus of glycine. In order to asses the relative extent of DKP formation among these dipeptides, a peak that can be used for comparison is needed. A major EI product for dipeptides with glycine as the N-terminus was the N-terminal cleavage (α - cleavage) product giving rise to m/z 30. When the N-terminal residue is fixed as glycine in a series of dipeptides, the relative extent of the thermal cyclizations can be assessed among the different dipeptides using the m/z 30 peak as a reference.

Several factors, including steric, electronic, and intramolecular interactions were expected to affect the DKP formation during pyrolysis. Table XIII summarizes the ratio of DKP to N-terminal peaks for the 20 dipeptides with glycine as the N-terminus. The dipeptides with

glutamic acid, aspartic acid, and arginine as the C-terminus did not form DKPs. The various factors affecting DKP formation in other dipeptides are discussed below.

The dipeptides with aliphatic alkyl substituents on the C-terminus (glycine, alanine, leucine, isoleucine, and valine) represent a series in which DKP formation should be controlled primarily by steric effects. If steric factors control the DKP formation, Gly-Gly would be expected to form the most DKP in relation to the N-terminal cleavage product, since the hydrogen substituent of glycine produces the least steric hinderance to cyclization. The methyl substituent of alanine poses the next least steric hinderance, followed by leucine, valine and isoleucine (77).

Figure 42 shows a pyrolysis mass spectrum of glycyl-glycine. The peaks at m/z 114 and 85, are from the DKP and its major EI fragment, while m/z 30 represents the N-terminal cleavage product. The mass spectra of the five dipeptides of this group are primarily described by the dipeptide molecular ion peak, the DKP peak and its fragments and the N-terminal cleavage peak.

Figure 43 is a pyrolysis mass spectrum of glycyl-alanine. The DKP of Gly-Ala occurs at m/z 128. As previously mentioned, the mass spectrum of Gly-Ala does not show a significant peak at m/z 114 because the loss of the substituent from the alanine residue

Table XIII. Ratio of DKP Peaks to N-terminal Peak for Dipeptides with Glycine as the N-terminus

C-terminal Amino Acid	DKP / N-terminal ratio
Alanine	0.329
Arginine	0.000
Asparagine	0.100
Aspartic Acid	0.000
Cysteine	0.693
Glutamine	0.259
Glutamic Acid	0.000
Glycine	0.308
Histadine	0.769
Isoleucine	0.043
Leucine	0.078
Methionine	1.306
Phenylalanine	0.043
Proline	0.989
Serine	0.575
Threonine	0.663
Tryptophan	0.390
Tyrosine	2.895
Valine	0.041

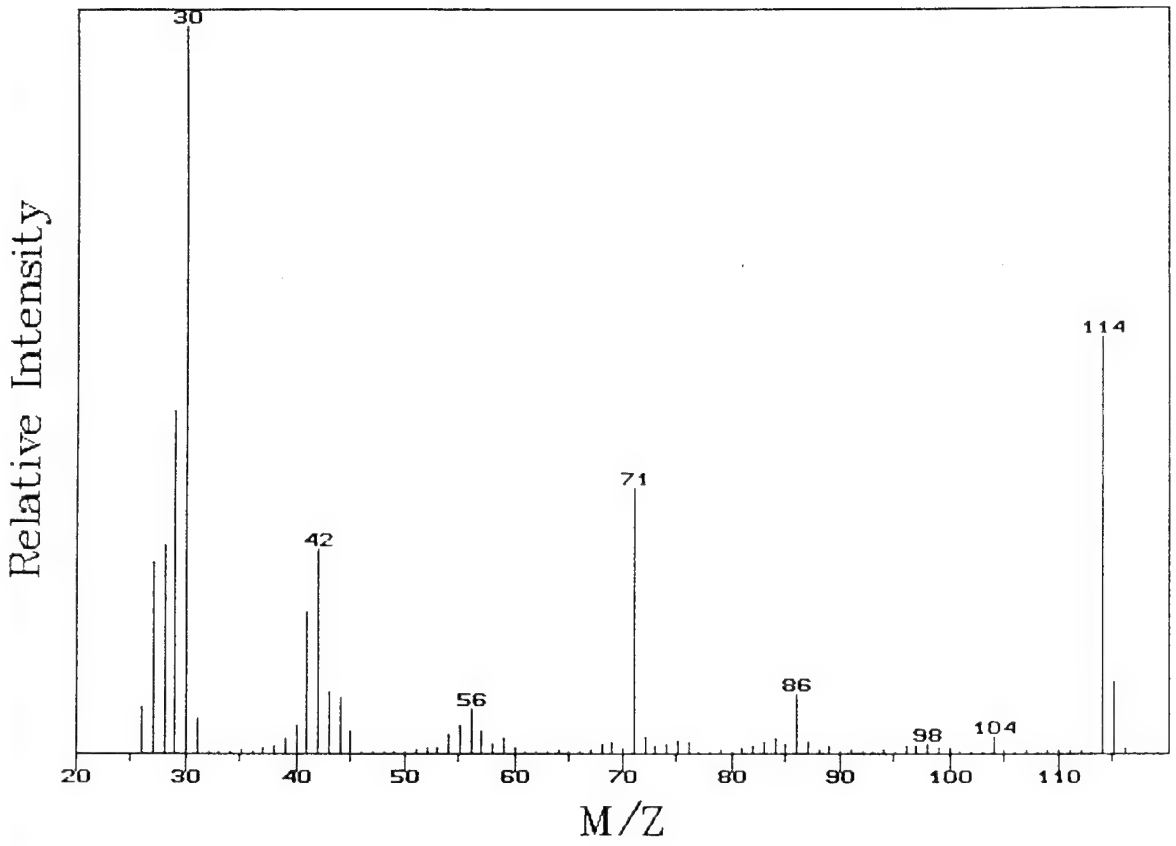

Figure 42. Pyrolysis Mass Spectrum of Gly-Gly

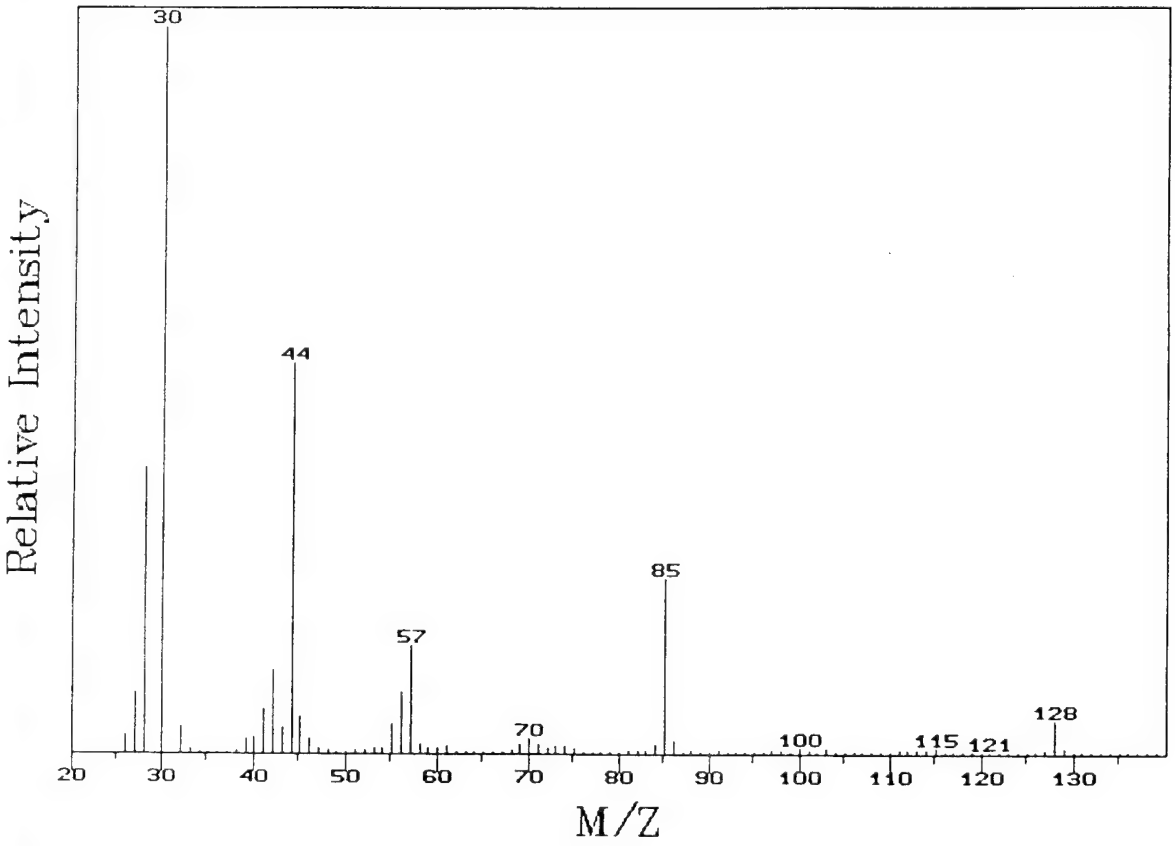

Figure 43. Pyrolysis Mass Spectrum of Gly-Ala

is not a favorable process. As in the pyrolysis mass spectrum of Gly-Gly, the peak at m/z 30 represents the N-terminal cleavage product of the dipeptide. The ratio of the DKP peaks to the m/z 30 peak demonstrates that Gly-Gly and Gly-Ala form similar amounts of DKP products, indicating that the presence of alanine on the C-terminus does not significantly hinder the DKP process.

A pyrolysis mass spectrum of glycyl-valine is shown in Figure 44. The peak at m/z 114 and the absence of the DKP molecular ion peak at m/z 156 is indicative of the loss of the isopropyl group from the intact DKP. This loss occurs more readily than substituent losses in Gly-Ala and Gly-Gly due to the increased stability of the 2° isopropyl radical formed in the cleavage. The ratio of the DKP peaks to the m/z 30 peaks in the spectrum is much smaller for Gly-Val than for Gly-Gly or Gly-Ala. This indicates a decreased tendency for the thermal cyclization, which is consistent with the added steric hinderance expected by the isopropyl group on the valine residue. Figure 45 is a pyrolysis mass spectrum of glycyl-leucine. Again a decreased amount of cyclization is observed, compared to Gly-Gly and Gly-Ala, due to the bulky isobutyl substituent in leucine. These results clearly indicate that the thermal cyclization process is affected by the bulkyness of the aliphatic substituents. Figure 46 graphically demonstrates this effect when the ratio of DKP to N-terminal peaks are compared among these dipeptides. Three replicate spectra were averaged for each dipeptide in the plot. Hammet plots using σ^+ values for each specific substituent showed no linearity (78).

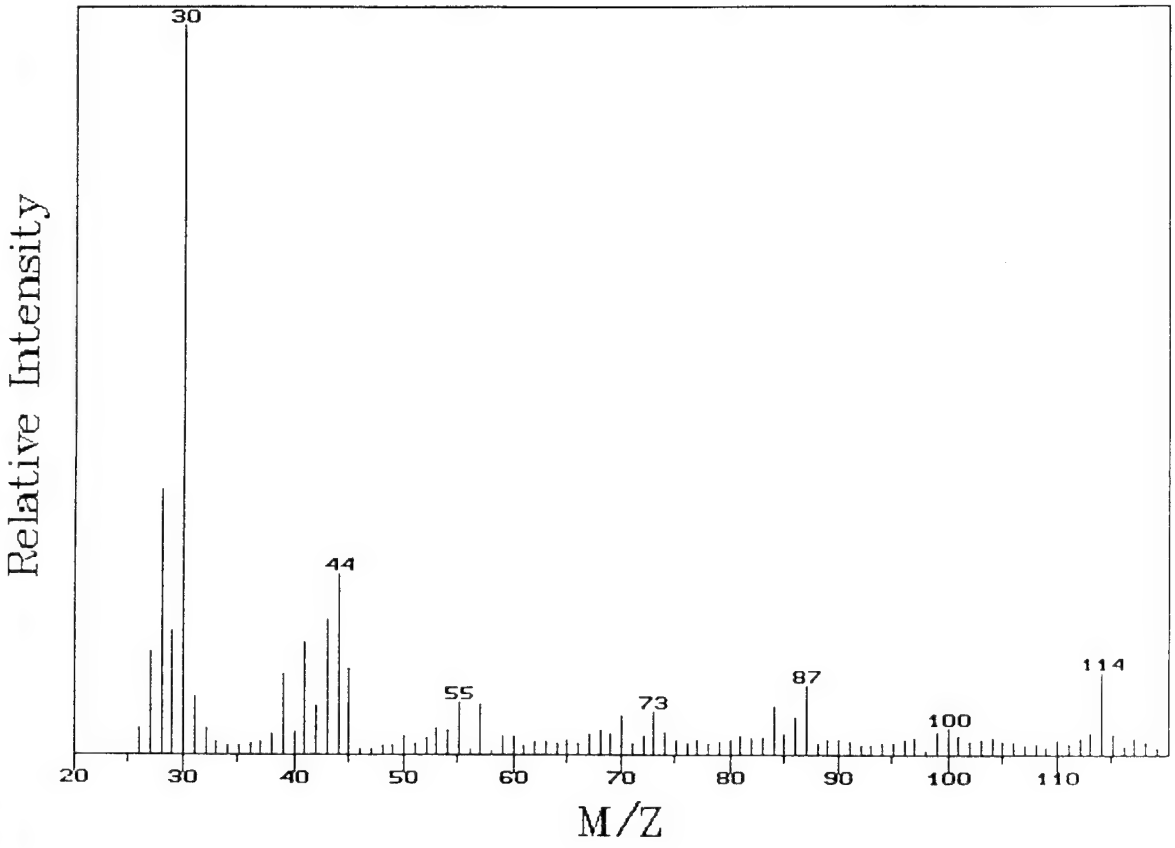

Figure 44. Pyrolysis Mass Spectrum of Gly-Val

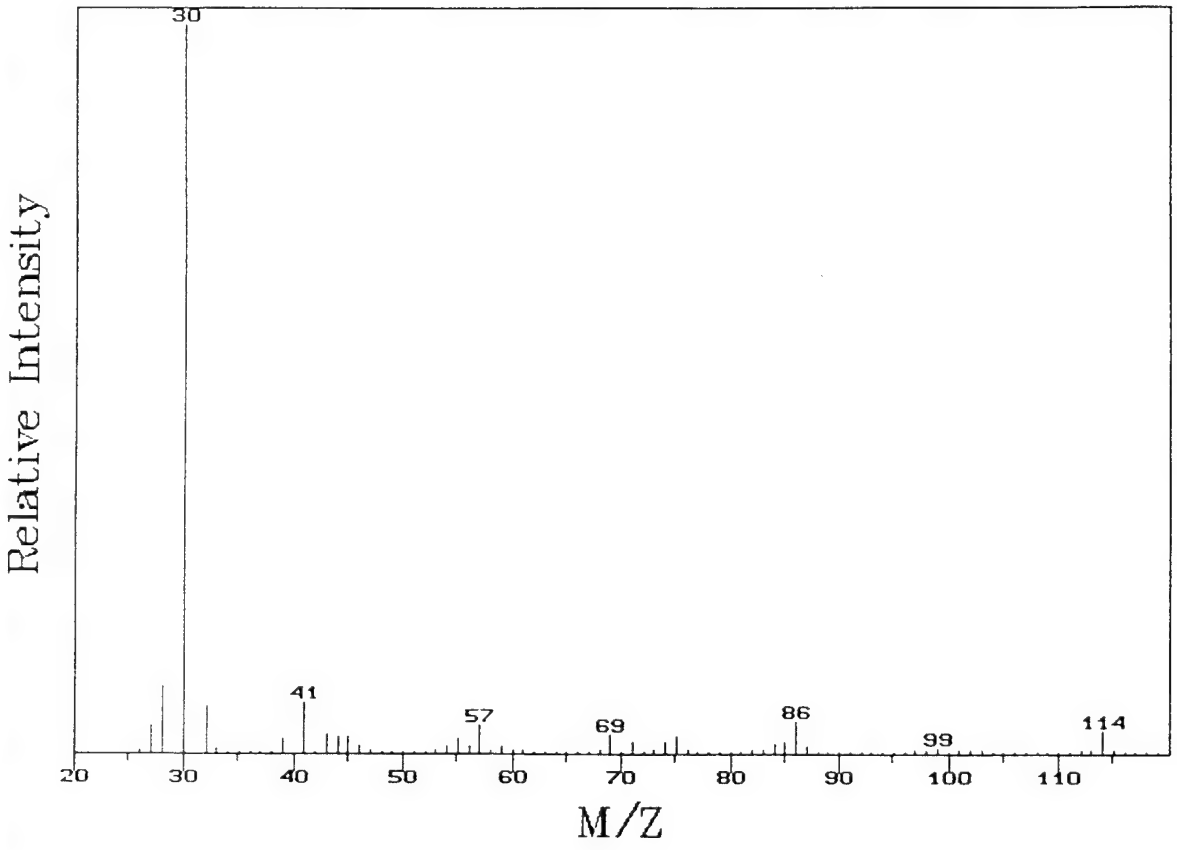

Figure 45. Pyrolysis Mass Spectrum of Gly-Leu

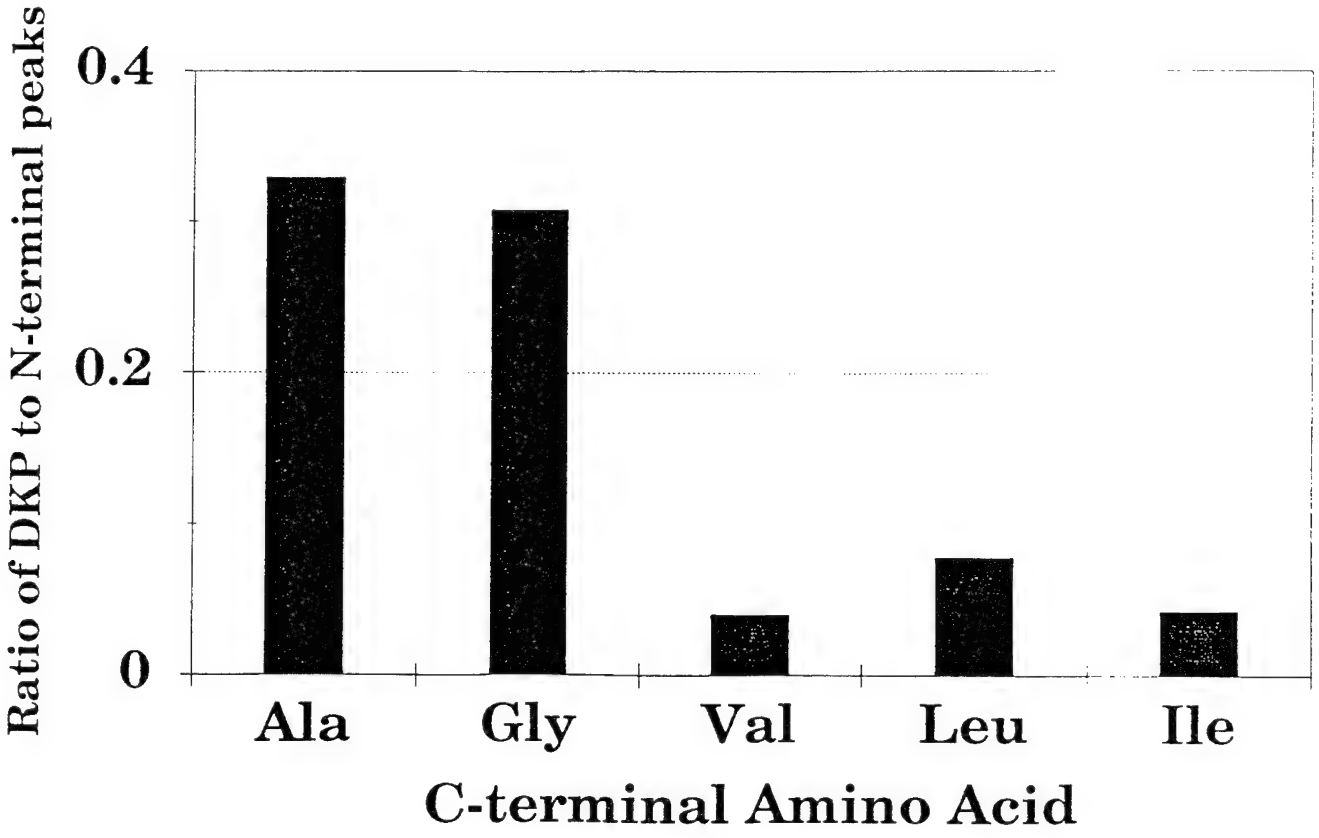

Figure 46. Ratio of DKP to N-terminal Peaks for Dipeptides with Aliphatic Hydrocarbon Substituents on C-terminal Amino Acid and Gly as the N-terminal Amino Acid

The presence of heteroatoms such as sulfur, nitrogen and oxygen in the substituents significantly affects the distribution of electron ionization products by increasing the possible number of ionization sites and fragmentation pathways. Hence, other EI reactions can make the N-terminal cleavage peak at m/z 30 inconsistent for dipeptides containing these types of substituents. The influence of different substituent functionalities on the formation of DKP and EI products is too complex to fully characterize. However, some of these dipeptides can be grouped according to the functionality of the substituent.

The amino acids, serine, threonine, and cysteine, which contain OH or SH functionalities on their substituents are structurally quite similar. Figure 47 represents the ratio of the DKP peaks to the m/z 30 peak from the EI α-cleavage process for Gly-Ser, Gly-Thr and Gly-Cys. These dipeptides show a larger ratio of DKP peaks to m/z 30 when compared to dipeptides with alkyl substituents on the C-terminus, as demonstrated by Gly-Gly used in Figure 47 as a reference. For all of these dipeptides, the hydrogen on the heteroatom of the substituent is in the γ position to the carbonyl oxygen, providing a favorable 6-membered ring geometry for hydrogen bonding. This should result in polarization of the C-terminal carbonyl bond rendering the carbonyl carbon more susceptible to nucleophilic attack and subsequent DKP formation.

The substituents of the amino acids can also influence competing reactions during pyrolysis mass spectrometry. These reactions can occur prior to, or after electron ionization. For example, Gly-Phe undergoes a unique reaction during pyrolysis and prior to EI to form

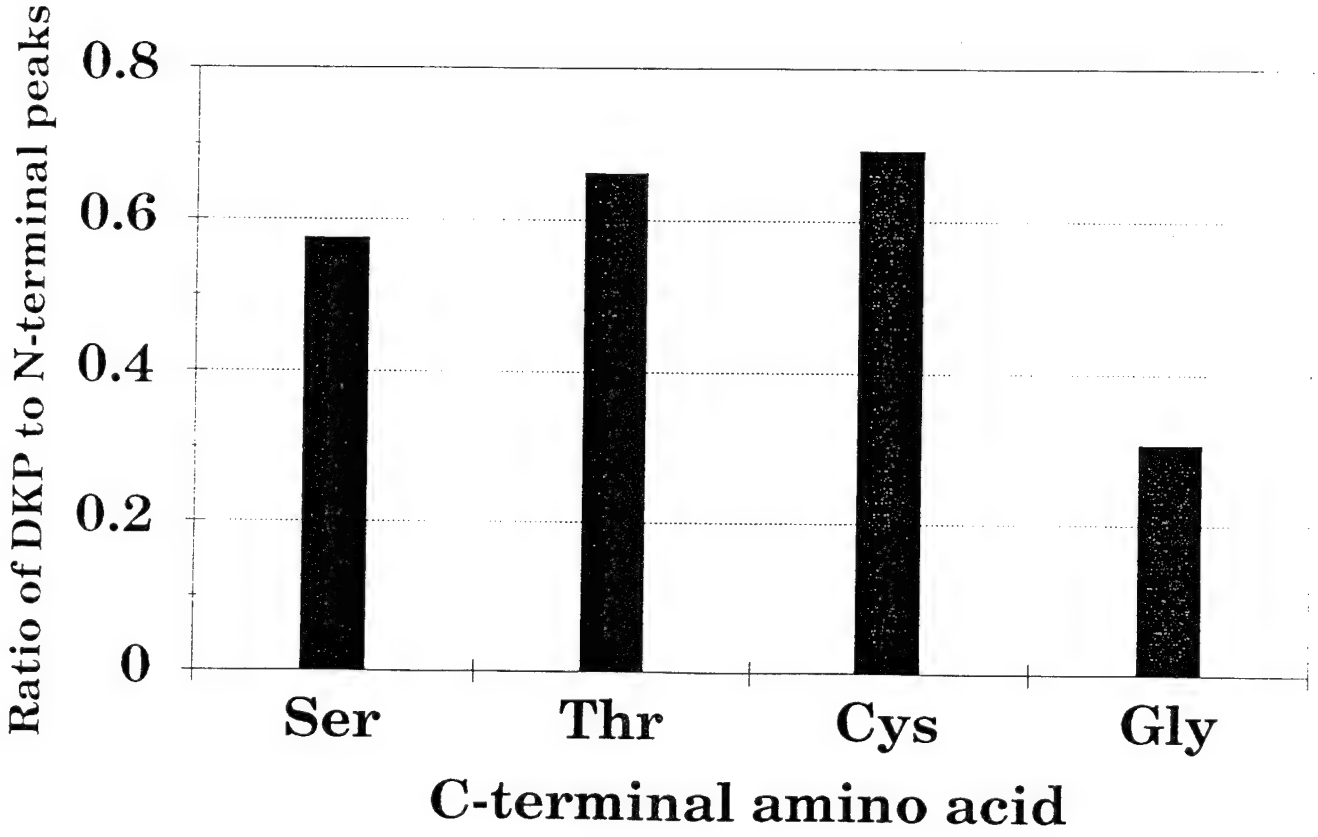

Figure 47. Intensity Ratio of DKP to N-terminal Peaks for Dipeptides with OH or SH Substituents on C-terminal Amino Acid and Gly as the N-terminal Amino Acid

cinnamic acid, which increases the DKP/N-terminal ratio. The mechanism for this process is summarized in Figure 48. Figure 49 is a pyrolysis mass spectrum of glycyl-tryptophan. The peak at m/z 130 corresponds to a product formed by the cleavage of the tryptophan substituent. This ion can be formed directly from the parent dipeptide as shown by the reaction scheme in Figure 50. The peak at m/z 243 represents the Gly-Trp DKP. A smaller N-terminal cleavage peak is observed at m/z 30 possibly due to the relative stability of the m/z 130 fragment ion. Svec and Junk observed pathways similar to this for certain dipeptides, but the dipeptide backbone, rather than the substituent retained the charge (57).

Figure 51 represents the pyrolysis mass spectrum of glycyl-proline. The peak at m/z 154 corresponds to the Gly-Pro DKP. The proline DKP does not fragment in a similar manner to other DKPs. For example, no peak at m/z 114 is observed for the unsubstituted DKP. Proline is the only amino acid which contains a cyclic substituent, preventing its cleavage as previously discussed for the other DKPs. Thus Gly-Pro cannot be compared with the other dipeptides having glycine as the N-terminus. However, it is interesting to note that the cyclization process occurs to a relatively high extent for this dipeptide, as demonstrated by the prominent peak at m/z 154. Samples containing proline have been shown to cyclize readily, including dipeptide esters and free dipeptides (57).

The pyrolysis mass spectrum of Gly-His is shown in Figure 52. The substituent of histidine contains an aromatic ring and is similar to the substituent in tryptophan. As discussed earlier, the stability of the tryptophan substituent drives a competing

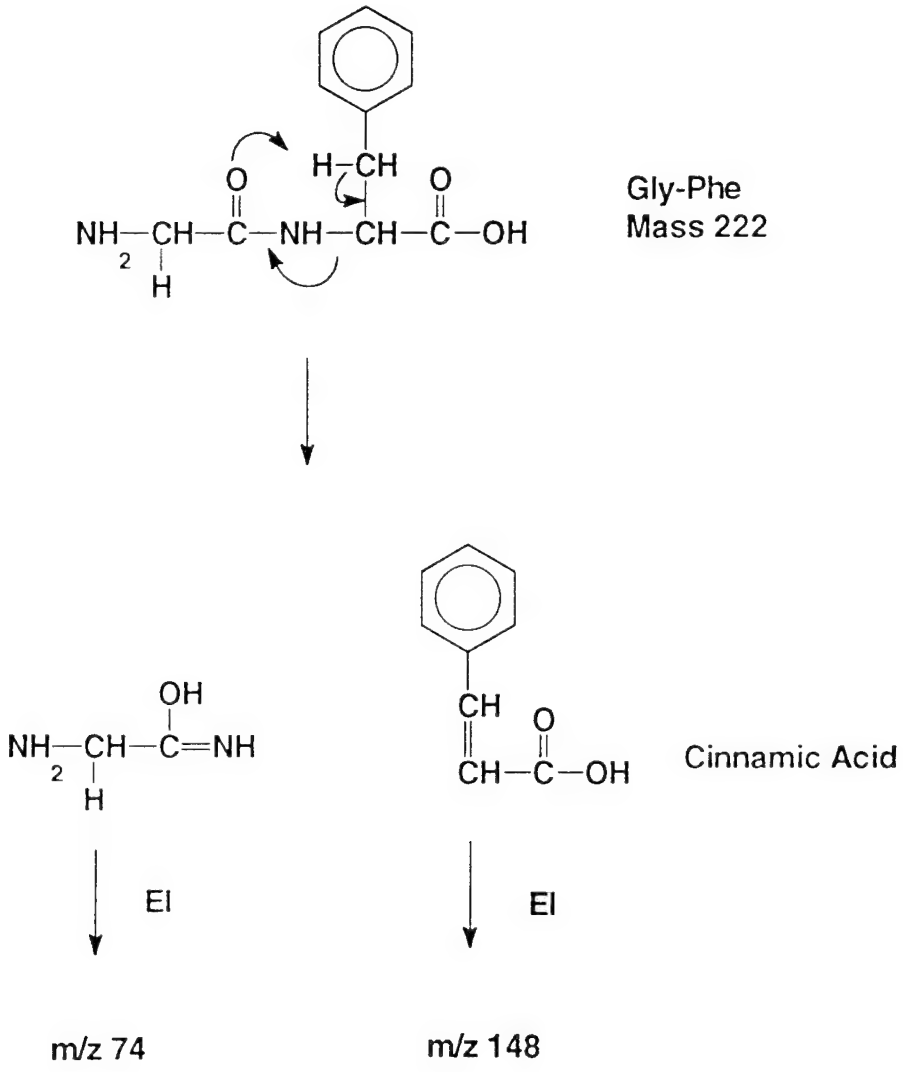

Figure 48. Mechanism of Cinnamic Acid Formation as Observed in Gly-Phe

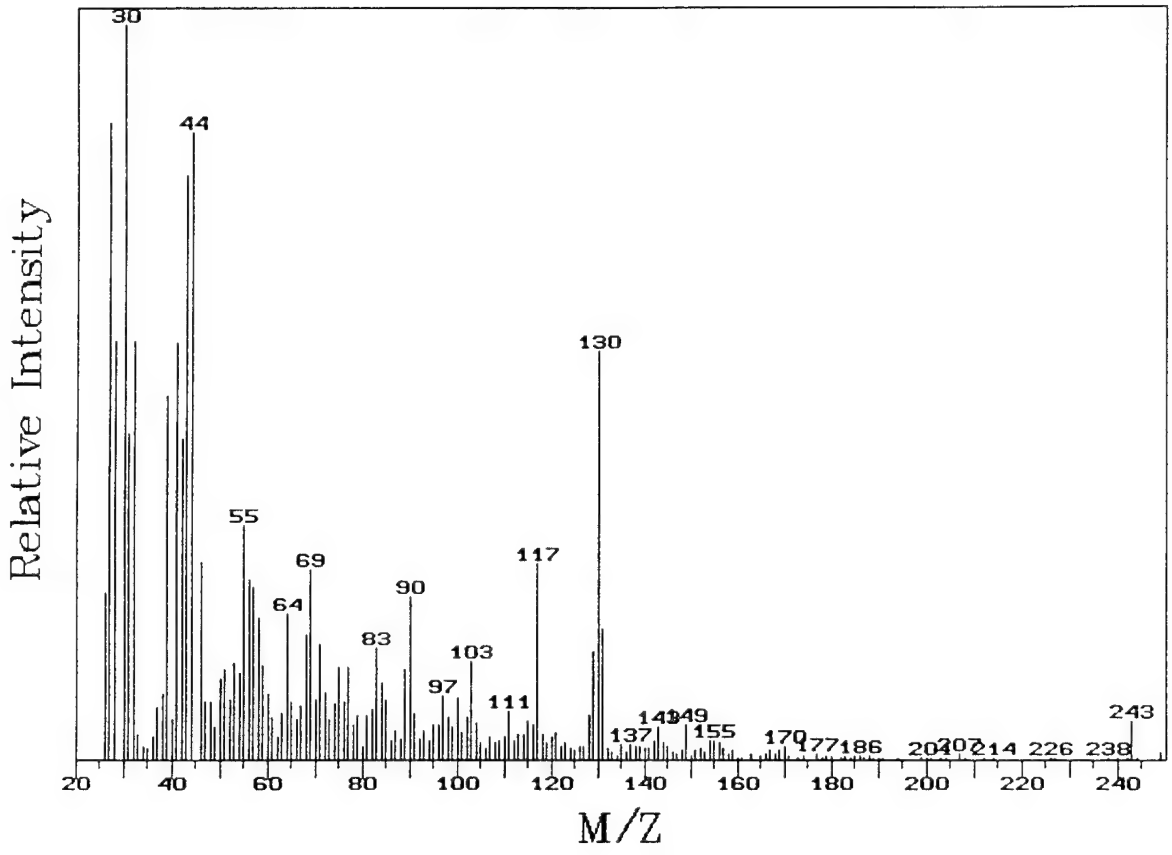

Figure 49. Pyrolysis Mass Spectrum of Gly-Trp

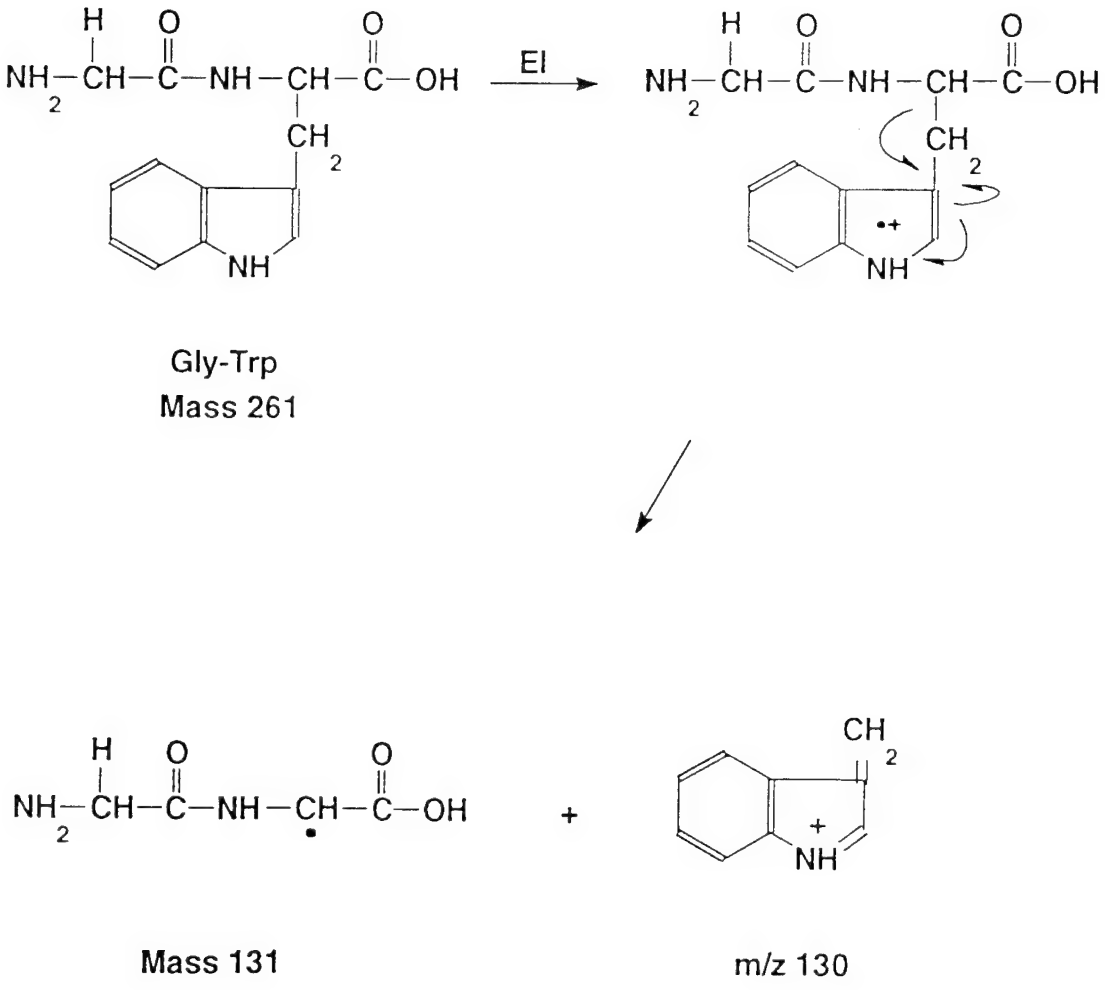

Figure 50. A Stable Additional Fragmentation Pathway as Observed in Gly-Trp

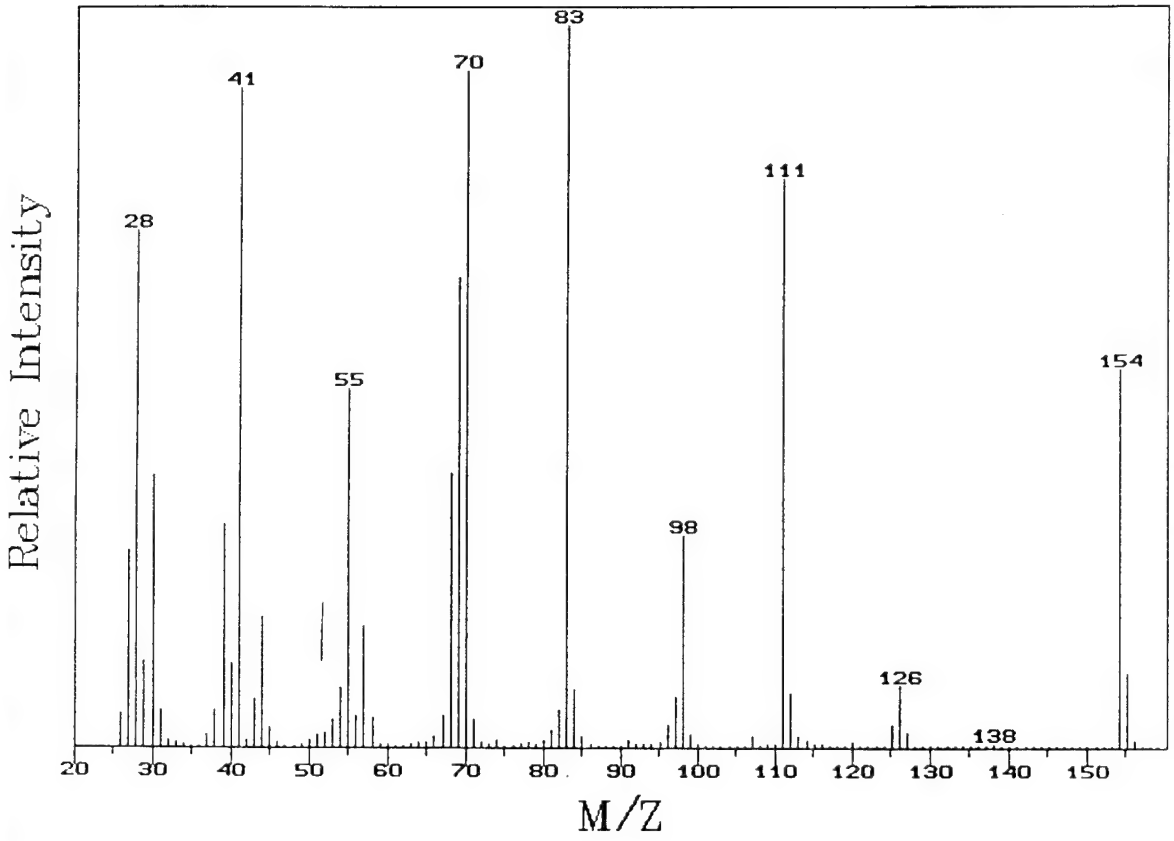

Figure 51. Pyrolysis Mass Spectrum of Gly-Pro

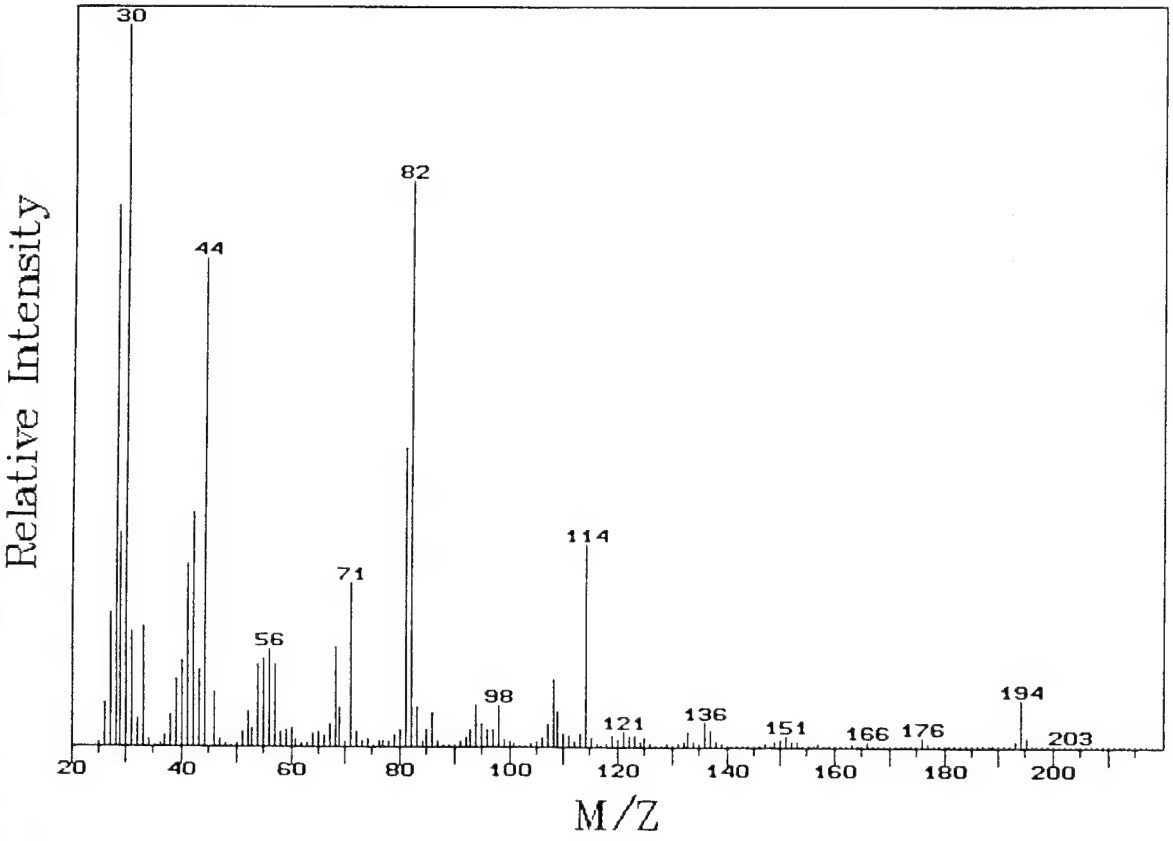

Figure 52. Pyrolysis Mass Spectrum of Gly-His

reaction (Figure 48). A similar reaction is observed with Gly-His. The loss of the histidine substituent produces a m/z 71 peak, but it does not dominate the mass spectrum, as the m/z 130 peak did in the Gly-Trp spectrum. The pyrolysis mass spectrum of Gly-His shows large peaks at m/z 194 and m/z 114, respectively representing the fully substituted DKP and the DKP after loss of the histidine substituent. Gly-His cyclizes readily to form a DKP, possibly due to the rigid nature of the histidine substituent which imposes less steric hinderance to the process.

The pyrolysis mass spectrum of Gly-Tyr is shown in Figure 53. Peaks at m/z 220 and m/z 114 represent the fully substituted and unsubstituted DKP. The base peak at m/z 107 occurs from the loss of the substituent from the tyrosine residue which can readily stabilize the positive charge through the phenyl ring. Due to the stability of this fragment ion, the competing N-terminal cleavage reactions is significantly reduced for this dipeptide, hence the relatively small peak at m/z 30.

Methionine contains a substituent with a thioether functionality which would not be predicted to enhance the nucleophilicity of the carbonyl carbon on the C-terminus as was the case with cysteine in Gly-Cys. Figure 54 is the pyrolysis mass spectrum of Gly-Met. The peak at m/z 206 has been assigned to the dipeptide molecular ion. The substituted DKP occurs at m/z 188 and the unsubstituted form at m/z 114.

Dipeptides containing lysine also cyclize to form DKPs in minor amounts. The DKP fragments by a characteristic loss of NH_3 from the lysine residue prior to loss of the remaining lysine substituent. Lysine and histidine were the only amino acids that

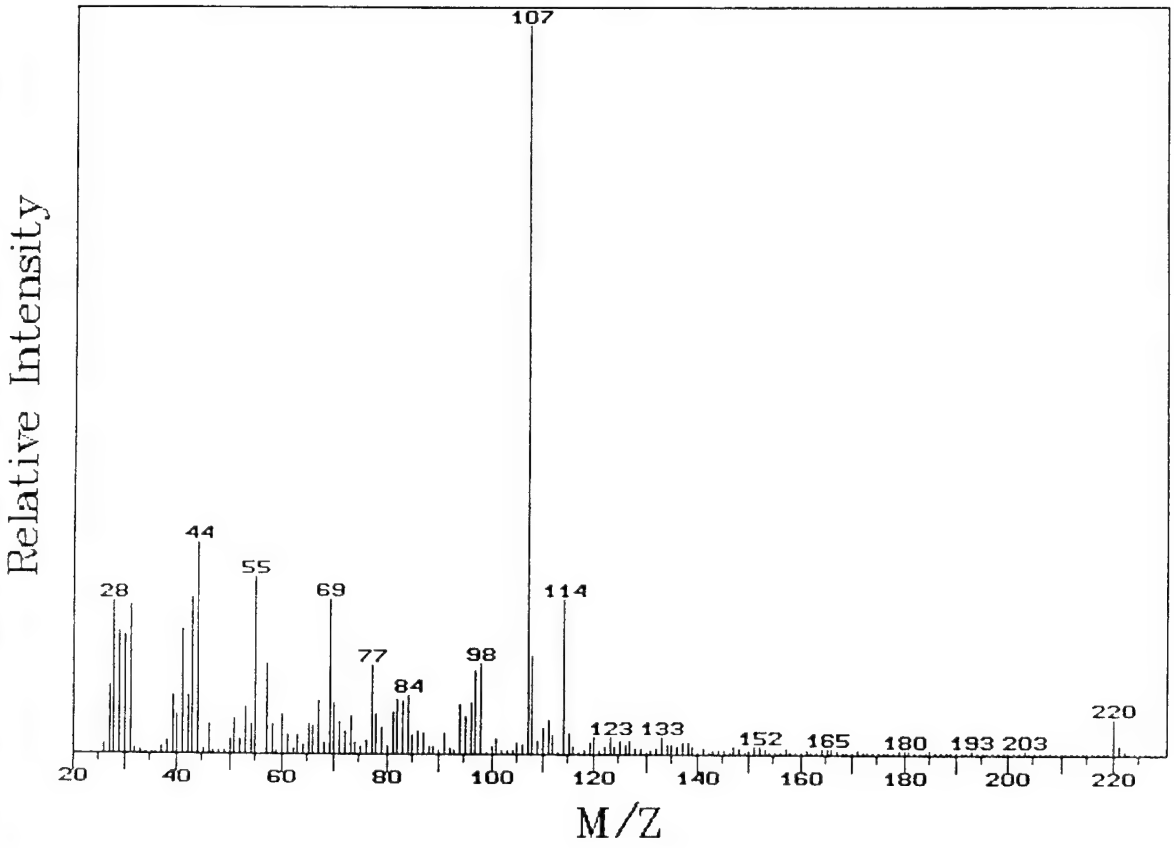

Figure 53. Pyrolysis Mass Spectrum of Gly-Tyr

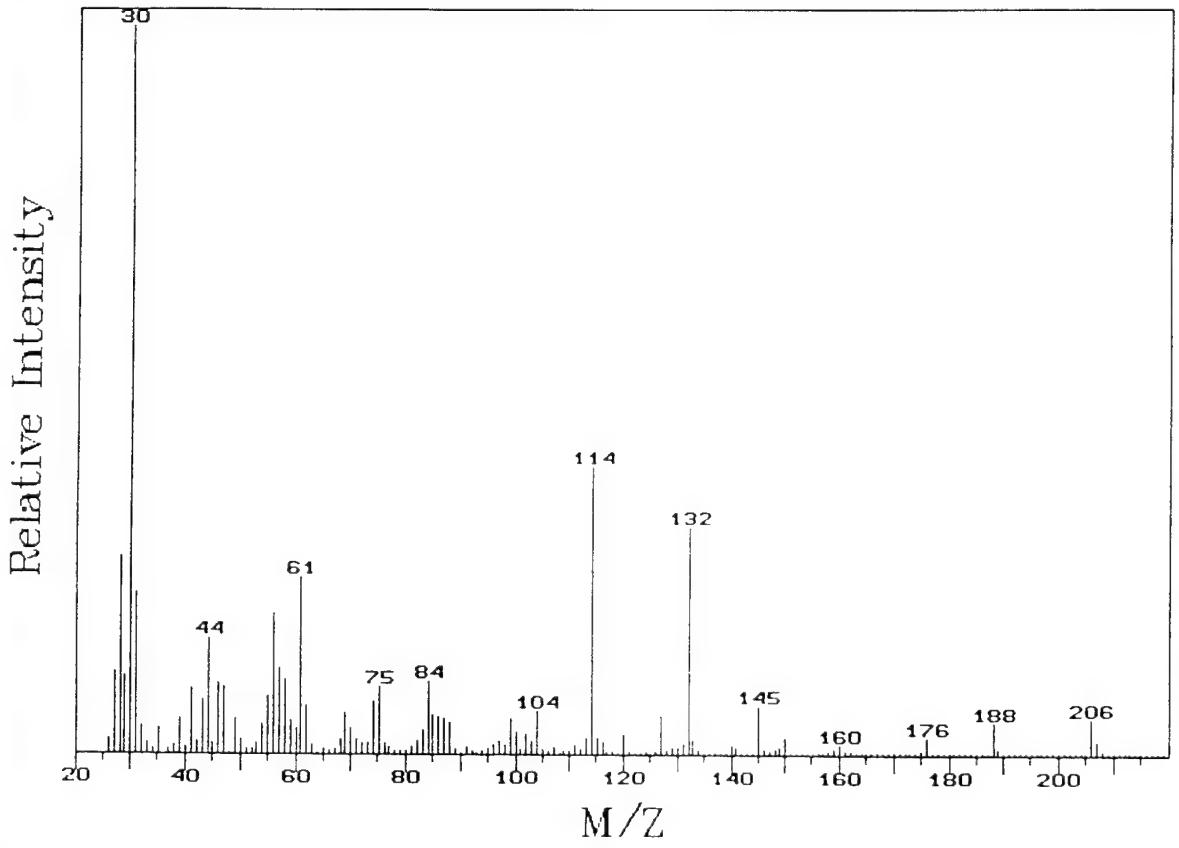

Figure 54. Pyrolysis Mass Spectrum of Gly-Met

contained an amino group in their substituents and reacted primarily via the DKP pathway. Asparagine and glutamine show minimal tendency for thermal cyclization to produce DKPs. As mentioned previously, dipeptides containing arginine did not cyclize to form DKPs. The increase in likely ionization sites can open more favorable decomposition pathways than the DKP process for these dipeptides.

The presence of additional carboxylic acid functionalities appeared to inhibit the DKP process. Therefore, it is not surprising that dipeptides containing aspartic acid and glutamic acid showed no tendency for thermal cyclization to form DKPs. The alternate pathways for the amino acids which do not form DKPs have not been explored fully.

Interestingly, the hydrophilicity "physical property" as defined by Hellberg *et al.* shows some correlation to DKP formation (76). The five amino acids described as the most hydrophilic (aspartic acid, asparagine, glutamic acid, arginine, and lysine) all show relatively small or no DKP formation. This is probably due to the fact that an increased number of electronegative atoms in the amino acids not only increase the hydrophilicity, but also the number of likely ionization sites, creating additional EI pathways.

2. Dipeptides with Glycine as the C-terminus

Dipeptides with glycine as the C-terminus have also been investigated. The N-terminus of these dipeptides was varied among the 20 common amino acids. Results indicate that DKP and EI processes occur to similar extents whether glycine is fixed as the C-terminus or the N-terminus of the dipeptide. However, when the N-terminus is varied, EI products such as N-terminal cleavage also vary. This eliminates a common peak for comparison of the spectra.

Qualitatively, dipeptides can be categorized as good, average, or poor for thermal DKP formation by examining the relative size of the substituted DKP peak and the m/z 114 peak to the other peaks in the mass spectrum of that particular dipeptide.

Figure 55 is a pyrolysis mass spectrum of Met-Gly. This dipeptide is categorized as one in which the DKP process is good. The DKP peaks at m/z 188 and m/z 114 (substituted and unsubstituted DKP) dominate other peaks in the spectrum. The results are similar to those obtained for the dipeptide Gly-Met which also formed large amounts of DKP products. In the pyrolysis mass spectrum of Lys-Gly, Figure 56, DKP peaks at m/z 114 and m/z 185 exist, but are fairly small in comparison to other peaks. Dipeptides with spectra similar to Lys-Gly are classified as 'average' for the cyclization process. Figure 57 is a pyrolysis mass spectrum of Trp-Gly. Processes discussed earlier for Gly-Trp (see Figure 49) dominate over the DKP process in this dipeptide as well, and therefore it is classified as 'poor' for the DKP process. Table XIV. summarizes the 20 dipeptides with glycine as the C-terminus and classifies them as good, average, or poor. Information can be gained as to the general nature of the dipeptide from this classification. Dipeptides containing hydrocarbon substituents on the N-terminus all form DKP products to a large extent, which is similar to the results obtained when these amino acids were on the C-terminus. Also, many of the dipeptides which were shown to undergo DKP production to a small, or no extent when glycine was on the N-terminus also

Table XIV. Classifications of DKP forming dipeptides with glycine as the C-terminus

Good	Average	Poor
Ala-Gly	His-Gly	Arg-Gly
Cys-Gly	Ile-Gly	Asn-Gly
Gly-Gly	Lys-Gly	Asp-Gly
Leu-Gly	Thr-Gly	Gln-Gly
Met-Gly	Tyr-Gly	Glu-Gly
Phe-Gly		Trp-Gly
Pro-Gly		
Ser-Gly		
Val-Gly		

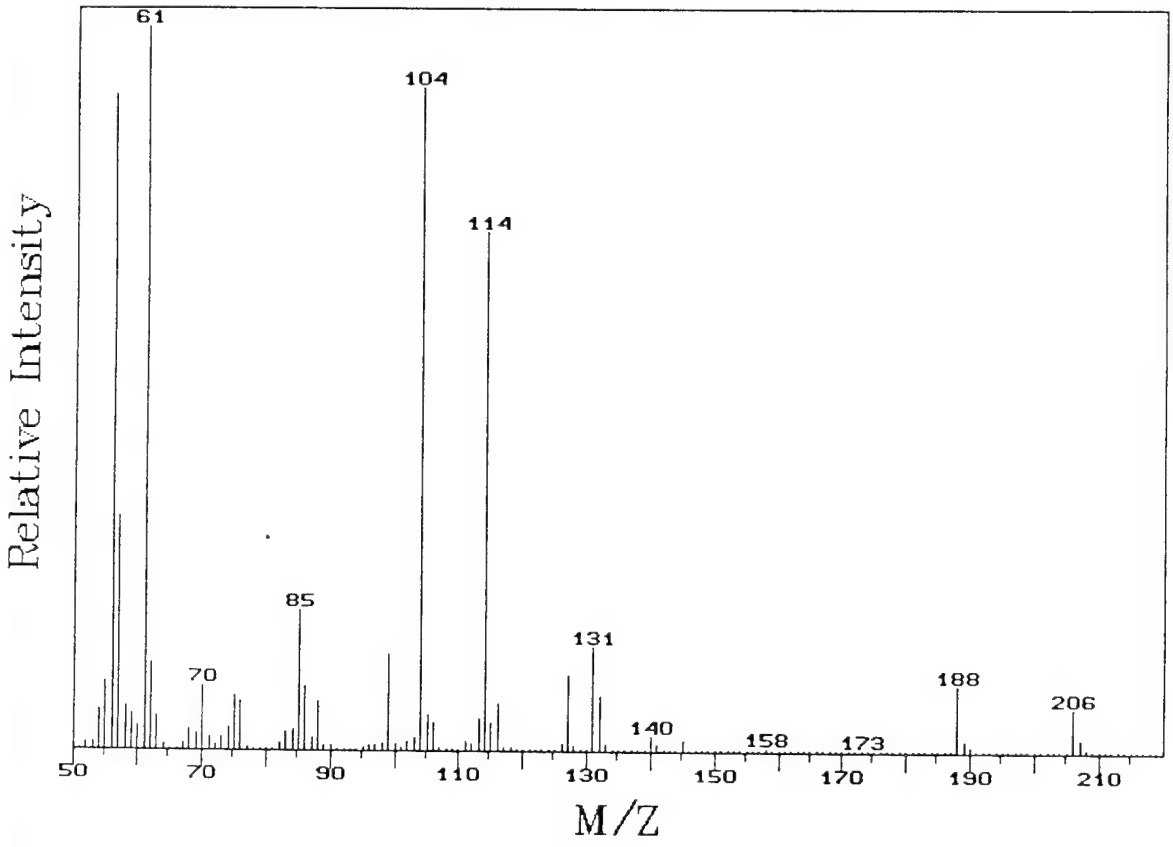

Figure 55. Pyrolysis Mass Spectrum of Met-Gly

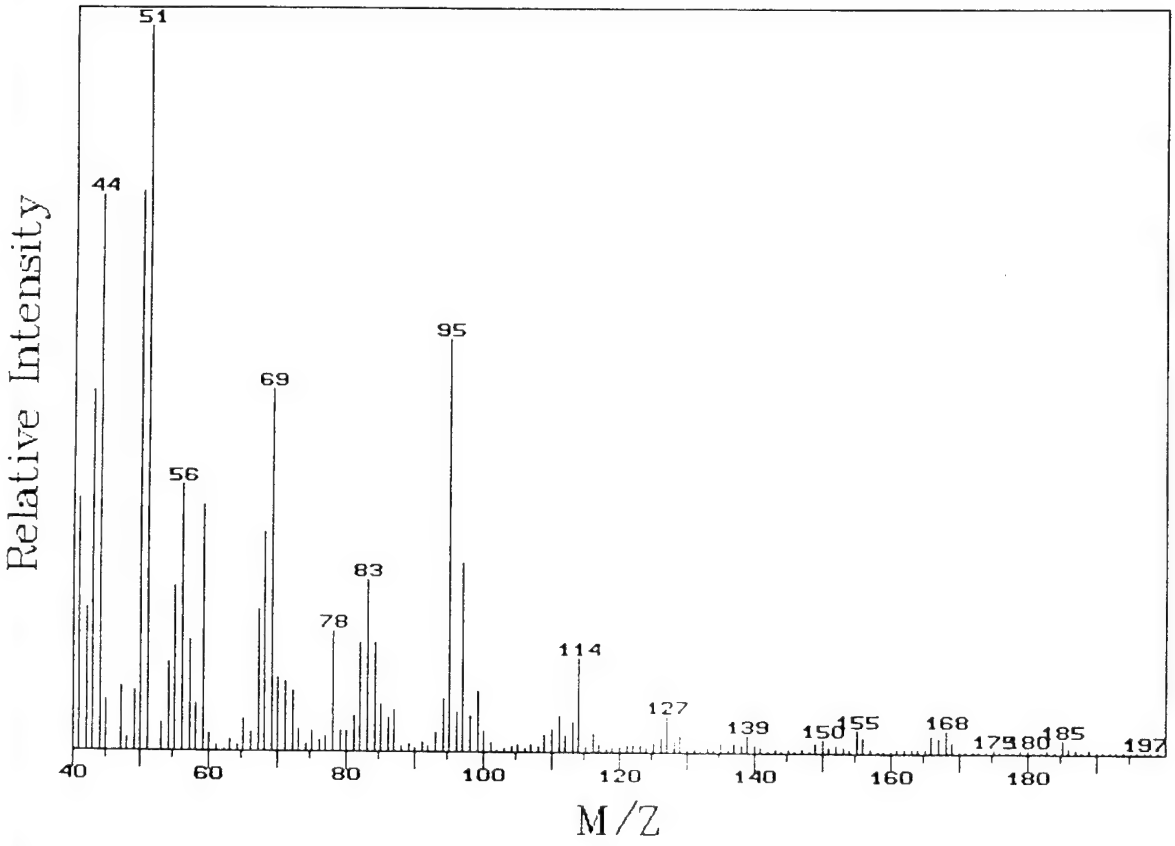

Figure 56. Pyrolysis Mass Spectrum of Lys-Gly

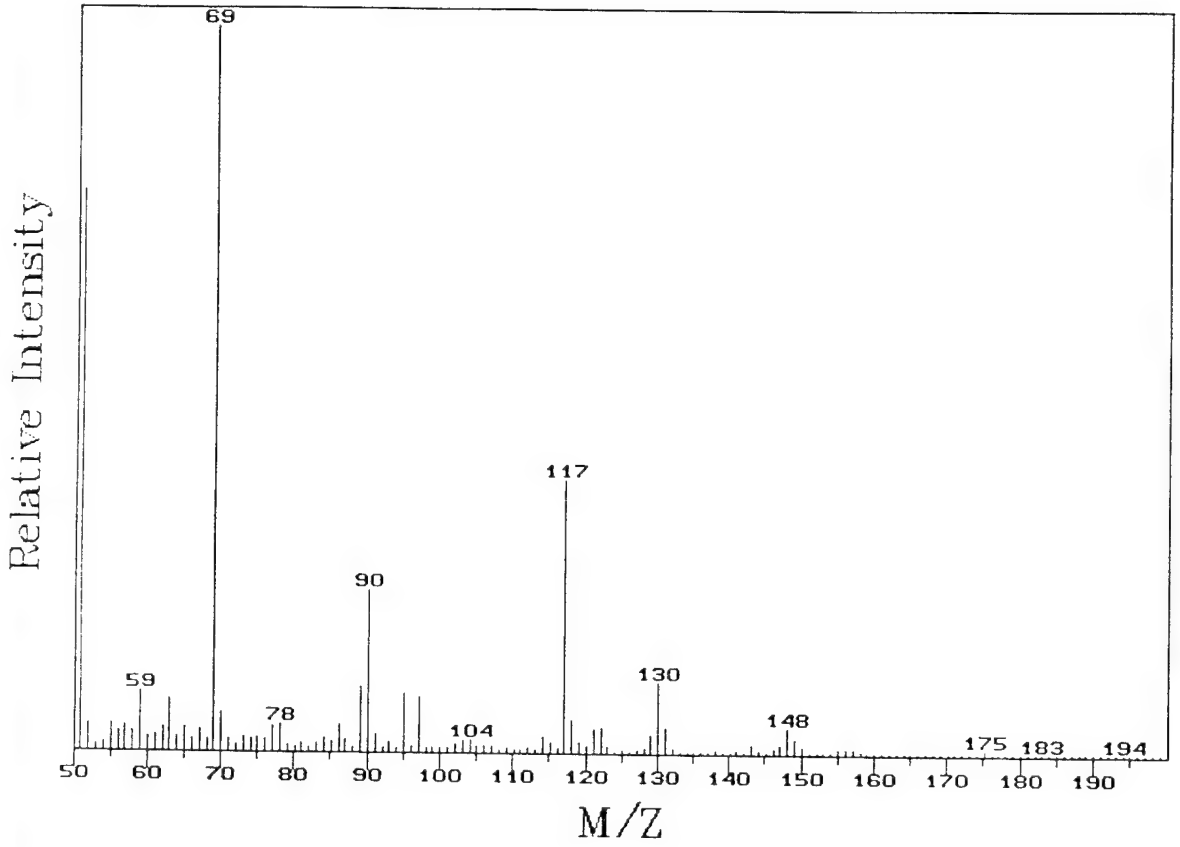

Figure 57. Pyrolysis Mass Spectrum of Trp-Gly

show a similar trend when glycine is the C-terminus.

3. Conclusions on dipeptide study

Thermal cyclization of dipeptides to form DKPs during pyrolysis has been shown to occur for a variety of dipeptides during pyrolysis mass spectrometry. The extent of the process has been related to the size and chemistry of the substituents on the varying amino acids. Controlling factors were similar to those discussed by Hellberg *et al* (76) (steric and electronic).

For dipeptides with glycine as the N-terminus several groups of amino acids have been established as having similar chemistry. The extent of the DKP formation was related to the steric hinderance created from the substituent in dipeptides with no heteroatoms in the aliphatic substituents (Gly-Gly, Gly-Ala, Gly-Leu, Gly-Ile, Gly-Val). Electrophilic/nucleophilic character were also established as factors which can assist or hinder the process. Hydrogen bonding to the carbonyl on the C-terminal amino acid can aid in the cyclization process in Gly-Cys, Gly-Ser, and Gly-Thr. Substituents containing nitrogen and oxygen can cause other reaction pathways, as for Gly-Asp, Gly-Asn, Gly-Glu, Gly-Gln, and Gly-Arg. The formation of stable neutral products or charged fragments can be favored as in the case of Gly-Phe and Gly-Trp respectively. Other dipeptides were classified qualitatively according to the extent of DKP formation.

DKP markers, unique for most dipeptides can be a useful method for identifying dipeptides in solutions, or from mixtures of dipeptides. In addition, DKP products have been shown to form from peptides with chain lengths up to six amino acids. Identification of

dipeptides from DKP formation observed in pyrolysis mass spectrometry is more rapid than analysis by gas chromatography-mass spectrometry, and involves no derivatization or involved sample preparation.

III. Biomarker Identification

The rationale for the application of the CBMS to bacterial and toxin identification has been to use a series of daughter-parent mass spectral peaks as biomarkers which serve to differentiate the various background and biological samples. The biomarkers were chosen due to either their biological or statistical significance. Based on work conducted at Dugway Proving Grounds, nineteen ions were chosen as biomarkers for the evaluation tests. The need to identify the chemical species and the biochemical precursors for each selected biomarker becomes apparent in developing a rapid chemotaxonomic microorganism identification system. This type of in-depth investigation using model compounds, daughter ion scans, and parent ion scans will provide a data base to interpret the information generated in ongoing tests.

The results from the daughter and parent scans for the 19 ions are shown in Table XV. The parent scans for most of the biomarker ions indicate several biochemical precursors for each ion. Therefore, identifying the chemical species that produces each biomarker becomes more difficult. The following presents possible chemical species and pyrolysis mechanisms for the biomarkers that are best understood. For some of the ions, high resolution mass spectrometry will be required to elucidate the possible structures.

Table XV. Major Ions Identified in the Daughter and Parent Scans of the Biomarker Ion

BIOMARKER	DAUGHTER IONS	PARENT IONS
67	39,41	82,95,109
81	41,53,67	96, 98,108,109,110, 116,123,135,195,215, 231
82	41, 54, 55, 67	97,1101125,151
89	39,63	115,1161117
91	65	107,118,119,120,133, 147
95	41, 55, 67, 68, 81	110,112,123,124,137, 138,151,152,165,166
102	31,76,77	129,130
103	51,76,77	120,130
105	77, 78, 79, 87	133,1471161
115	70,87,97	143,157,169,185,195, 209,223,237
117	37, 62, 90, 99	132,144,145,153,186, 200
128	57, 72, 77, 84, 100, 101, 113	145,146,155,156
129	55, 57, 73, 84, 87,102	146,156,157,171,185, 197
131	77,86,91,103,104	146,148,158,159,174, 187,200,202,216, 230,243
135	81,108	163,178,191

a. m/z 67

Figure 58 demonstrates the ions associated with m/z 67. One possible source of m/z 67 may be the nucleic acid base cytosine. Cytosine produces a m/z 95 ion (loss of -NH2) which further fragments to m/z 67. There is some speculation that m/z 67 is a fragment of ethylfuran, however, this has not been substantiated by the parent ion spectra.

b. m/z 81

One of the biochemical sources of m/z 81 is nucleic acids. The parent spectrum of m/z 81 contains m/z 108, 135, 151, 215, and 231 as seen in Figure 59. All of these ions have been identified by Wiebers and Dudek as fragments of the nucleic acid bases adenine and guanine (79,80). Pyrolysis-mass spectral analysis of a mixture of model DNA building blocks (TMP, CMP, AMP, and GMP) show the same fragmentation mechanisms that were observed in the whole cell. Furthermore, daughter ion scans of m/z 215 and 231 contain the m/z 81 fragment.

Another possible source of m/z 81 could be from ethylfuran which results from the pyrolysis of carbohydrates. Ethylfuran (m/z 96) fragments to 81 (loss of -CH3) and then further fragments to 67 (loss of -CH2). This fragmentation was observed in the daughter ion and parent ion spectra of m/z 81.

c. m/z 91

The m/z 91 ion likely has several sources because it is a very favorable ion in mass spectrometry. One suggested source is the amino acid phenylalanine (m/z 165) which fragments to m/z 120 (loss of -COOH) which can further fragments to m/z 91. M/z 91 is also known to occur during pyrolysis from most compounds.

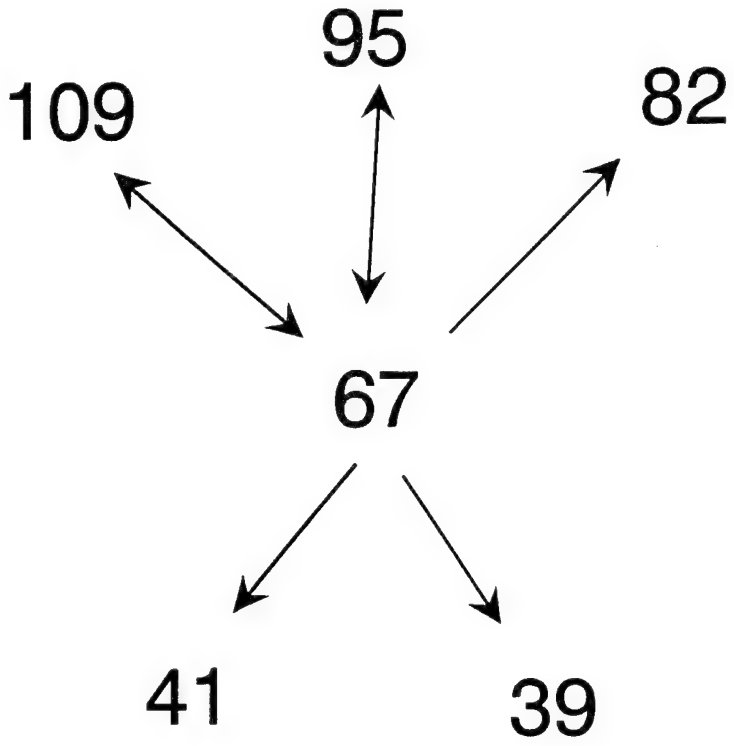

Figure 58. Precursor/product relationships of m/z 67.
↔ confirmed both directions, → confirmed one direction.

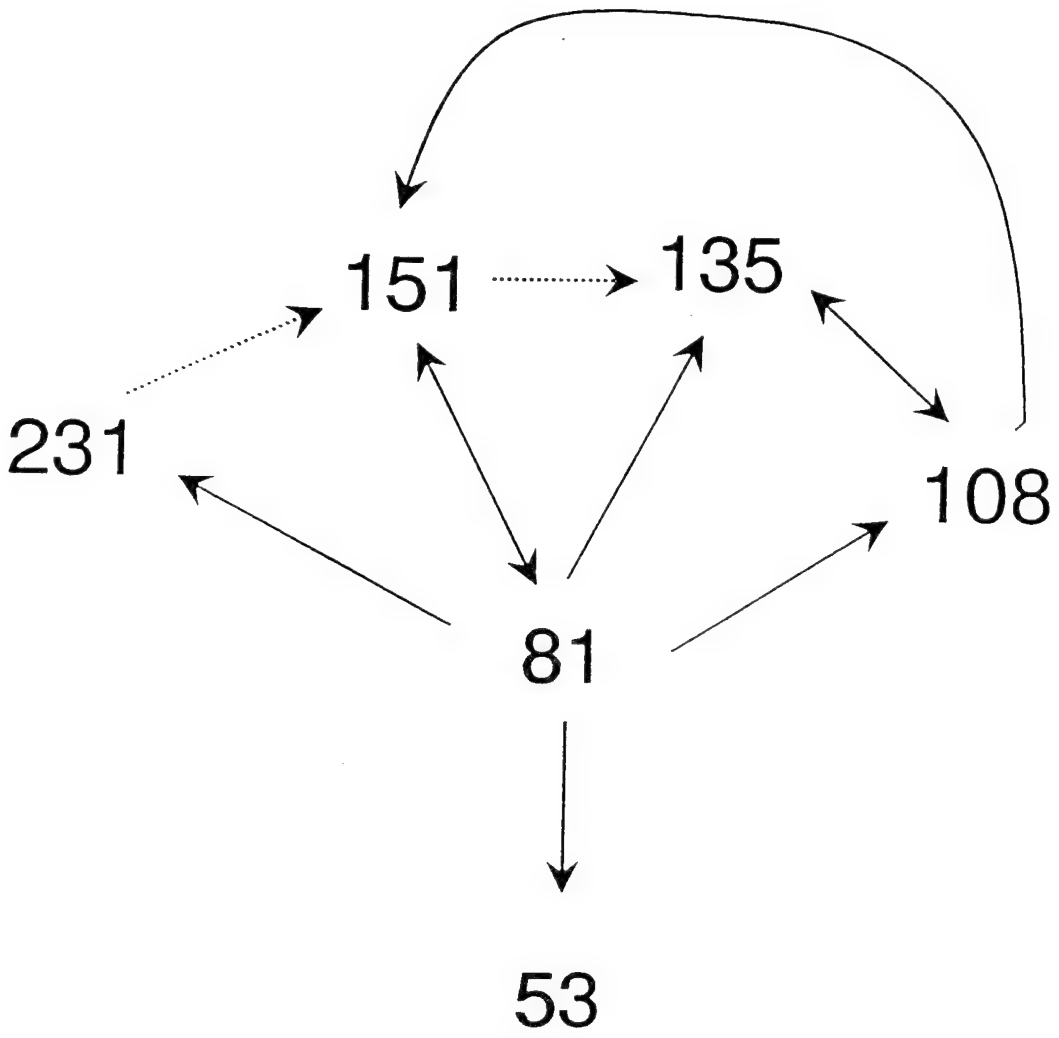

Figure 59. Precursor/product relationships of m/z 81.
↔ confirmed both directions, → confirmed one direction,
⇢ noted in literature.

d. m/z 103

The sources of m/z 103 are primarily the amino acids phenylalanine and tryptophan. The major fragments of phenylalanine (mw=120) are m/z 120, 103 and 77. Tryptophan (mw=130) fragments under electron ionization to m/z 117, 103, and 77. The only major ions for m/z 103 in the parent ion scan are m/z 120 and 130 (Figure 60).

e. m/z 115

The ion at m/z 115 most likely fragments from D-ribose (m/z 150) or RNA. Ribose fragments to m/z 133 which further fragments to 115. The other sources of m/z 115 have not been identified yet and will require high resolution mass spectrometry to be separated.

f. m/z 117

Like m/z 115, m/z 117 has multiple sources. The m/z 117 can result from nucleic acids or more precisely, deoxyribose (m/z 134) or from the amino acid tryptophan. Deoxyribose fragments to m/z 117 (loss of -OH) which further fragments to 99 (loss of H_20). Full scan spectra of DNA extracts from various bacteria also show a peak at 186 just as the parent scan of 117 does, demonstrating the feasibility that DNA is a major biochemical precursor of m/z 117.

As mentioned, tryptophan (m/z 204) also fragments to indole (m/z 117). This may be another source of m/z 117. There are several other biochemical sources of ion 117. However, not all of the parent ions have been identified. Ion 117 is most likely more than one chemical species.

g. m/z 128

M/z 128 has been reported in the spectra of the pure component dipeptide alanyl-glycine (m/z 146) as the diketopiperazine. Therefore, one source of 128 is the diketopiperazine of these two amino acids. Furthermore, m/z 146 was observed in the parent scan of m/z 128.

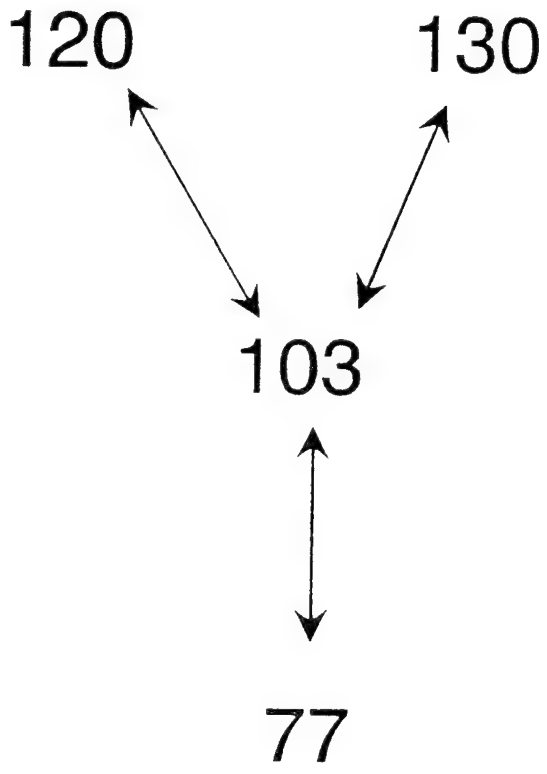

Figure 60. Precursor/product relationships of m/z 103.
↔ confirmed both directions.

Unlike some of the other biomarker ions, m/z 128 has very few ions in the parent scan. M/z 155 and 156 are present in the parent spectrum but have not been identified yet. Figure 61 also shows the many fragments of m/z 128 seen in the daughter scan.

h. m/z 129

The most likely source of the m/z 129 fragment is the C16:0 fatty acid (m/z 256). The C16:0 fatty acid fragments to m/z 227, 185, 171, 157, 129, 87, and 73. All of these fragments were observed in the parent and daughter ion scans of 129 (Figure 52). However, there are several other ions in both the parent and daughter spectra that cannot be attributed to palmitic acid. These ions are 55, 57, 84, 102, 146, 156, and 197 (Figure 62). Therefore, it is highly probable that m/z 129 has more than one biochemical precursor.

i. m/z 131

This ion is a known fragment of tryptophan (m/z 204). Tryptophan fragments to 131 which fragments further to 103. Also, m/z 243 is the diketopiperazine of gly-trp and was seen in the parent spectrum of 131. However, ions like 146, 148, 158, 159, 174, 187, 200, 202, 216 and others observed in the parent spectra have not been identified and require high resolutions mass spectrometry to be elucidated.

j. m/z 135

Figure 63 summarizes the ions observed in both the parent and daughter ion scans. As was mentioned earlier, m/z 135 was observed in the parent spectrum of m/z 81. The daughter ion scan of m/z 135 demonstrates fragmentation to m/z 108 and 81. Interestingly, the daughter scan of m/z 135 for the pure component 2'-deoxyadenosine is identical to that of the whole cells from *B. neotomae*.

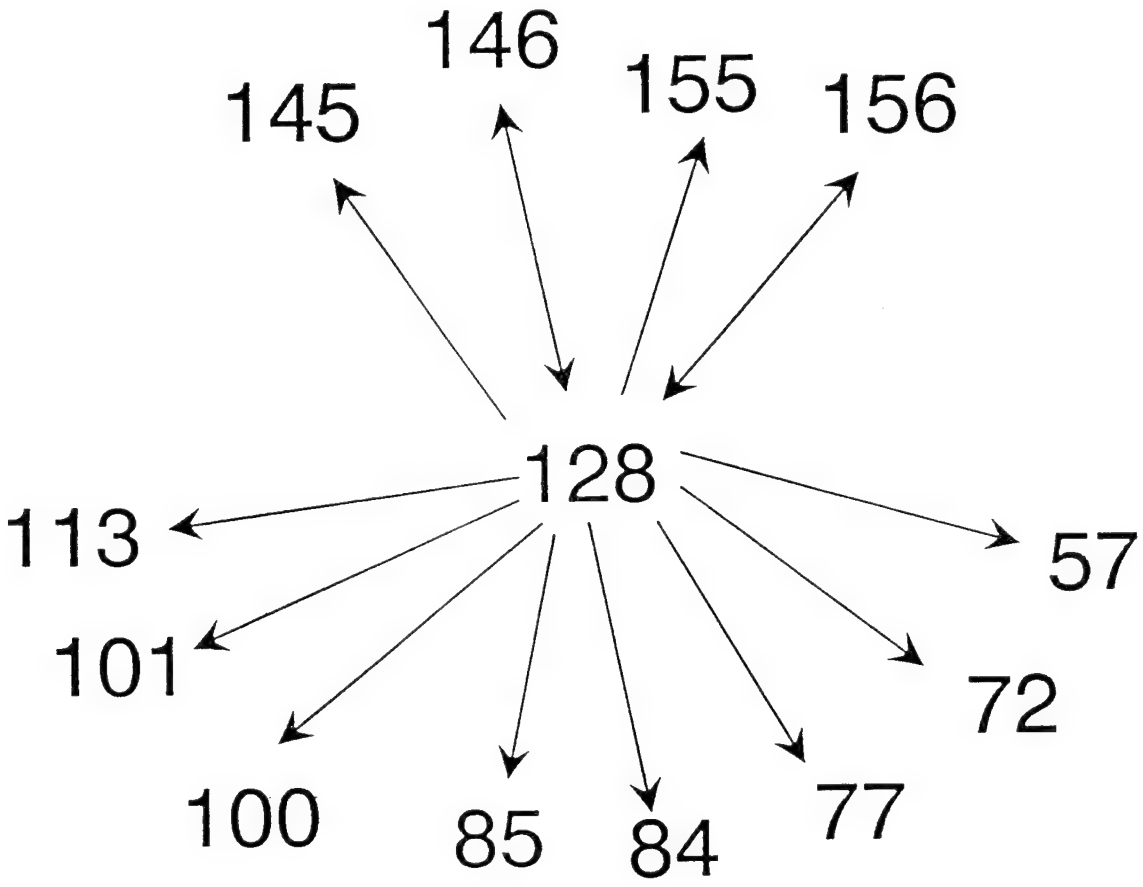

Figure 61. Precursor/product relationships of m/z 128.
↔ confirmed both directions, → confirmed one direction.

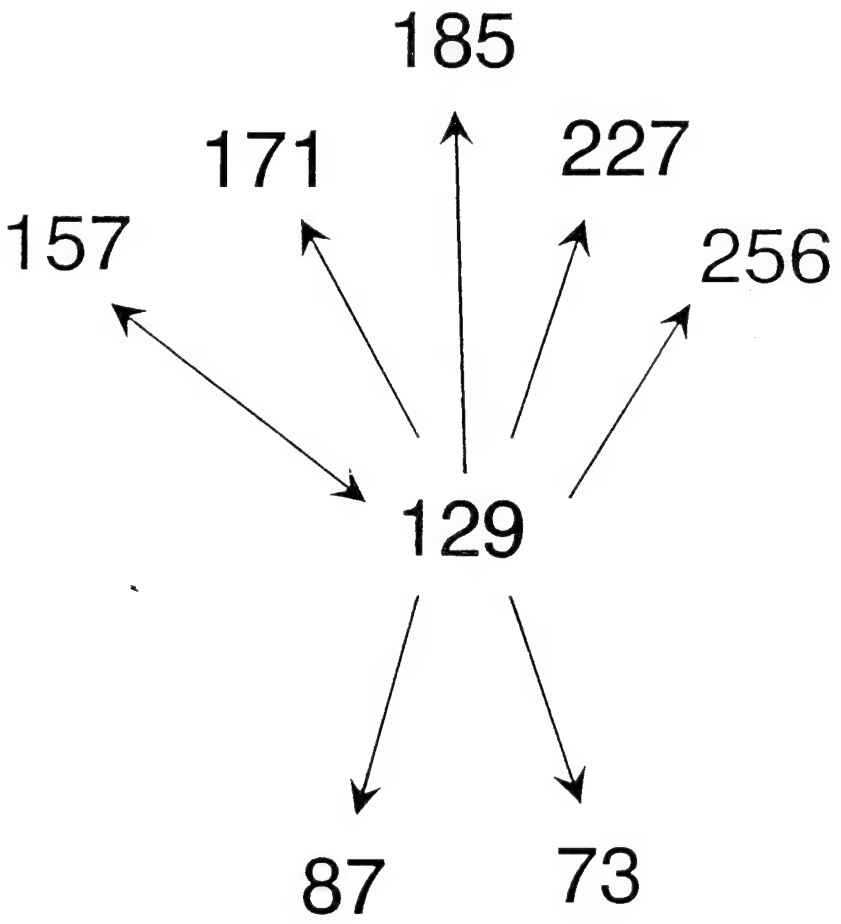

Figure 62. Precursor/product relationships of m/z 129.
↔ confirmed both directions, → confirmed one direction.

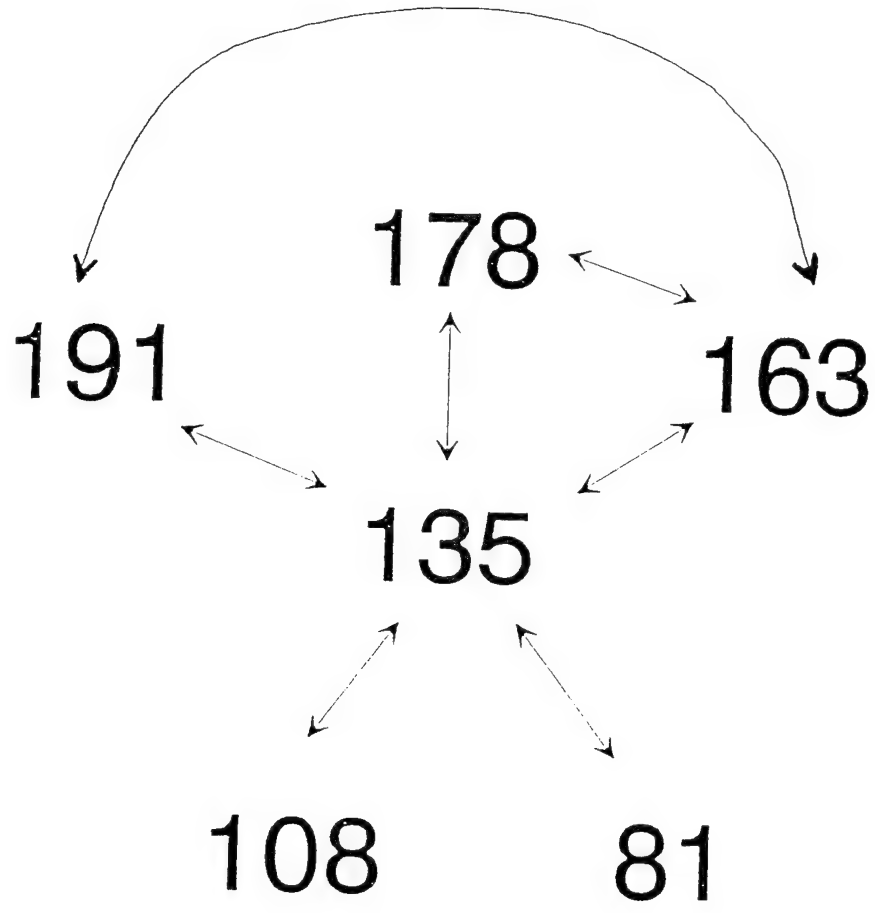

Figure 63. Precursor/product relationships of m/z 135.
↔ confirmed both directions.

Furthermore, ions found in the parent ion scan of m/z 135 of the whole cell are also observed in the full scan spectrum of 2'-deoxyadenosine. It is therefore very possible that the chemical species for m/z 135 is adenine, due to the information collected on 2'-deoxyadenosine.

k. Conclusions on biomarker study

The biomarker ions of interest are a collection of fragments from peptides, nucleic acids, and lipids. The work done previously on pure cell components and pure standards has been demonstrated to be reproducible in the whole bacterial cells. In other words, the work done on the pure dipeptide phenylalanyl-leucine has aided in identifying m/z 103 as a fragment of this dipeptide as one of its biochemical precursors. Although most of the biomarker ions have more than one source, several of the sources have been identified therefore allowing chemical species identification of the biomarker.

IV. DNA Studies

Past investigations have shown that pyrolysis mass spectrometry (Py-MS) can be applied to DNA yielding information concerning the qualitative composition of DNA, the detection and identification of modified nucleosides and the base sequence of DNA fragments. This paper will demonstrate that quantitative compositional information can also be obtained via Py-MS. Mass spectra of DNA exhibit major peaks at the mass values for all of the purine and pyrimidine bases. Therefore, measurement of the base peaks reflects the amount of a base present (79). However, the volatility of the various bases is not the same and is in the order

of C > T > A > G.

The technique of Py-MS demonstrates how the standard curve may be used in the quantitative analysis of the G/C molar ratio of DNA extracts from bacteria and G/C molar ratios of amplified PCR products. It is important to note however, that a G/C ratio is an exclusionary determinant rather than a supportive one. GC ratios are useful for determining unrelatedness, but cannot be used to support the claim that two organisms are related. Two organisms may have similar GC ratios, but their sequence of the bases may vary dramatically.

a. Construction of the Standard Curve

Mass spectral analysis was carried out on three individual samples of each of the following sources: **G/C** molar ratios of 100%, 75%, 67%, 58%, 46%, 33%, 25%, and 0%. From the mass spectra, the peaks of the nucleic acid bases were identified. The 24 samples were then analyzed via principal component analysis software. The first principal component plot (Figure 64) demonstrates how the pure standards separated out. A second principal component plot was constructed using the 8 most centric points from each of the respective clusters of the pure standards and then allowing the PCA software to exhaust its component capabilities to produce a linear plot, Figure 65. The standard curve that was produced with the pure standards may have the capability to determine the G/C molar ratio of an unknown DNA extract or PCR product. However, the curve is slightly less than linear. The next step for this procedure would be to test the validity of the curve with an unknown pure standard and then with a pure bacterial DNA extract and with an amplified PCR product. The amplified PCR results would be predicted to be more accurate than the DNA extract because

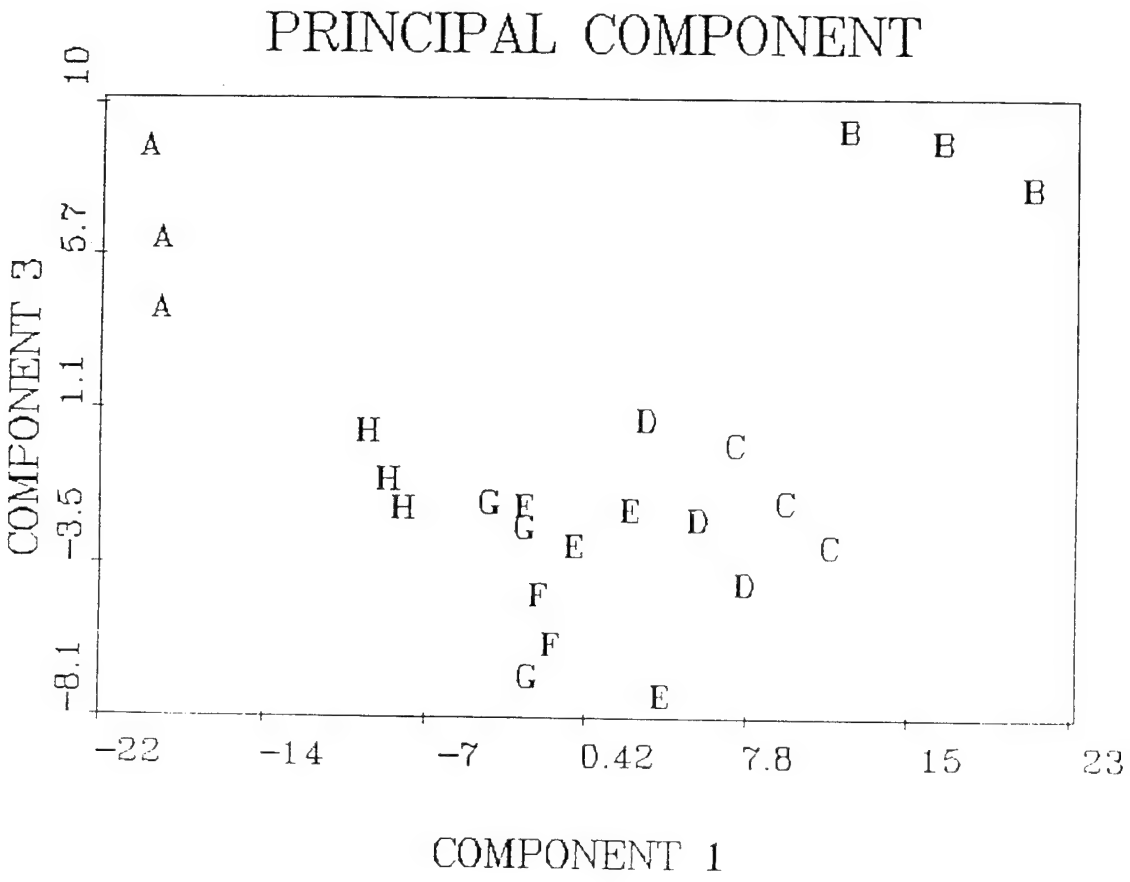

CATEGORY	CONTENT
A	ALL G+C
B	ALL A+T
C	25% G+C
D	33% G+C (B. anthracis)
E	46% G+C (Y. pestis)
F	58% G+C (B. melitensis)
G	67% G+C (P. aeruginosa)
H	75% G+C

Figure 64. Principal Component Plot of various G+C ratios.

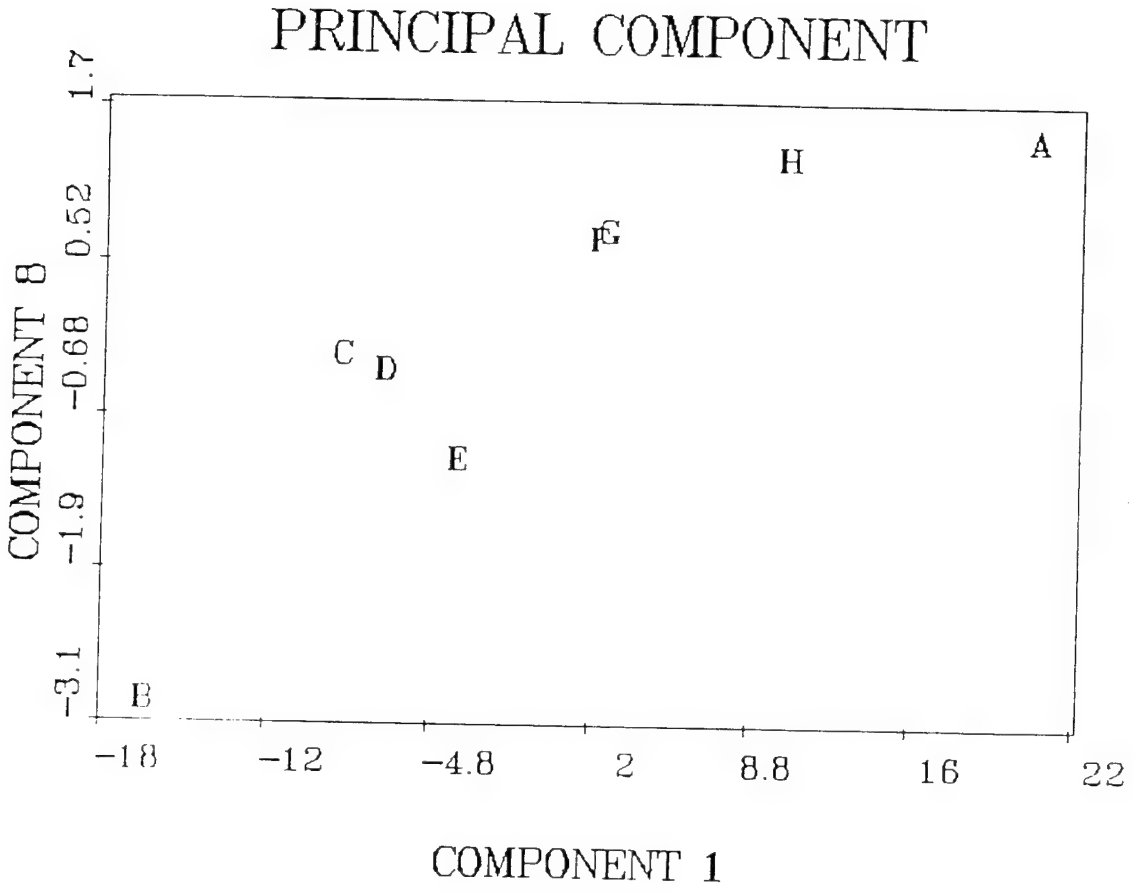

Figure 65. Principal Component Plot of various G+C ratios to demonstrate a linear relationship.

the RNA has been eliminated in the PCR product. Microbial cells have a much larger quantity of RNA than of DNA.

Other methods exist to calculate G/C molar ratios, but the mass spectral method has the advantage of analyzing very limited amounts of DNA. The forte of the mass spectral procedure lies in its extreme sensitivity (79). In summary, this technique could prove to be a powerful tool for the quick identification of G/C molar ratios in both bacterial DNA extracts and amplified PCR products.

CONCLUSIONS

The research described in this REPORT has expanded the Py-MS knowledge base on a comprehensive array of biomarkers present in bacteria. Many of these biomarkers have provided taxonomic information to allow identification and differentiation by pyrolysis-mass spectrometry of biological threats in the presence of an environmental background. Proteins, nucleic acids, and lipids are among the biomarkers that have been extensively studied. The ability to perform *in situ* chemical reactions during pyrolysis is an exciting outgrowth of this research. These reactions and the use of quadrupole ion trap technology to perform selective, and sensitive detection of biomarkers have added great deal of specificity in the identification of bacteria.

In situ derivatization of lipids has been the most promising approach for immediate addition to the Army's CBMS detection scheme. Similar results have been obtained using the in situ process with mass spectrometry detection as the conventional Microbial ID, Inc.

system.

The studies on the pyrolysis of proteins has developed an understanding of the factors affecting the formation of the major pyrolysis product, diketopiperazines. As work advances in this area, it is anticipated that some sequencing of selected proteins will be accomplished. Pyrolysis of nucleic acids has shown that ratios of the DNA and RNA bases can be obtained. The use of the base ratios has been an important microbiological parameter for genus differentiation. The investigations described in this REPORT have been designed to provide the maximum amount of information from each biomarker class. Multiple ions for a selected class have been used in all laboratory investigations. All these advances are being currently implemented into the CBMS instrument. Research into both the methodology and instrumentation have taken a parallel development during the course of this study.

REFERENCES

1. K.J. Voorhees; S.J DeLuca and A. Noguerola; J. Anal. Appl. Pyrol., **24**, 1 (1992).

2. S.J. DeLuca; E.W. Sarver; P. de B. Harrington; K.J. Voorhees; Anal. Chem., **62**, 1465 (1990).

3. F. Basile; K.J. Voorhees and T.L. Hadfield; Appl. and Env. Microbiol., **61**, 1534-1539 (1995).

4. F. Basile; K.J. Voorhees and T.L. Hadfield; "Differentiation of Microorganisms based on Py-MS and Principal Components Analysis of Fatty Acid Methyl Esters", in the Proceedings The 42nd ASMS Conference on Mass Spectrometry and Allied Topics, 108 (1994).

5. S.J. DeLuca; E.W. Sarver and K.J. Voorhees; J. Anal. Appl. Pyrol., **23**, 1 (1992).

6. K.J. Voorhees; W. Zhang; A.D. Hendricker and B. Murugaverl; J. Anal. Appl. Pyrol., **30**, 1 (1994).

7. A. Noguerola; B. Murugaverl and K.J. Voorhees; J. Amer. Soc. Mass. Spectrom., **3**, 750 (1992).

8. A.D. Hendricker; P.B. Harrington; W. Zhang; K.J. Voorhees; A. Mahmoudi; "An Investigation of Oligopeptides by Curie-point Py-Tandem MS", Paper 038, Pittsburgh Conference Atlanta, GA, March 8, 1993.

9. A. Hendricker; B. Muragaverl and K.J. Voorhees; " Steric Effect in the Thermal Cyclization of Peptides", ERDEC Scientific Technology Meeting, Edgewood, MD, November 1993.

10. A.D. Hendricker; B. Murugaverl and K.J. Voorhees; "Steric Effects in The Thermal Cyclization of Peptides", J. Anal. Appl. Pyrol., accepted.

11. A.D. Hendricker; B. Murugaverl and K.J. Voorhees; "Steric Effects in The Thermal Cyclization of Peptides", in the Proceedings The 42nd ASMS Conference on Mass Spectrometry and Allied Topics, 635 (1994).

12. A. Noguerola; "Curie-point Pyrolysis-Mass Spectrometry and Tandem Mass Spectrometry of Some Fundamental Biomaterials and Foundations for a Learning System for Classifying Mass Spectra", Ph.D. Thesis to the Colorado School of Mines, 1992.

13. K.J. Voorhees and W. Zhang; unpublished results.

14. C.D. Mowry; A. Sonesson and K.J. Voorhees; "Bacterial Isoprenoid Profiling using Curie-point Py-MS" in the Proceedings The 42nd ASMS Conference on Mass Spectrometry and Allied Topics, 152 (1994).

15. H-R. Schulten and W. Gortz; Analyt. Chem, **50**, 428 (1978).

16. R. Tsao and K.J. Voorhees, Anal. Chem., **56**, 368 (1984).

17. H.L.C. Meuzelaar; J. Haverkamp; F.D. Hileman; "Pyrolysis Mass Spectrometry of Recent and Fossil Biomaterials, Compendium and Atlas", Elsevier: Amsterdam, 1982, p.34.

18. P.B Harrington and K.J. Voorhees; Anal. Chem., **62**, 729 (1990).

19. K.J. Voorhees, P.B. Harrington, T.E. Street, S. Hoffman, S.L. Durfee, J.E. Bonelli and C.S. Firnhaber, (1990), "Approaches to Py-MS Data Analysis of Biological Materials," Computer-Enhanced Analytical Spectroscopy, **2**, 259.

20. L.T. Miller; J. Clin. Microbiol., **16**, 584 (1982).

21. G. Holzer, T.F. Bourne and W. Bertsch, J. Chromatogr. **468**, 181 (1989).

22. C.W. Moss, J. Chromatogr. **203**, 337 (1981).

23. A. Fox, and G.E. Black, Identification and detection of carbohydrate markers in bacteria. Derivatization and gas-chromatography mass spectrometry, Chapter **8.** In Catherine Fenselau (ed.), Mass Spectrometry for the Characterization of Microorganisms. **ACS** Symposium Series **541,** American Chemical Society, Washington, D.C, 1994.

24. D.N. Heller, R.J. Cotter, C. Fenselau, and 0.M. Uy, Anal. Chem. **59**, 2806 (1987).

25. P.A. Snyder, P.B.W. Smith, J.P. Dworzanski and H.L.C. Meuzelaar, Pyrolysis-gas chromatography-mass spectrometry. Detection of biological warfare agents, Chapter 5. In Catherine Fenselau (ed.), Mass Spectrometry for the Characterization of Microorganisms. ACS Symposium Series 541, American Chemical Society, Washington, D.C, 1994.

26. D. Naumann, V. Fijala, H. Labischinski and P. Giesbrecht, J. Mol. Struct. **174**, 65, 1988.

27. R.A. Dalterio, W.H. Nelson, D.Britt, and J.F. Sperry, Appl. Spectro. **41**, 417 (1987).

28. C. Edwards, The significance of *in situ* activity on the efficiency of monitoring methods, Chapter 1. *In* C. Edwards (ed.), Monitoring Genetically Manipulated Microorganisms in the Environment. John Wiley & Sons, New York, 1993.

29. K.D. Hughes, D.M. Huber and F.E. Lytle, Anal. Chem. **61**, 1656 (1988).

30. F. Basile, K.D. Hughes, P.E. Wisniowski, D.G. Gorenstein, F.E. Lytle, T.S. McCay-Buis, D.M. Huber and B.C. Hemming, Anal. Biochem. 211, 55 (1993).

31. M. Costas, B. Holmes, S.L.W. On and D.E. Stead, Identification of medically important Pseudomonas species using computerized methods, pp. 15-18. In R.G. Board, D. Jones, F.A. Skinner (ed.), Identification Methods in Applied and Environmental Microbiology. Society for Applied Bacteriology. Blackwell Scientific Publications, Oxford, U.K., 1992.

32. C.W. Moss, The Use of Cellular Fatty Acids for Identification of Microorganisms, Chapter **4.** *In* Alvin Fox, Stephen L. Morgan, Lennart Larsson, and G6ran Odham (ed.), Analytical Microbiology Methods: Chromatography and Mass Spectrometry. Plenum Press, New York, 1990.

33. Microbial ID, Inc. 1993. Microbial Identification System operating manual, ver. **3.0.** Microbial ID, Inc., Newark, DE.

34. R.J. Cotter, Pyrolysis and desorption mass spectrometry, Chapter 2. *In* K. J. Voorhees (ed.), Analytical pyrolysis. Techniques and applications. Butterworth & Co., London, U.K., 1984

35. R.C. Murphy, Mass Spectrometry of Lipids, pp. 75-77. In Fred Snyder (ed.), Handbook of Lipid Research, vol. 7. Plenum Press, New York, 1993.

36. N. Shaw, Lipid Composition as a Guide to the Classification of Bacteria, p. 97, *In* D. Periman (ed..), Advances in Applied Microbiology. Academic Press, New York, 1974.

37. Dodd, C. E. R., R. H. Dainty, Identification of *Brochothrix* by intracellular and surface biochemical composition, pp. 299-304. *In* R.G. Board, D. Jones, F.A. Skinner (ed.), Identification methods in applied and environmental microbiology. Society for Applied Bacteriology. Blackwell Scientific Publications, Oxford, U.K., 1992.

38. W.M. O'Leary, S.G. Wilkinson, Gram-positive bacteria, **pp. 120-129.** *In* C. Ratledge and S. G. Wilkinson (ed.), Microbial Lipids, vol. 1. Academic Press, New York, 1988.

39. N.J. Jensen and M.L. Gross, Lipids, **21**, 362 (1986).

40. S.E. Stein, R.S. Donald, J. Am. Soc. Mass Spectrom. **5**, 859 (1994).

41. R.C.W. Berkeley, R. Goodacre, R.J. Helyer, T. Kelley, Pyrolysis mass spectrometry in the identification of *Bacillus* species, pp. 257-262. *In* R. G. Board, D. Jones, F. A. Skinner (ed.), Identification Methods in Applied and Environmental Microbiology. Society for Applied Bacteriology. Blackwell Scientific Publications, Oxford, U.K., 1992.

42. D.N. Heller, R.J. Cotter, C. Fenselau, J.A. Platt, 0.M. Uy, Anal. Chem. **60**, 1415 (1988).

43. A. Fox, J. Gilbart, and S.L. Morgan, Analytical Microbiology: **A** Perspective, Chapter 1. *In* Alvin Fox, Stephen L. Morgan, Lennart Larsson, and Goran Odbam (ed.), Analytical Microbiology Methods: Chromatography and Mass Spectrometry. Plenum Press, New York, 1990.

44. X.L. Hronowski, R.J. Cotter, N. Qureshi and K. Takayama, Program Abstr. Proceedings of the 41st Annual ASMS Conference on Mass Spectrometry and Allied Topics, abstr. 431a, 1993.

45. G. Eglinton, D.H. Hunnernan, and A. McCormick, Org. Mass Spectrom. **1**, 593 (1968).

46. S.G. Wilkinson, Gram-negative Bacteria, p. 449. *In* C. Ratledge and S.G. wilkinson (ed.), Microbial Lipids, vol 1. Academic Press, New York, 1988.

47. F. Basile, T.L. Hadfield, K.J. Voorhees, Program Abstr. 36th Rocky Mountain Conference on Analytical Chemistry, abstr. 257, 1994.

48. F. Basile, T.L. Hadfield, D.W. Sickenberger, K.J. Voorhees, Program Abstr. ERDEC Scientific Conference on Chemical and Biological Defense Research, abstr. 2, 1994.

49. C. Arnold, Software Specialist, MIDI, Inc., Newark, Del. Private Communication.

50. F. Basile; T.L. Hadfield; K.J. Voorhees, Appl. Environ. Microbiol., **61**, 1534-1539 (1995).

51 . K. Abel, H. deSchmertzing; J.L. Peterson, J. Bacteriol., **85**, 1039 (1963).

52. J.R. Vestal and D.C. White, BioScience, **39**, 535-541 (1989).

53. R.G. Board; D. Jones F.A. Skinner, (Eds), Identification Methods in Applied and Environmental Microbiology; Blackwell Scientific Publications: London, 1992.

54. P.B. Harrington; T.E. Street; K.J. Voorhees; F. Radicati di Barzolo; R.W. Odom, Anal. Chem., **61**, 715-719 (1989).

55. P.D. Nichols; W.R. Mayberry; C.P. Antworth; D.C. White, J. of Clin. Microbiol., **21**, 738-740 (1985).

56. R.E. March, personal communication, 1995.

57. H.J. Svec, and G.A. Junk, J. Am. Chem. Soc., **86**, 2278-2282 (1964).

58. A.S. Noguerola, B. Murugaverl and K.J. Voorhees, J. Am. Soc. Mass Spectrom., **3**, 751-756 (1992).

59. G.G. Smith, G.S. Reddy and J.J. Boon, Chem. Soc. Perkin Trans II, 203-211 (1988).

60. G.A. Junk and H.J. Svec, Anal. Biochem., **6**, 199-202 (1963).

61. M.A. Ratcliff, E.E. Medley and P.G. Simmonds, J. Org. Chem., **39**, 1481-1490 (1973).

62. K. Biemann, "Mass Spectrometry: Organic Chemical Applications; McGraw Hill: New York, 1962, pp 283-296.

63. N. Lichtenstein, J. Am. Chem. Soc., **60**, 560-563 (1938).

64. A.B. Mauger, Chem. Comm., 39-40 (1971).

65. D. Gross and G. Grodsky, J. Amer. Chem. Soc., **77**, 1678-1680 (1955).

66. D.W. Bowers, S. Delbert, L.R. Hunter and T.R. McIver, J. Amer. Chem. Soc., **106**, 7288-7289 (1984).

67. D.H. Robertson and C. Merritt, Jr., J. Gas Chromatogr., **5**, 96-98 (1967).

68. C.V. Bradley and W.H. Dudley, Biochem. and Biophy. Res. Comm., **104**, 1223-1230 (1982).

69. L. Li and M. Lubman, Rapid Comm. Mass Spectrom., **3**, 12-15 (1985).

70. T.O. Munson and J. Vick, J. Anal. Appl. Pyrol., **8**, 493 - 501 (1985).

71. T.O. Munson and D.D. Fetterolf, J. Anal. Appl. Pyrol., **11**, 15 -24 (1987).

72. J.J. Boon and J.W. DeLeeuw, J. Anal. Appl. Pyrol., 11 (1987) 313-327.

73. G. Mauntado and C. Puglisi, Thermal Degradation of Condensation Polymers, in Comprehensive Polymer Science, First Supplement, Paragram, Oxford, 1992, pp 227-249.

74. NIST/EPA/NIH Mass Spectral Database, Version 4, 1992.

75. R.D. Cramer III, J. Amer. Chem. Soc., **102**, 1837-1849 (1986).

76. S. Hellburg, M. Sjöström, B. Skagerberg and S. Wold, J. Med. Chem., **30**, 1126-1135 (1987).

77. R.W. Taft, Separation of Polar, Steric and Resonance Effects in Reactivity in Steric Effects in Organic Chemistry ed. M.S. Newman, John Wiley & Sons inc., New York, 1956 598-599

78. R.W. Taft, Separation of Polar, Steric and Resonance Effects in Reactivity in Steric Effects in Organic Chemistry ed. M.S. Newman, John Wiley & Sons inc., New York, 1956 571-574

79. D.M. Hawley and J.L. Wiebersy, Nucleic Acids Research **5**, 4949-4956 (1978).

80. J.M. Rice and G.O. Dudek, J. Amer. Chem. Soc. **89,** 2719-2725 (1967).